Loss Mechanisms in Turbine Tip Clearance Flows

by

Arthur Huang

Submitted to the Department of Aeronautics and Astronautics
in partial fulfillment of the requirements for the degree of
Master of Science in Aeronautics and Astronautics
at the
MASSACHUSETTS INSTITUTE OF TECHNOLOGY
June 2011

Author .....
Department of Aeronautics and Astronautics
May 19, 2011

Certified by .....
Edward M. Greitzer
H.N. Slater Professor of Aeronautics and Astronautics
Thesis Supervisor

Certified by .....
Choon S. Tan
Senior Research Engineer
Thesis Supervisor

Certified by .....
Steven G. Gegg
Manager, Turbine Aerodynamics, Rolls-Royce Corporation
Thesis Supervisor

Accepted by .....
Eytan H. Modiano
Associate Professor of Aeronautics and Astronautics
Chair, Graduate Program Committee

Loss Mechanisms in Turbine Tip Clearance Flows

by

Arthur Huang

Submitted to the Department of Aeronautics and Astronautics
on May 19, 2011, in partial fulfillment of the
requirements for the degree of
Master of Science in Aeronautics and Astronautics

Abstract

Numerical simulations of tip clearance flow have been carried out to define the loss generation mechanisms associated with tip leakage in unshrouded axial turbines. Mixing loss between the leakage, which takes the form of a strong embedded streamwise vortex ($u_\theta/u_x \geq 1$ in the vortex core), and the mainstream flow is found to be the main source of loss. Vortex line contraction, and consequent vortex core expansion, and also vortex breakdown, are identified as the two important mechanisms that determine mixing loss. Because of these vortex dynamic features, the behavior is different from the conventional view of the effect of pressure level on mixing of non-uniform flows. More specifically, it is shown, through control volume arguments and axisymmetric computations, that as a strongly swirling flow passes through a pressure rise, the *mixed-out loss can either decrease or increase*, the latter occurring if the deceleration becomes large enough to initiate vortex breakdown. It is further shown that tip vortices in turbines experience pressure rises large enough to cause vortex breakdown. The effect of pressure distribution on tip leakage losses is illustrated through examination of two turbine blades, one designed with a forward loaded tip and one with an aft loaded tip. The computations show a 16% difference in tip clearance loss between the two, due to the lower pressure rise encountered by the clearance vortex, and hence lower vortex breakdown losses, with the forward loaded blade. Other computational experiments, on the effects of blade loading, incidence, and solidity, are also shown to be consistent with the ideas developed about blade pressure distribution effects on vortex breakdown and hence clearance mixing loss.

Thesis Supervisor: Edward M. Greitzer
Title: H.N. Slater Professor of Aeronautics and Astronautics

Thesis Supervisor: Choon S. Tan
Title: Senior Research Engineer

Thesis Supervisor: Steven G. Gegg
Title: Manager, Turbine Aerodynamics, Rolls-Royce Corporation

Acknowledgments

"Come unto me, all you who are weary and burdened, and I will give you rest"

-Matthew 11:28

This work was carried out with the support of the Rolls-Royce Whittle fellowship, in collaboration with the Turbine Aerodynamics group at Rolls-Royce Corporation in Indianapolis.

I would like to thank my thesis advisors, Prof. Edward Greitzer and Dr. Choon Tan, without whom this work would not have been possible. Their constructive critiques never let me settle for less, and their encouragement let me know that I was capable of more. I am also indebted to Prof. Nick Cumpsty for his helpful comments on this work.

Thanks is also due to several engineers at Rolls-Royce for their friendship and deep technical involvement in this work. Ed Turner, Steve Gegg, and Eugene Clemens have all contributed vitally to the technical thought behind this thesis. Specifically, I would like to thank Steve for his great advice and management of the Whittle Fellowship program, Ed for his help in designing new airfoil geometries, and Eugene for putting up with all the times I went running to him with CFD issues. Likewise, I'd like to thank Kurt Weber, who good-naturedly endured my countless questions about CFD.

I would also like to thank my colleagues at the Gas Turbine Lab for their friendship, advice, and support. I am especially grateful to Dorian Colas and David Hall for enlightening discussions on vortex dynamics, mixing losses, and basketball.

My time at MIT would have been far less meaningful if I had never become friends with Yunji Wu, Justin Lai, Jeremy Lai, Orton Huang, James Won, Yu Xu, Albert Chi and Ed Kao. Thank you for sharing your lives with me. In addition, thanks to Joey Sung and Eddie Wu for their friendship which has continued since childhood.

Finally, I want to thank my family for their support and love through the years. Alex and Allen have been the best of brothers, each in his own way. I never see my dad so excited as when he discusses research with me, and I am grateful for his love, patience, and wisdom. As for my mom, I know that no one loves me more, and it is to her that this thesis is dedicated.

Contents

List of Figures

List of Tables

Nomenclature

ϵ	Leakage angle, relative to mainstream
η	adiabatic efficiency
Γ	circulation
μ_{eff}	effective viscosity
Ω	blade rotational speed
Φ	dissipation function
ϕ	flow coefficient $= v_x/\Omega r$
ψ	work coefficient $= \Delta h_t/(\Omega r)^2$
ρ	density
σ	solidity
ξ	loss coefficient
A	area
AR	Area ratio
c	blade axial chord
C_p	pressure rise coefficient $= \frac{p-p_{inlet}}{0.5\rho U^2}$
c_p	specific heat at constant pressure

g	tip clearance
h	Duct height or blade span
h_t	stagnation enthalpy
M	Mach number
m_{leak}	leakage massflow
m_{main}	mainstream massflow
p	pressure
p_t	stagnation pressure
PR	stagnation-to-static pressure ratio
R	gas constant
r, θ, z	cylindrical coordinates
r_e	vortex core edge radius
Re	Reynolds number
S	swirl number
s	specific entropy
T	temperature
t	time
T_t	stagnation temperature
u, U	wake, freestream streamwise velocities
u, v, w	x,y,z-velocities
V	velocity

v_θ swirl velocity

VR velocity ratio = $\frac{u}{U}$

x, y, z Cartesian coordinates

y^+ dimensionless wall distance

Chapter 1

Introduction

Turbomachines have a small clearance, referred to as the tip clearance or tip gap, between the outer radius of the rotating blades and the stationary casing. The existence of the clearance results in losses as the flow leaks through the clearance, and there is observed to be a decrease in efficiency of turbomachinery that varies roughly linearly with gap size [1]. This change in efficiency with clearance level is known as the leakage loss slope. Typical clearances for axial turbines lie in the range of 1-2% gap-to-span ratio [15].

Rotating blade rows can be classed into two categories: shrouded and unshrouded. Shrouded blade rows are characterized by a shroud, a ring of material linking the blades at the tip so that flow cannot leak over the tip, with the clearance gap between the shroud and the casing. Unshrouded blade rows have no shroud, and the flow passes through the clearance gap between the blade tip and the casing. This thesis examines loss mechanisms in unshrouded turbines.

For an unshrouded turbine, the tip clearance loss is about one-third of the total loss [6]. The leakage loss slope has been observed to range between 2 and 3 points in efficiency per 1% in clearance-to-span ratio [3]. The limits of quantitative understanding of the parametric dependence of tip clearance loss on stage design is one barrier to turbine optimization. Providing such understanding is the objective of this work.

1.1 Background

Tip clearance flows in turbines have been studied extensively, and only a summary of the fluid mechanics and attempts to model loss are given below.

Characteristic flow features have been observed in tip clearance flows over flat tipped blades. Figure 1-1 shows a 2-D cartoon of the flow within the tip gap [3]. Flow enters the gap on the pressure side. If the corner is sharp, a separation bubble will form on the tip at the pressure side corner. If the thickness to clearance ratio is greater than 2 or so, the flow will reattach [11]. Downstream of reattachment, viscous stresses reduce the relative stagnation pressure and mix the momentum. When the flow exits the gap, its velocity vector is misaligned with the freestream velocity and a shear layer (vortex sheet) exists between the clearance flow and the mainstream. As the flow progresses downstream, the vortex sheet rolls up into a vortex.

Figure 1-2 shows contours of relative stagnation pressure in a turbine passage, along with streamlines in the tip clearance vortex, from a 3-D turbine computation. The vortex remains adjacent to the suction surface corner and is characterized by low stagnation pressure relative to the freestream. As the vortex convects downstream, it mixes with the freestream, generating loss.

In modeling the clearance flow, it has been standard to divide the process into two fluid dynamic modules [3], [7], [22]. The first considers the flow passing through the gap. The second considers the interaction between the leakage flow and the mainstream.

In the first module, the stagnation-to-static pressure ratio across the gap and the viscous losses in the gap determine the state of the flow at the gap exit. Moore and Tilton, building on the work of Rains in compressors, viewed the gap as an orifice [15], with the separation bubble as a vena contracta, where the contraction coefficient could be determined through potential flow analysis. A control volume model was used to mix the flow out within the gap. The model produced a discharge coefficient which matched a low speed cascade experiment. Heyes and Hodson added viscous losses from the endwalls to this model and developed a control volume method to

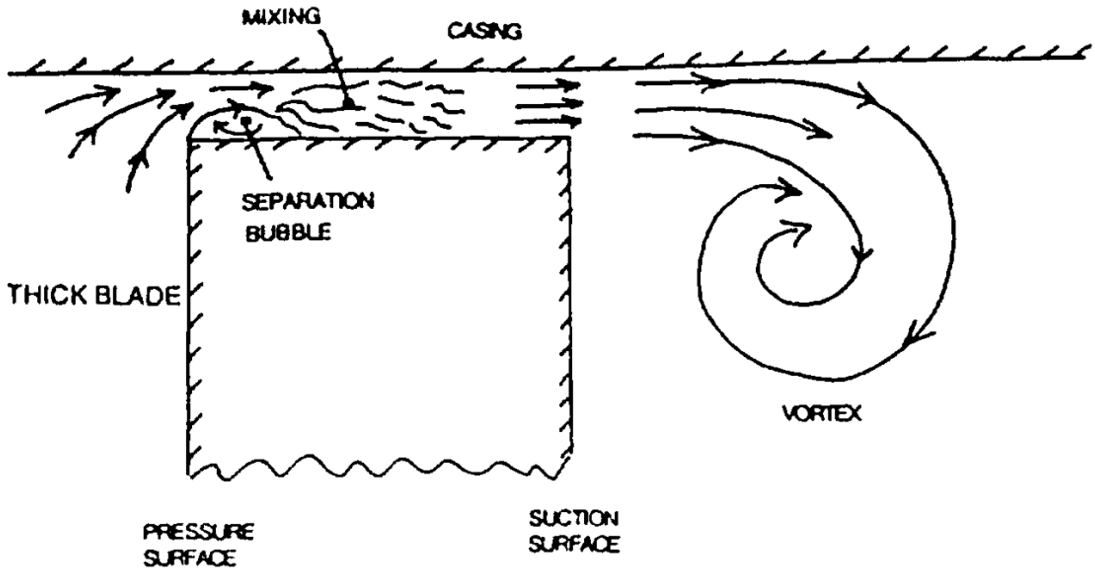

Figure 1-1: 2D sketch of tip clearance flow features [3]

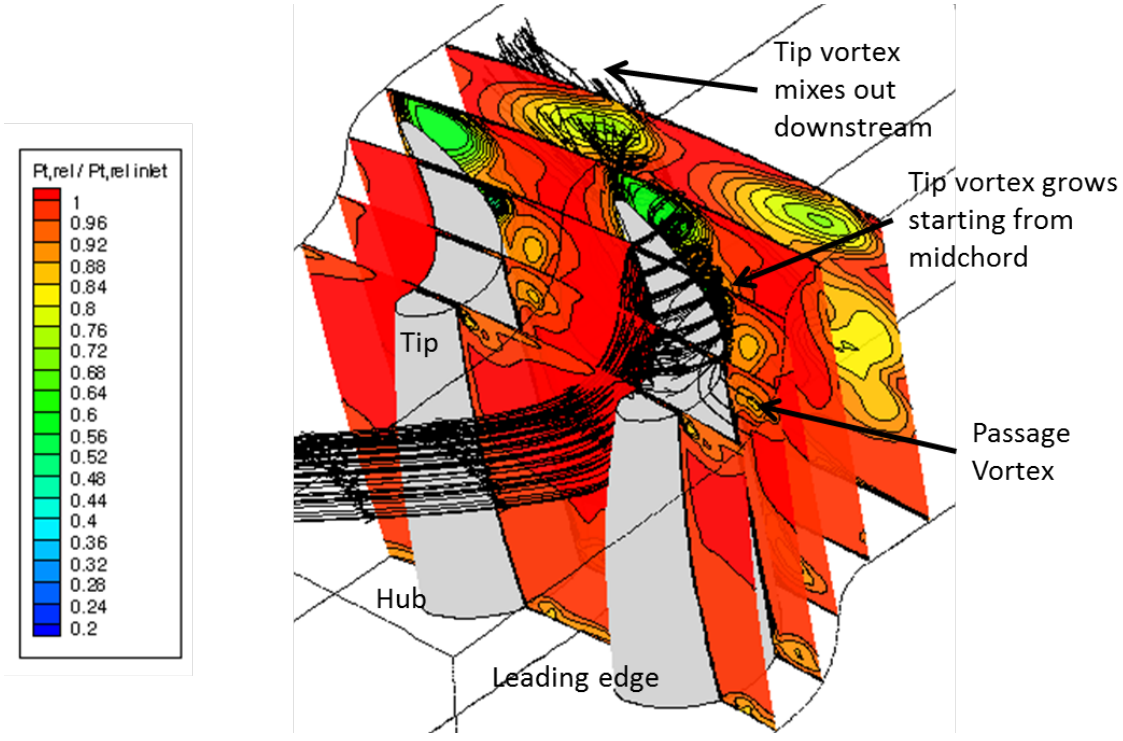

Figure 1-2: Computed turbine rotor flowfield at 2% clearance. Streamlines and contours of relative stagnation pressure

calculate the angle at which the flow exited the gap [7]. The model matched results from a low speed turbine cascade, but it required knowledge of the static pressure at the gap inlet and exit. This is the most useful model for tip leakage massflow that the author has found in the literature.

The second fluid dynamic module, which is the focus of this work, looks at what happens to the flow *after* it exits the gap. Sjolander found that the losses within the tip gap comprised only 10-15% of the tip clearance loss, with most of the clearance loss tied to the mixing of the tip clearance flow with the mainstream [22]. Denton suggested a control volume model for estimating these mixing losses [3]. However, there has been no work to assess the applicability of Denton's model or to examine the flow for additional loss sources. Up to now, the loss within the gap and the mixing loss have been the only clearance loss mechanisms identified in the literature.

Recent work has focused on computational efforts to model the effects of various geometrical modifications to the tip on the flow and heat transfer within the clearance gap. [12], [14]. These modifications, known as tip treatments, attempt to reduce the leakage massflow, and hence the clearance loss by adding rims around the tip gap (squealers), or extending the tip into a winglet or partial shroud. Tip treatments have been shown to reduce the tip clearance loss, but can be difficult to cool [12]. Li et al. showed a 0.2% improvement in turbine efficiency at 0.5% clearance-to-span for a squealer configuration with the pressure side rim angled away from the tip [14].

The author has not seen information in the literature on how best to choose turbine airfoil shapes or design parameters to minimize tip losses. The simplest correlations assume the tip loss slope is independent of turbine design. Kacker and Okapuu give a correlation which estimates tip clearance loss based on the blade exit angle, although they do not present a physical rationale [8]. The control volume model of Denton is a useful tool, but it has not been shown whether such a control volume model gives an accurate estimate of loss.

1.2 Research Questions

The goal of this work is to identify and quantify loss mechanisms in turbine tip clearance flow, and thus provide guidelines for the design of unshrouded high pressure turbines. The research questions to be addressed are as follows:

- How well does the Denton model for mixing losses capture tip clearance losses?
- Are the mixing losses affected by the presence of the clearance tip vortex?
- How should a turbine rotor be designed to reduce tip clearance loss?

1.3 Methodology

To answer the research questions, three-dimensional computations of clearance losses are carried out for a variety of turbine designs in order to identify the major loss mechanisms. Since only 15% of the loss takes place within the gap, the present work focuses on the mixing of the tip leakage flow with the mainstream and on the development of the tip clearance vortex.

Viscous computations of ducts with slip-walls are used to illustrate the effect of area expansions on vortex behavior. Specifically: (i) The Denton control volume model is evaluated for mixing losses due to flow injection in rectangular ducts with area changes, and (ii) a control volume model for the evolution of a Rankine vortex in a pressure gradient is evaluated using axisymmetric calculations.

The 3-D turbine computations are used to evaluate tip clearance losses and investigate behavior of tip vortices in the turbine environment. Based on the results of the duct calculations, it was hypothesized that reducing the pressure rise experienced by the tip vortex would reduce the tip clearance loss in a turbine. Implementation of such a turbine design was found to decrease the tip clearance loss by 9%.

1.4 Contributions

The main contributions to turbine aerodynamics from the present work are as follows:

- Because turbine tip clearance vortices are strong swirling flows (in contrast to compressor tip vortices), the mixing loss is sensitive to pressure gradients in a different manner than for compressors. In particular mixing loss decreases with pressure level until the onset of vortex breakdown. Once breakdown is encountered the mixing loss increases with pressure rise. The first of these effects is qualitatively different from compressor tip clearance flow, in which, as with a wake in a pressure gradient, mixing loss increases with pressure level.

- The control volume analysis proposed by Denton estimates turbine tip clearance loss due to mixing to within 40%. The discrepancy occurs because the leakage vortex mixes out over a range of pressures rather than at constant pressure, as Denton assumed.

- Tip vortex breakdown is a loss mechanism in turbine tip clearance flows.

- Tip clearance loss can be reduced by decreasing the pressure rise experienced by the tip vortex. A 9% reduction in leakage loss has been obtained by using a tip designed to reduce losses due to vortex breakdown.

1.5 Organization of Thesis

The remainder of the thesis is organized as follows: Chapter 2 illustrates the important features of tip clearance flows using the computed flowfield around a representative high pressure turbine blade. Chapter 3 describes a control volume analysis for mixing losses and its assessment against a simplified duct geometry and against turbine calculations. Chapter 4 gives a control volume model description of a Rankine vortex in a pressure gradient and its implications for tip leakage vortex mixing losses. Chapter 5 describes the reasoning behind the turbine blade design for low leakage loss and the mechanisms through which the leakage loss was decreased. Chapter 6 evaluates the effect on tip clearance losses of further changes to the pressure distribution through changes in blade loading, incidence, and solidity. Chapter 7 gives a summary and recommendations for future work.

Chapter 2

Features of Tip Clearance Flows

2.1 Introduction

This chapter discusses features of tip clearance flow relevant to loss. The loss sources, the flow exiting the tip gap, and the vortex core are characterized based on a representative 3-D turbine blade computation. The key observations are listed below.

- The main source of loss is the mixing between the leakage flow and the mainstream flow.
- The leakage flow can be roughly regarded as pressure driven with a discharge coefficient of approximately 0.8.
- The tip vortex formed by the leakage flow passes through a pressure rise and breaks down (for this turbine design). The vortex breakdown location is correlated with the region of highest loss per unit axial distance.

2.2 Computational Study of Tip Clearance Flow

To determine the connections between tip clearance flow features and losses, a computational study was performed on a subsonic high pressure turbine blade with tip clearance ranging from 0 to 2% of span. The calculation was done for a single rotor

blade with constant area ducts upstream and downstream. A hybrid mesh was used, with a structured mesh in the mainstream and an unstructured prism mesh at the center of the tip gap. Figure 2-1 shows the mesh on the rotor blade and the hub, Table 2.1 shows the turbine parameters, and Table 2.2 shows the details of the mesh. At the inlet of the domain, stagnation pressure and temperature profiles were specified. The inlet conditions were determined from a separate calculation including the stator and the rotor connected by a mixing plane interface. The exit static pressure boundary condition was defined by holding the hub exit static pressure constant as the clearance changed and using simple radial equilibrium to set the radial pressure distribution. Periodic boundary conditions linked the left and right sides of the domain. No-slip, adiabatic wall boundary conditions were used for the solid surfaces, and the blade rotated as the casing remained motionless. The Reynolds-Averaged Navier Stokes (RANS) equations were solved using ANSYS Fluent, a commercial finite volume solver. Turbulence was modeled using the Spalart-Allmaras turbulence model [18]. The mesh had an average y^+ of 1 in the first cell from solid surfaces in order to resolve the boundary layers.

2.3 Loss Sources

Figure 2-2 shows the computed rotor loss coefficient ξ, defined in Equation 2.1, as a function of tip clearance. The loss coefficient is defined as the lost work due to entropy generation normalized by the turbine work. [1] The loss coefficient rises linearly with clearance level, as seen in the literature. The tip clearance loss is defined as the difference in loss coefficient between the blade with a given tip clearance and the zero clearance case.

$$\xi = \frac{T_{exit}\Delta s}{c_p(T_{t,inlet} - T_{t,exit})} \tag{2.1}$$

A loss breakdown was conducted to determine the sources of clearance loss. The

[1] It is more common to refer to a leakage loss slope as a change in turbine adiabatic efficiency per percent gap to span ratio. In this work, an entropy based metric is used instead because it is the entropy generation due to tip clearance which should scale linearly with the tip clearance, and the efficiency changes non-linearly with loss.

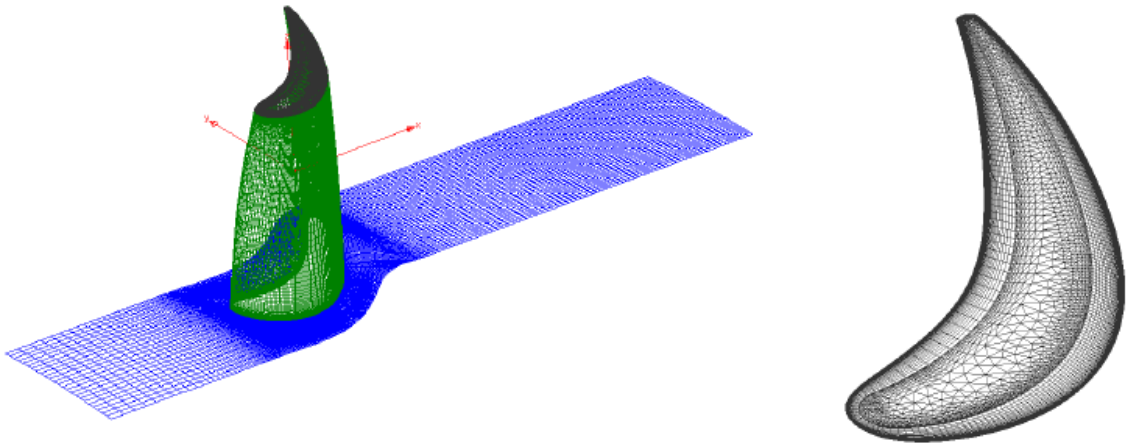

Figure 2-1: Mesh on the hub, blade surface, blade tip

Table 2.1: Turbine Parameters

Work Coefficient	2.13
Flow Coefficient	0.584
Midspan Relative Inlet Angle	54.3°
Midspan Relative Exit Angle	64.6°
Exit Mach Number	0.755
Stagnation-to-Static Pressure Ratio	2.22
Solidity	0.966
Aspect Ratio	1.25
Exit Relative Re_c	3.8×10^6

Table 2.2: Mesh Details

Cell count (2% clr)	2.8×10^6
Avg near-wall y^+	1
Cells across tip gap (2% clr)	36
Inlet plane location (chords upstream of leading edge)	1.35
Exit plane location (chords downstream of trailing edge)	2.55

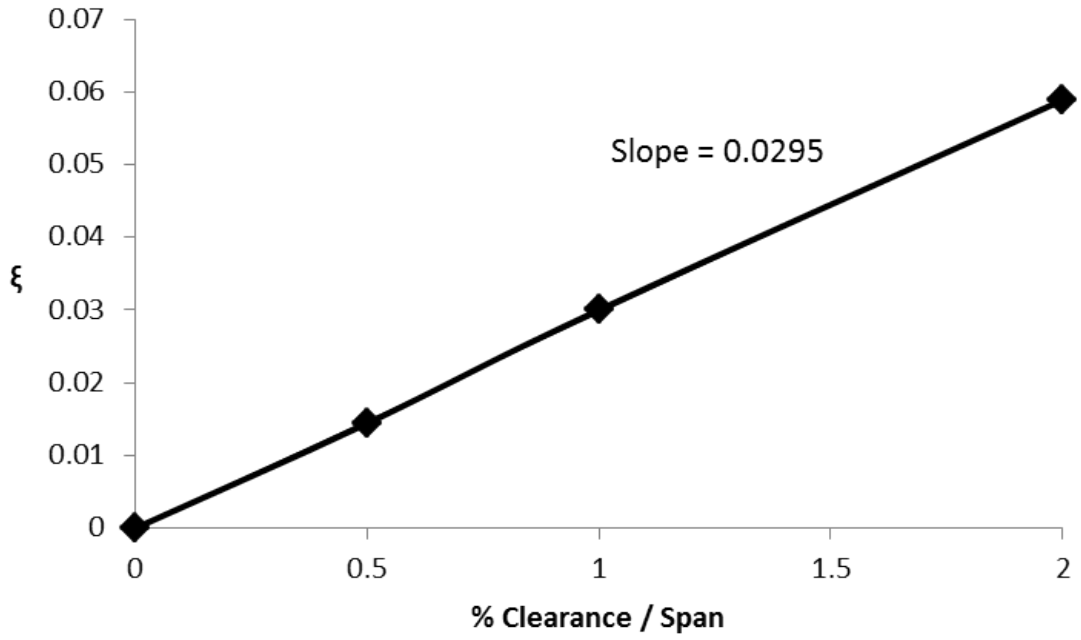

Figure 2-2: Tip clearance loss coefficient for model subsonic HP turbine as a function of clearance-to-span ratio

domain was split into four volumetric regions: the clearance gap, the blade and hub boundary layers, the lower half of the mainstream, and the upper half of the mainstream, which includes the tip clearance vortex. Figure 2-3 shows the normalized volume integral of the entropy generation rate over each region at zero and two percent clearance. The volumetric entropy generation rate $\rho\frac{ds}{dt}$ was calculated from the dissipation function Φ, neglecting irreversible entropy generation due to heat transfer which is responsible for only 7% of the loss [13].

$$\rho\frac{ds_{visc}}{dt} = \frac{\Phi}{T} \tag{2.2}$$

$$= \frac{2\mu_{eff}}{T}\left[\left(\frac{du}{dx}\right)^2 + \left(\frac{dv}{dy}\right)^2 + \left(\frac{dw}{dz}\right)^2 + \frac{1}{2}\left(\frac{du}{dy} + \frac{dv}{dx}\right)^2 + \frac{1}{2}\left(\frac{du}{dz} + \frac{dw}{dx}\right)^2 + \frac{1}{2}\left(\frac{dv}{dz} + \frac{dw}{dy}\right)^2 - \frac{1}{3}\left(\frac{du}{dx} + \frac{dv}{dy} + \frac{dw}{dz}\right)^2\right] \tag{2.3}$$

The changes in loss for the blade and hub boundary layer and lower half of the

mainstream are small relative to the change in loss in the upper half of the mainstream and together account for a negligible change in loss. The gap losses are also a relatively small fraction (15%) of the tip clearance loss, and the losses in the upper half of the mainstream, where the tip leakage flow emerges and mixes out, account for 85% of the tip clearance loss.

The loss per unit axial distance was obtained by taking the difference (between the case with clearance and the case without clearance) of the surface integral of the volumetric entropy generation on an axial plane. Figure 2-4 shows the normalized leakage loss per unit axial distance, $\frac{d\xi}{d(x/c)}$ as described in equation 2.4.

$$\frac{d\xi}{d(x/c)} = \frac{T_{exit}c}{m_{main}\Delta h_t}\int_{axialslice}\rho\frac{ds}{dt}dA \tag{2.4}$$

Upstream of $x/c = 0.75$, the leakage loss is generated mainly within the gap, but downstream of $x/c = 0.75$, the mixing losses account for almost all of the leakage loss. The main loss mechanism of tip clearance loss is the mixing between the leakage flow and the mainstream flow.

2.4 Characterization of Gap Exit Flow

Since the tip clearance loss is predominantly due to mixing losses and since control volume models show that mixing loss scales directly with the leakage massflow and the square of the leakage velocity, the state of the flow exiting the tip gap is of interest. Figure 2-5 shows the ratio of massflow exiting the gap between the leading edge and a specified axial location to the passage massflow, as a function of axial position, for a 2% clearance. It is observed that 85% of the massflow exits the gap aft of 50% axial chord. The massflow through the gap is determined by the exit area, the relative stagnation-to-static pressure ratio at the exit, the viscous losses within the gap, and the angle ϵ between the leakage flow velocity vector and the gap contour (extension of the tip airfoil suction surface into the clearance). A value of $\epsilon = 90^\circ$ indicates that the leakage flow is emerging normal to the gap surface.

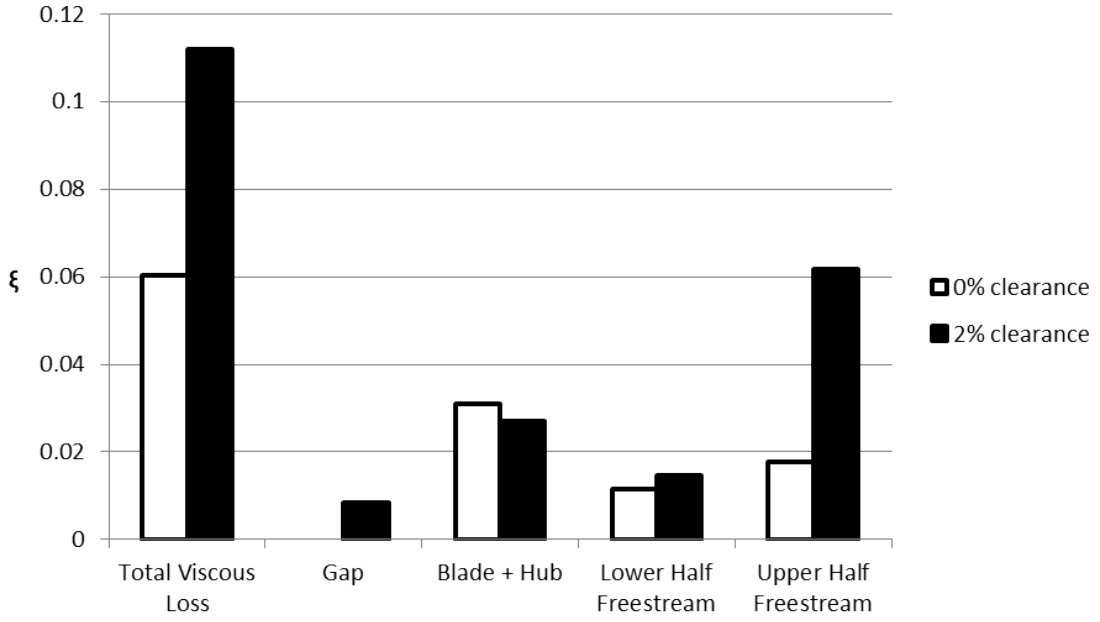

Figure 2-3: Normalized entropy generation in gap, blade and hub boundary layers, lower half freestream, and upper half freestream, for subsonic HP turbine at 0, 2% clearance

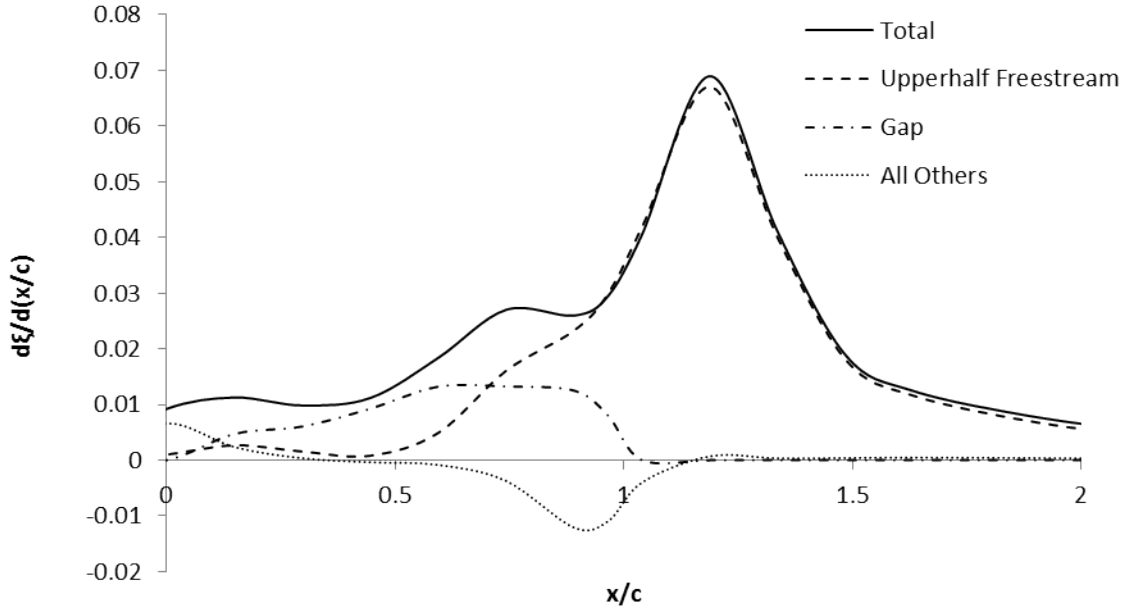

Figure 2-4: Normalized leakage loss per unit axial distance as a function of axial distance for subsonic HP turbine. Volumetric entropy generation rate integrated over axial planes and allocated to loss sources. Difference taken between 0, 2% clearance cases to obtain leakage loss

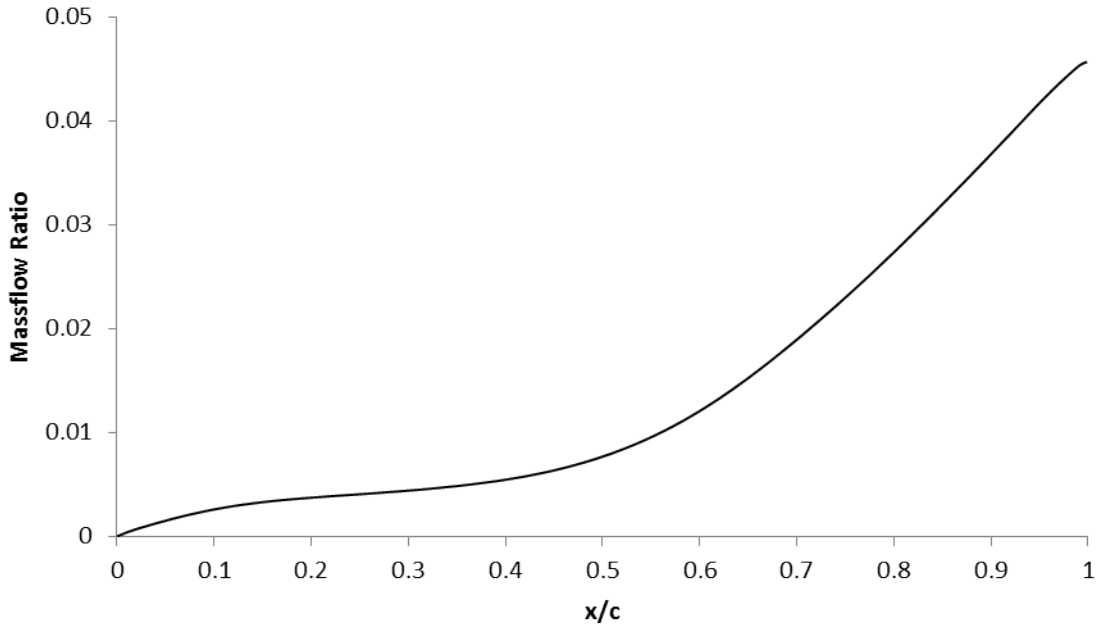

Figure 2-5: Leakage massflow between leading edge and specified axial position, normalized by passage massflow. Subsonic HP turbine at 2% clearance.

$$m = \rho(\vec{V} \cdot d\vec{A}) = \rho V A sin(\epsilon) \tag{2.5}$$

2.4.1 Gap Pressure Ratio and Discharge Coefficient

The gap can be viewed as an orifice, with the ratio of the relative stagnation pressure to the exit static pressure determining ρV. The static pressure at the gap exit can be significantly different from the pressure on the blade suction surface [7], [20]. Heyes and Hodson cited work from Dishart and Moore which showed that for a 2D cascade, the static pressure in the tip clearance gap in the forward 50% axial chord is higher than that at the midspan [7]. Yang, Yu, and Feng showed that the static pressure near the leading edge tip increases, relative to a linear cascade, when the casing is rotated relative to the blade, and when Coriolis and centrifugal forces are included [20]. The computations presented in this work similarly show a static pressure in the forward tip gap region higher than that at 80% blade span. Figure 2-6 shows the isentropic Mach number on the suction surface at 80% span, averaged across the tip

gap. In the first 40% axial chord, the Mach number in the gap is half that at midspan and only 6% of the leakage flow emerges from the gap in that region. Between 40-60% axial chord, the gap exit Mach number approaches that at the suction surface, and between 60% to 100% axial chord, the two are approximately equal.

Figure 2-7 shows the gap discharge coefficient C_d (defined as the ratio of the actual gap massflow to the ideal gap massflow, calculated assuming isentropic flow through the gap for the same stagnation-to-static pressure ratio) as a function of axial location. The discharge coefficient is near 0.8 over most of the aft 50% axial chord. It falls approaches 0.6 toward the trailing edge. In this region, the flow does not reattach (the tip thickness is smaller), and the separation bubble decreases the effective gap exit area and hence the discharge coefficient.

2.4.2 Gap Exit Area

As implied in Equation 2.5, the leakage massflow is proportional to the leakage area. A useful metric for the leakage area is the derivative of the gap perimeter with respect to axial distance, i.e., the leakage area per unit axial distance divided by the gap height. This is shown in Figure 2-8. As the blade curves away from the axial direction, the gap area per unit axial distance increases so that 70% of the gap exit area is located downstream of 50% axial chord.

2.4.3 Leakage Angle

The streamline angle is the final factor which gives the leakage massflow. Figure 2-9 shows the mass-averaged leakage angle as a function of axial position. Between 20% and 60% axial chord, the angle between the leakage and the freestream drops to 45°, $sin(\epsilon)$ is low, and the massflow is reduced. Downstream of 50% axial chord, where most of the massflow exits, the leakage angle peaks around 75% axial chord, where the tip gap pressure ratio is lowest and the normal component of the velocity vector is highest.

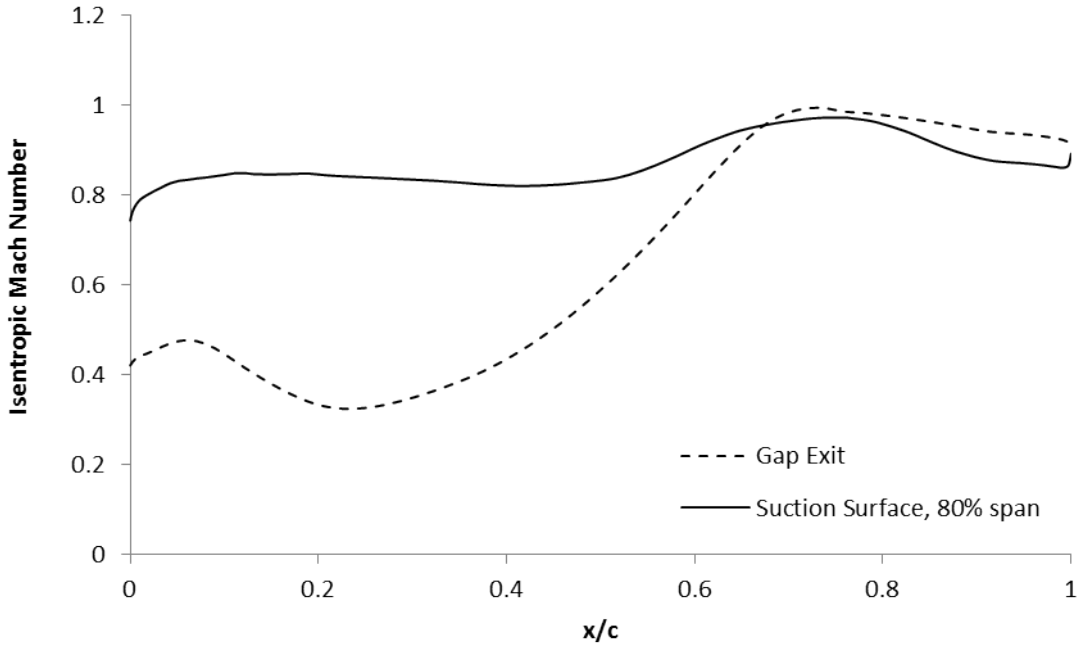

Figure 2-6: Relative isentropic Mach number in the tip gap and on the blade suction surface at 80% span as a function of axial position. Subsonic HP turbine at 2% clearance.

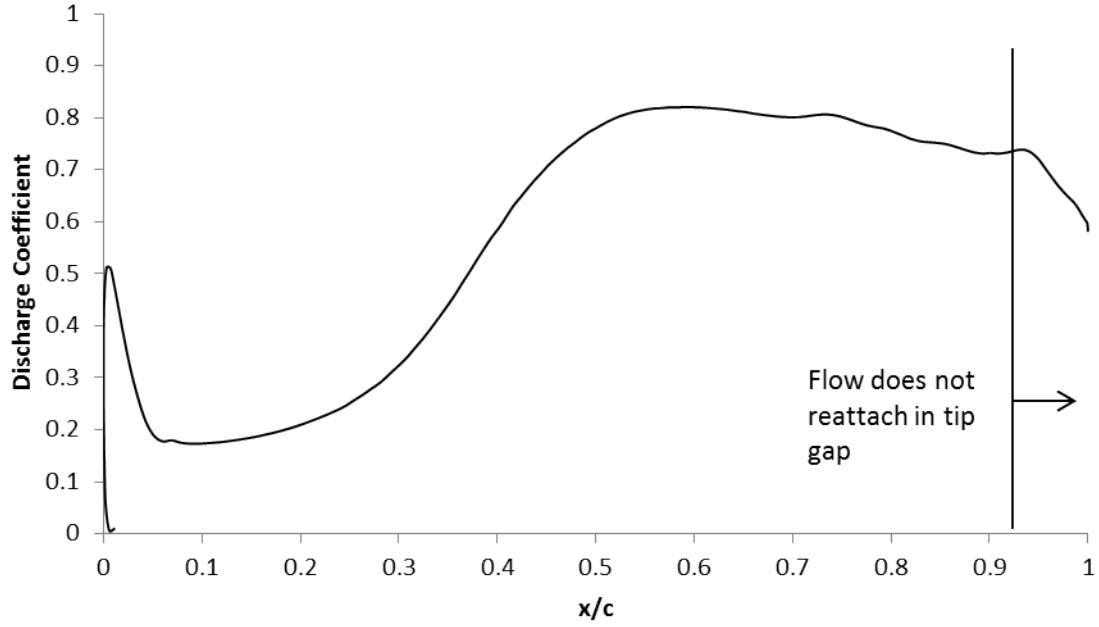

Figure 2-7: Tip gap discharge coefficient as a function of axial position. Subsonic HP turbine at 2% clearance.

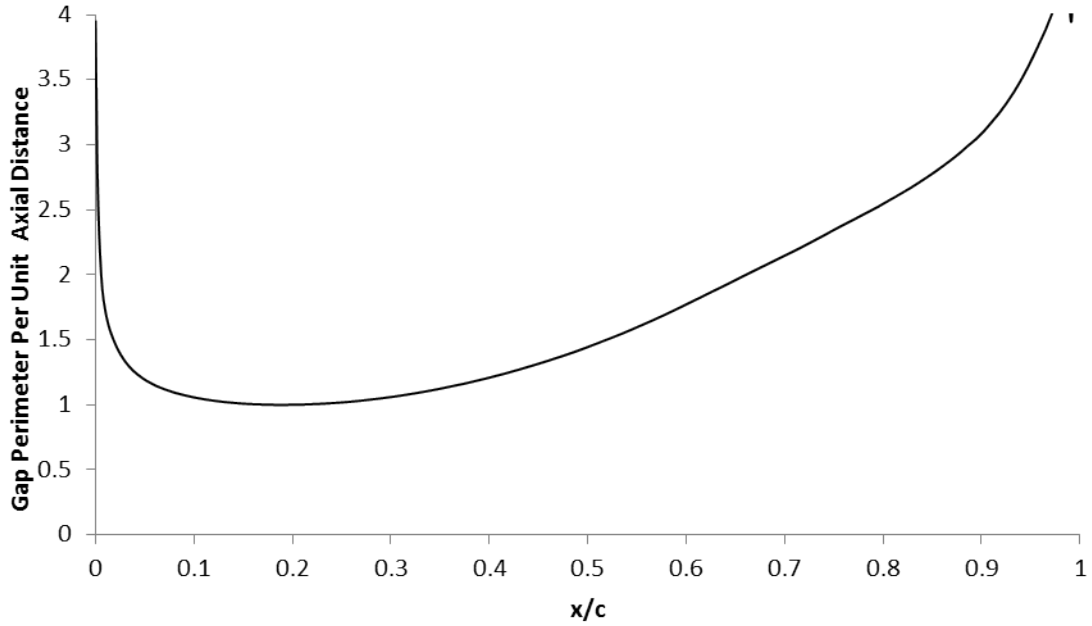

Figure 2-8: Derivative of gap perimeter with respect to axial distance. Subsonic HP turbine at 2% clearance.

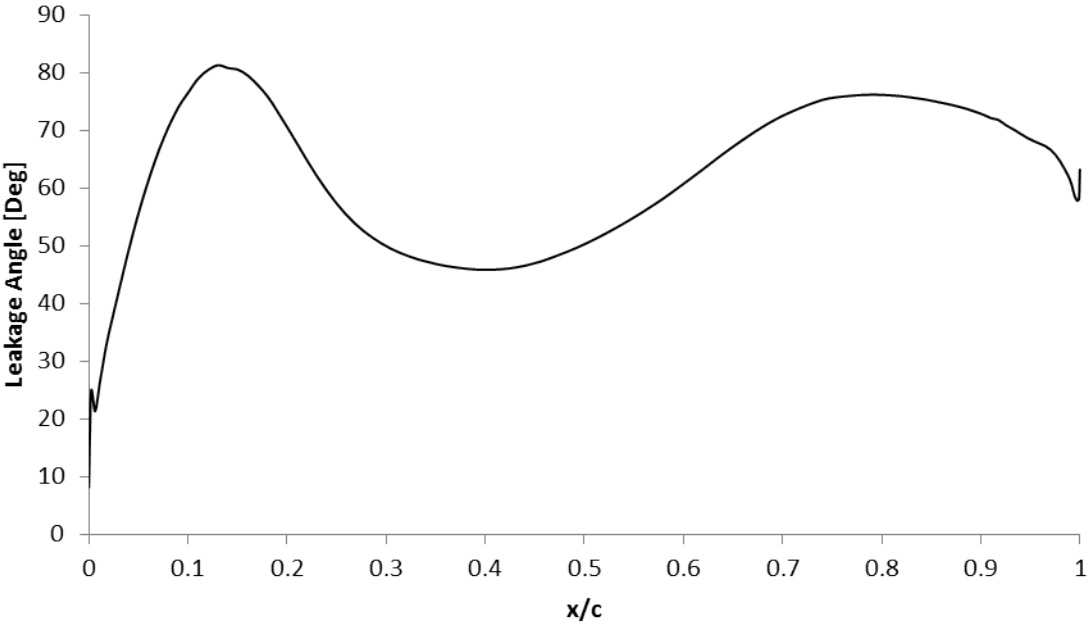

Figure 2-9: Leakage flow angle as function of axial position. Subsonic HP turbine at 2% clearance.

2.4.4 Leakage Flow Modeling

Since 85% of the massflow exits aft of 50% axial chord, one model for tip clearance flow in this range of clearances might be to neglect the forward 50% axial chord, where the flow is more complex and the gap pressure differs from the suction surface pressure in a way that is difficult to predict *a priori*. In the aft 50% axial chord, the gap exit pressure is close to the suction surface pressure, and the discharge coefficient is approximately equal to 0.8. If a leakage flow angle is estimated, or calculated via the method of Heyes and Hodson [7], the gap exit massflow and velocities can be estimated. For the subsonic HP turbine, the leakage massflow is estimated to within 10% by assuming the flow exits downstream of midchord, is driven by the stagnation-to-static pressure ratio at 80% span, has a discharge coefficient of 0.8, and exits the gap at a 70° angle (this is the mass-averaged leakage angle).

2.5 Characterization of Tip Clearance Vortex

The previous section addressed estimation of the *tip leakage flow*. A second aspect of tip clearance flow modeling is estimation of *mixing loss once the leakage flow is specified*. The control volume analysis of Denton assumed the flow mixes out immediately to the suction surface velocity [3]. In reality, however, a vortex forms at the suction surface corner and mixing takes place downstream where the conditions are different. The vortex remains near the suction side corner and is strengthened by leakage flow exiting the gap further downstream.

The vortex core was extracted from the CFD results by excluding cells containing negative relative vorticity. [2] Slices are taken normal to the streamwise direction to reveal the evolution of the vortex core, and Figure 2-10 shows the vortex core vorticity, non-dimensionalized by turbine exit velocity and gap height. As tip leakage vortex progresses downstream, it expands and the vorticity falls.

Two important metrics for a vortex core are the swirl number and the streamwise

[2] In a rotating reference frame, all cells have relative background vorticity -2Ω, where Ω is the angular velocity of the rotor. In this work, the background vorticity has been subtracted from the relative vorticity so that positive vorticity refers to vorticity higher than the background level.

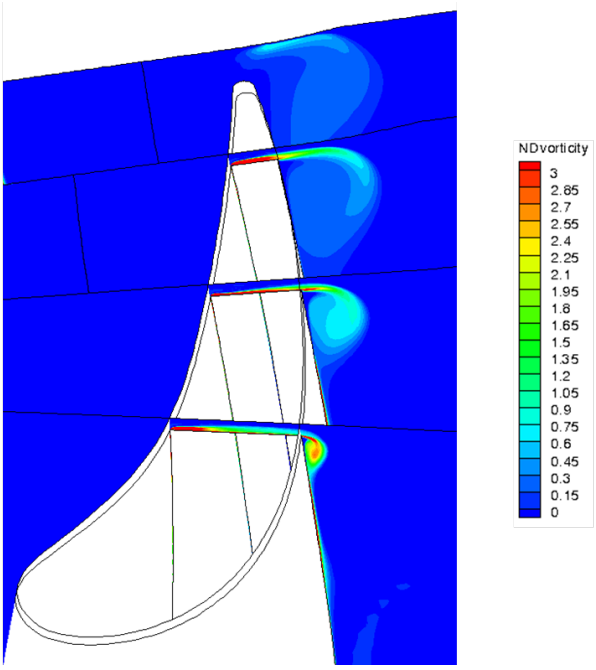

Figure 2-10: Contours of non-dimensionalized vorticity on crossflow planes. Subsonic HP turbine at 2% clearance.

velocity ratio. The vortex core area and circulation are used to define the maximum swirl velocity of a Rankine vortex, v_{max} and the swirl number is defined as the ratio of that maximum swirl velocity to the average core streamwise velocity u as in Equations 2.6 and 2.7.

$$v_{\theta,max} = \frac{\Gamma}{2\pi r_{core}} \tag{2.6}$$

$$S = \frac{v_{max}}{u} \tag{2.7}$$

The streamwise velocity ratio is defined in Equation 2.8 as the core average streamwise velocity divided by the freestream velocity U.

$$VR = \frac{u}{U} \tag{2.8}$$

The velocity ratio on the core centerline is also of interest, since that is the location where the velocity is most affected by pressure gradients. The core centerline is defined

as the lowest static pressure point in the vortex core at each streamwise location.

Figure 2-11 shows the swirl number, velocity ratio, and core centerline velocity ratio of the tip clearance vortex, from the point at which it is identifiable at 40% axial chord to a half chord downstream of the trailing edge. The tip clearance vortex has a swirl number above 1, indicating a flow in which the swirl dynamics have an important role. The streamwise velocity ratio drops sharply downstream of 75% axial chord, and then rises toward the freestream value as the vortex mixes. The centerline velocity ratio changes more than the average velocity ratio and becomes negative at the trailing edge, indicating flow reversal in the vortex core.

Comparing Figures 2-11 to 2-6 and 2-4, two things are observed. First, the region in which the core velocity ratio declines sharply is the region over which the freestream flow is diffusing. Second, much of the tip clearance loss occurs in this region. It has been well documented that under adverse pressure gradients, vortex cores can increase dramatically in area, a phenomena known as vortex breakdown. Vortex breakdown has been observed in turbine tip clearance vortices by Sjolander [21]. However, the author has not seen evidence that tip vortex breakdown is a source of loss in turbines.

2.6 Conclusions

Computations of the flow in a subsonic high pressure turbine showed that 85% of the leakage flow exits downstream of 50% axial chord, where the gap exit pressure is close to the freestream pressure. The gap has a discharge coefficient near 0.8. The massflow through the gap can be well predicted by estimating a discharge coefficient and a leakage flow angle using the control volume calculation of Heyes and Hodson [7]. Mixing losses are found to be the dominant source of tip clearance loss and much of that loss takes place in the region where the tip clearance vortex breaks down (between the $x/c = 0.9$ and 1.2).

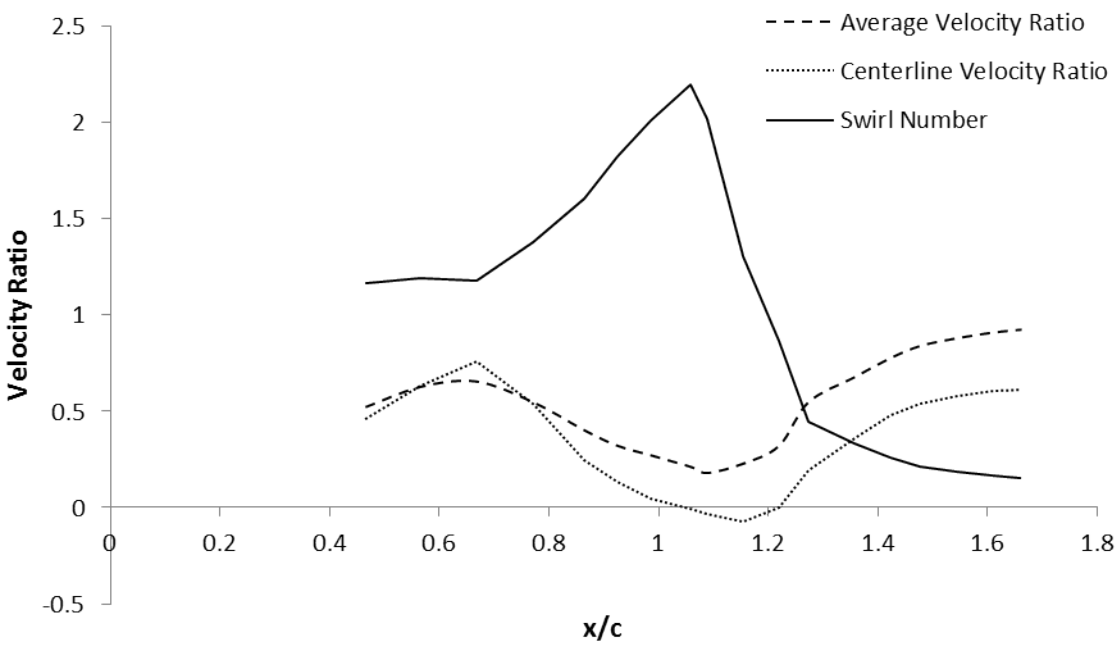

Figure 2-11: Tip clearance vortex core parameters as a function of axial chord: Average velocity ratio, centerline velocity Ratio, and swirl number. Subsonic HP turbine at 2% clearance.

Chapter 3

Estimation of Tip Clearance Mixing Losses with Control Volume Analysis

3.1 Introduction

In this chapter, we discuss the application of a control volume model to tip clearance loss estimation. The model is assessed against tip clearance flows in rectangular ducts and turbine geometries. When mixing takes place at constant area (roughly constant pressure for typical tip clearance massflow ratio), the control volume model gives an accurate estimate of loss. However, when mixing occurs in a pressure gradient, two phenomena can cause the control volume model to be less appropriate, the decrease in vortex mixing loss due to a pressure rise, and vortex breakdown. These effects will be made quantitative below.

3.2 Description of Control Volume Model

Denton provided a useful approximate description of tip clearance loss by modeling the situation as a compressible channel flow with mass injection [3]. The methodology for this approach is based on differential control volumes, as described by Shapiro [17],

i.e. the control volume analysis abstracts the turbine geometry to a compressible one-dimensional internal flow. The mainstream flow near the suction surface is given as a function of streamwise position and the leakage flow is modeled as an injection into the mainstream, with specified density, velocity, temperature, and angle to the freestream. The control volume is bounded by the duct walls and crossflow planes upstream and downstream of the injection location. Figure 3-1 shows a sketch of the control volume.

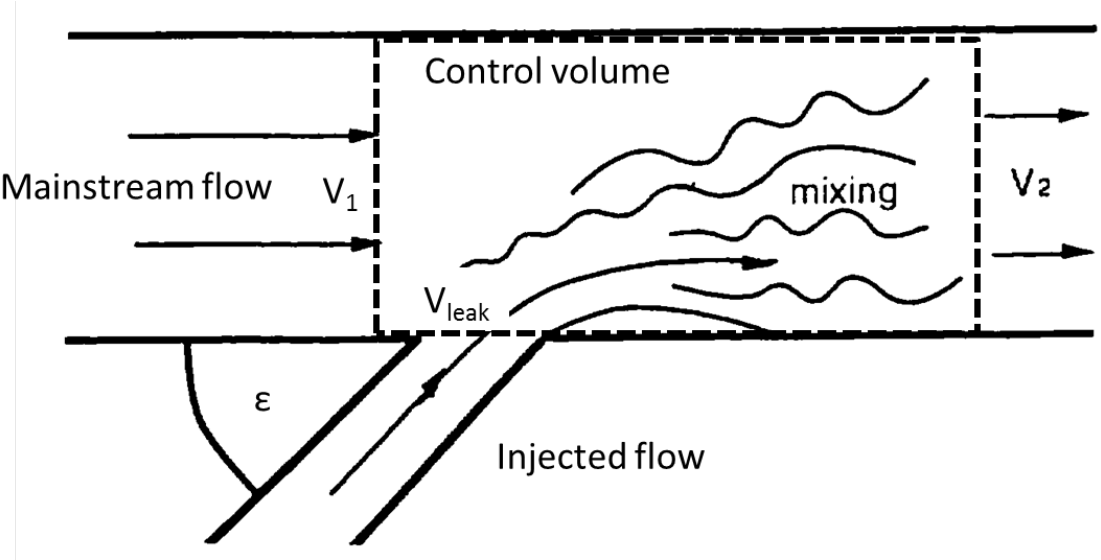

Figure 3-1: Control Volume Model for Mixing Losses [3]

The equations that define the exit state are conservation of mass, momentum, and energy. An expression for the entropy generated within the control volume due to irreversible processes is given by Equation 3.2 [4].

$$T\Delta s_{gen} = \frac{m_{leak}}{m_1}\left(\frac{1}{2}\left[V_{y,leak}^2 + (V_1 - V_{x,leak})^2\right] + c_p T\int_T^{T_{inj}} \frac{1}{T} - \frac{1}{\tau}d\tau\right) \tag{3.1}$$

$$\text{or } T\Delta s_{gen} = \frac{m_{leak}}{m_1}\left(\frac{1}{2}\left[V_{leak}^2 + V_1^2 - 2V_1 V_{leak} cos(\epsilon)\right] + c_p T\int_T^{T_{inj}} \frac{1}{T} - \frac{1}{\tau}d\tau\right) \tag{3.2}$$

Equation 3.2 gives the entropy rise as the product of the massflow ratio and three terms. The terms in the square brackets represent dissipation of kinetic energy. The first term represents dissipation of the kinetic energy associated with the crossflow

velocity, and the second represents the dissipation associated with equilibrating the leakage and mainstream velocities. The integral term represents irreversibility resulting from the static temperature difference between the two streams. This term is small (less than 5% of the total loss) compared to the other two terms because $T \approx T_{inj}$. From Equation 3.2 the estimated mixing loss is proportional to the leakage massflow ratio, rises with the square of the difference between mainstream and injected velocities, and decreases as the leakage flow angle ϵ decreases.

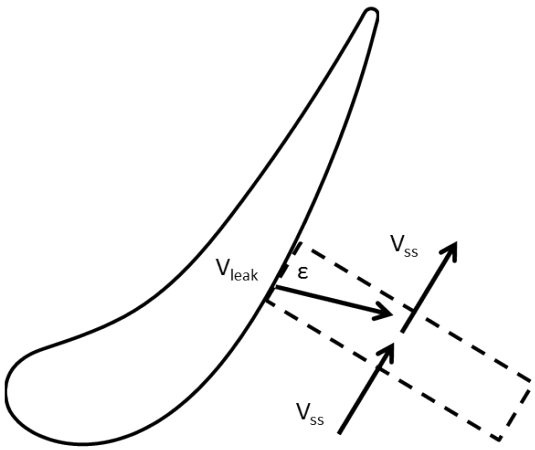

Figure 3-2: Control volume model applied to turbine tip clearance flow for mass flow ratio $\leq\leq 1$

The description of tip clearance loss, expressed in Equation 3.3 and shown in Figure 3-2, views the suction surface as a series of differential control volumes. The differential unit of leakage flow exiting the gap with velocity $\vec{V}_{leak}$ at each axial location is mixed out to suction surface velocity V_{SS} at constant pressure. The mixing of the leakage flow can thus generate different amounts of entropy depending on the local freestream conditions. The total estimated loss is an integral over the suction side gap.

$$T\Delta s_{gen} = \int_{gap} \frac{\rho V_{leak} sin(\epsilon)}{m_m} \left(\frac{1}{2} \left[V_{leak}^2 + V_{SS}^2 - 2V_{SS}V_{leak}cos(\epsilon) \right] + c_p T \int_T^{T_{inj}} \frac{1}{T} - \frac{1}{\tau} d\tau \right) dA \tag{3.3}$$

3.3 Assessment of Control Volume Model in Rectangular Ducts

We can assess the control volume description of mixing losses using the state of injected flow and the isentropic mainstream velocity extracted from the calculations. Before doing this for the turbine environment, however, we examine its validity for a simpler flow, injection into rectangular nozzles and diffusers with exit-to-inlet area ratios ranging from 0.5 to 1.7.

Figure 3-3 shows a nozzle geometry with exit-to-inlet area ratio 0.8. Color contours of the static pressure coefficient show that the pressure decreases as the nozzle area decreases. The duct height h is uniform everywhere, and is used to non-dimensionalize the lengths. The duct width w is equal to the height at the inlet ($x/h = 0$) and decreases to the exit width between $x/h = 1$ and 2. Flow is injected into the duct via the indicated rectangular slot, whose dimensions are $0.02h$ by h. Two injection slot geometries are considered: one introducing the injected flow normal to the mainstream, and one injecting flow at a 45° angle to the mainstream. The ratio of the duct inlet stagnation pressure to the exit static pressure is varied between 1.05 and 1.6, with the stagnation pressure at the injection inlet equal to that at the inlet. The mixing losses are defined by specifying no-slip walls (so that there are not viscous losses at the walls) and extracting the difference in loss between the case with flow injection and the case without an injection slot. The exit of the computational domain is four duct heights downstream of the slot.

Figure 3-4 presents streamlines of the leakage flow along with contours of entropy for an area ratio of 0.8. The streamlines imply a vortical structure that persists to the exit, indicating the flow at the exit plane is not completely mixed out. The control

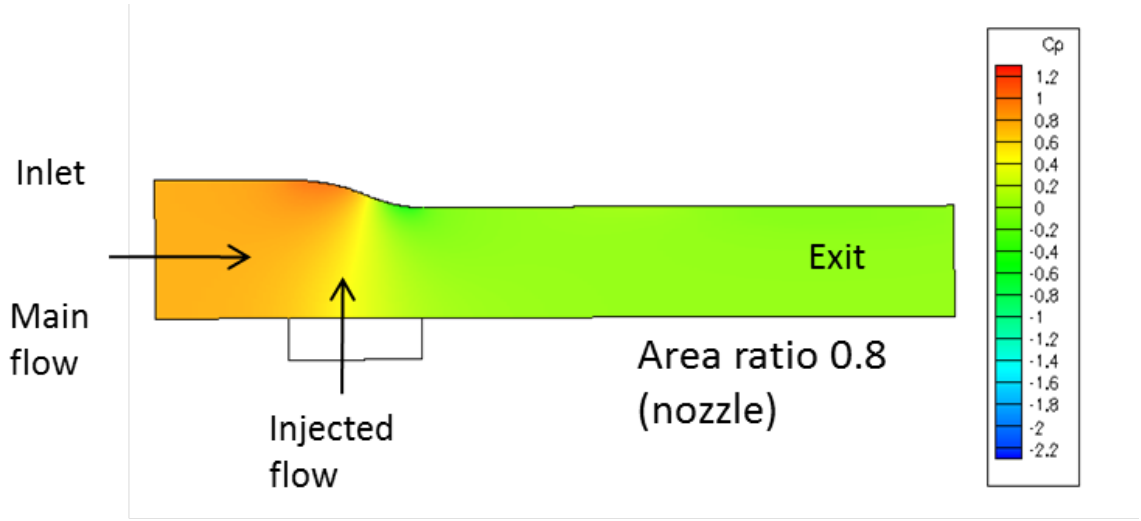

Figure 3-3: Geometry of rectangular nozzle with 90° flow injection, area ratio 0.8. Color contours of static pressure coefficient.

volume model, which produces a mixed-out analysis, is assessed against the difference between the mixed-out entropy flux at the domain exit and the inlet entropy flux. The mixed-out exit state is arrived at by placing a constant area control volume at the exit plane and conserving mass, momentum, and energy.

To obtain the control volume estimate for the losses, equation 3.3 was applied over the injection slot exit, mixing out the leakage flow to the freestream velocity at midspan. All losses for the duct cases are non-dimensionalized by the injected massflow and the square of the exit velocity to give the loss per unit injected flow: $\frac{m_{main} T \Delta s}{m_{leak} V_{exit}^2}$.

Figure 3-5 shows the mixed out loss (calculated mixing loss in the duct plus mixing losses downstream of the duct exit) per unit injected flow, as a function of pressure ratio for area ratio 0.8 with both 90° and 45° injection, along with the losses estimated from the control volume analysis. The control volume approach underestimates the loss by 20% but it gives the trends in change in loss with pressure ratio for both injection angles, showing that the scaling with velocity, leakage massflow, and injection angle are captured.

Figure 3-6 shows the mixed out loss as a function of the duct area ratio for pressure ratio 1.05 (essentially incompressible flow) and 90° injection. For area ratios between

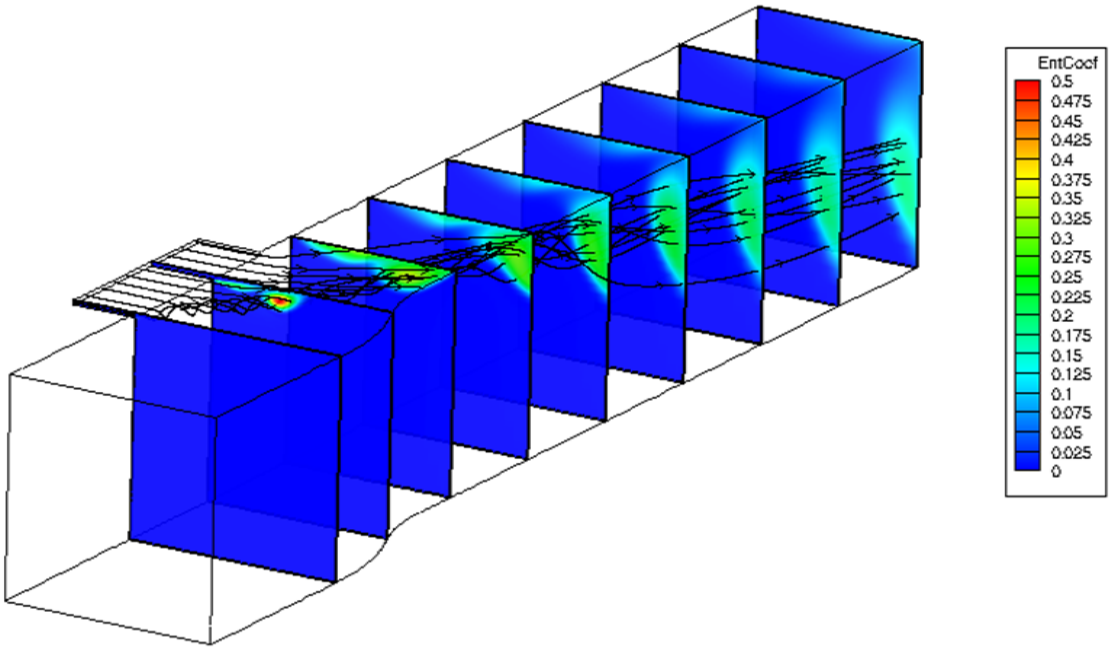

Figure 3-4: Contours of entropy, streamlines of the leakage flow for 90° flow injection into rectangular duct of area ratio 0.8.

0.5 and 1.5, the control volume model agrees with the computed loss to within 30%. At an area ratio of 1 (constant area duct), the control volume description and the calculation agree to within 2%; this is not surprising, since the control volume analysis is based on constant area mixing. For $AR \leq 1$, the rate of change of estimated losses with area radio is less than the rate of change of the computed losses, so that the mixing losses are thus underpredicted by the control volumes for $AR \leq 1$ and overpredicted for $1 \leq AR \leq 1.5$. However, at $AR = 1.3$, the computed loss slope becomes larger than the modeled loss slope, and for $AR \geq 1.5$ the control volume model underpredicts the loss.

The control volume description assumes that the injected flow mixes out immediately as it enters the mainstream. In reality, however, the injected flow forms a vortex, as shown in figure 3-4, which passes through a pressure change as it mixes with the mainstream. Figure 3-7 shows the vortex core centerline streamwise velocity ratio and swirl number at $x/h = 2$ as a function of duct area ratio. As the area ratio rises from $AR = 1$, the velocity ratio decreases. For $AR \geq 1$, the vortex area

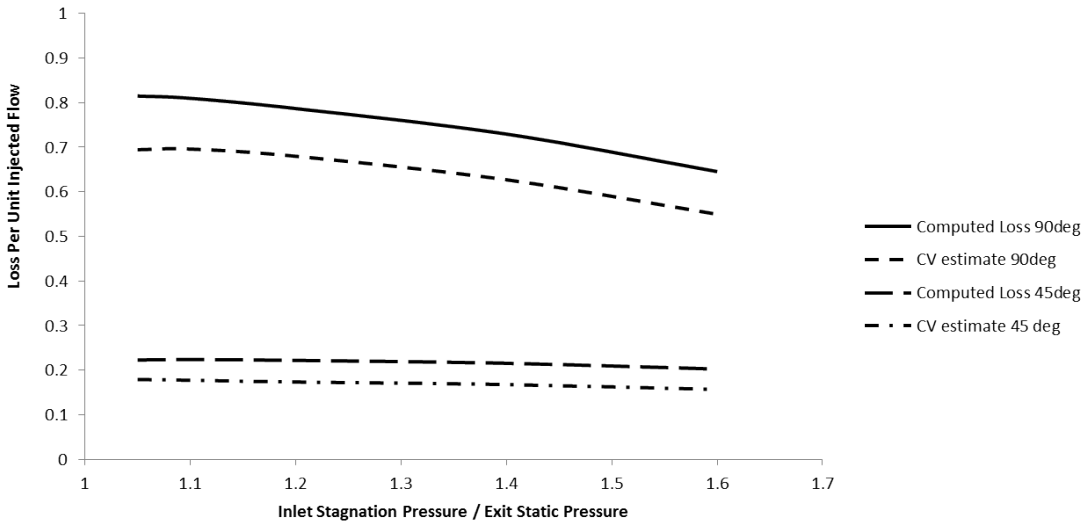

Figure 3-5: Mixing loss per unit massflow due to flow injection as function of pressure ratio. Comparison between calculation and control volume analysis at area ratio 0.8 for both 45° and 90° injection

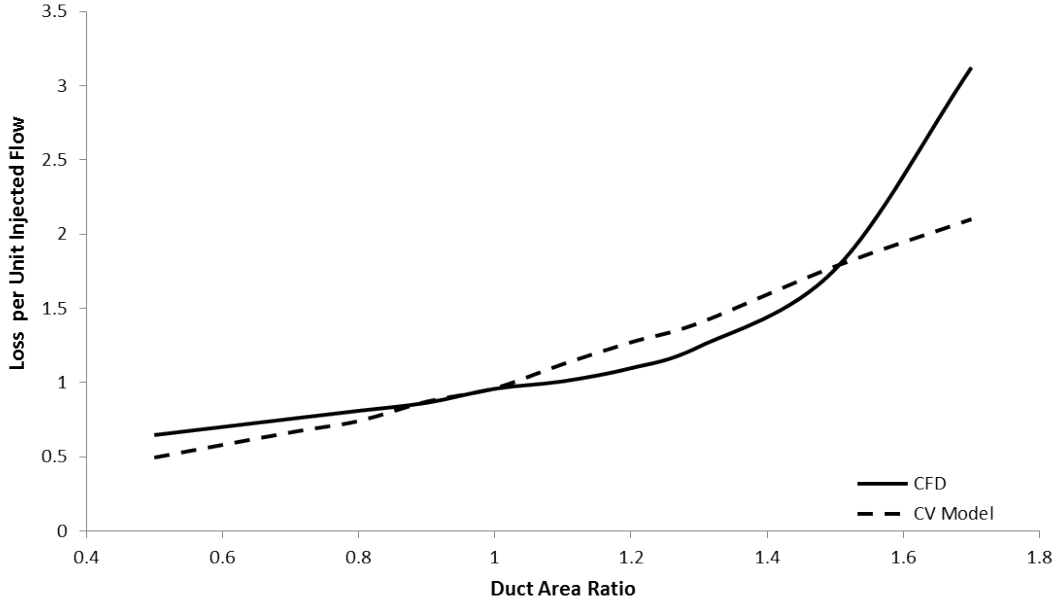

Figure 3-6: Mixing loss per unit massflow due to flow injection as function of area ratio. Comparison between calculation and control volume analysis for PR = 1.05, 90^{deg} injection

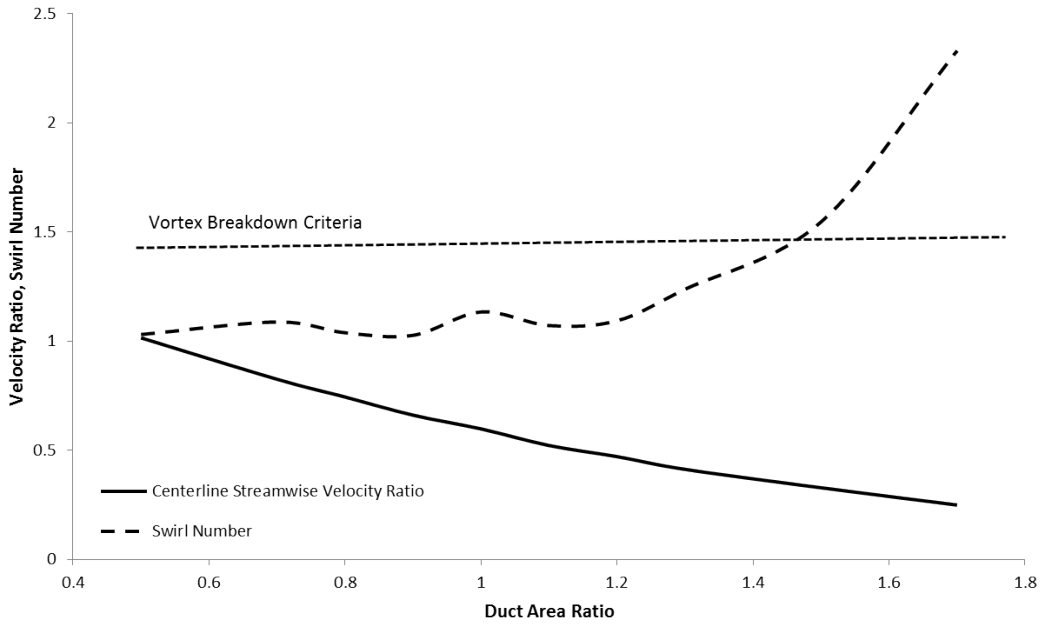

Figure 3-7: Average velocity ratio, swirl number for vortices at $x/h = 2$ in a rectangular duct, PR=1.05, AR=0.5-1.7

is increased and the swirl velocity decreased (by Kelvin's theorem), decreasing the mixed out losses associated with swirl. Conversely, for $AR \leq 1$, the swirl velocity and the losses decrease due to vortex stretching. For this reason, the control volume approach overpredicts the loss for $1 \leq AR \leq 1.5$ and underpredicts for $AR \leq 1$.

We view the loss behavior for $AR \geq 1.3$ as associated with vortex breakdown. As described in Chapter 4, if a vortex core reaches a swirl number of roughly $\sqrt{2}$, the vortex can experience a phenomena known as vortex breakdown, in which the flow in the vortex core stagnates. Figure 3-7 shows that the swirl number for $AR \geq 1.5$ is greater than $\sqrt{2}$, so vortex breakdown can occur. It is hypothesized that as the area ratio increases and the vortex is exposed to a larger pressure rise, the losses in vortex breakdown increase, resulting in the increase in the rate of change of loss with area ratio above $AR = 1.3$.

The two effects described above (vortex line contraction and vortex breakdown) account for the difference between computed losses and losses estimated by the control volume analysis. We conclude that the applicability of the control volume approximation depends on the pressure change over which vortex mixing occurs. If the vortex

does not break down, deceleration of the vortex core will result in lower swirl velocities and losses lower than that predicted using control volume analysis. However, there is a critical pressure rise above which vortex breakdown will occur, generating increased losses so that the control volume approach will underpredict the mixing loss.

3.4 Assessment of Control Volume Model of Mixing in Turbine Environments

We now evaluate the utility of the control volume description in realistic turbine geometries in comparison to 3-D computations for four turbine designs: a low pressure turbine (LPT), a subsonic high pressure turbine (HPT), a transonic high pressure turbine, and a supersonic high work turbine. These were chosen to span a range of design parameters, as shown in table 3.1. The flow coefficient ϕ is the the average axial velocity divided by wheelspeed at midspan. The work coefficient ψ is the ratio of work extracted by the turbine to the square of the midspan wheelspeed. Finally, the ratio of inlet stagnation pressure to exit static pressure determines the Mach number and the influence of compressibility. Cases were run for tip clearances ranging from 0 to 2%.

The tip leakage loss was defined as the difference between the loss with clearance and the loss at zero clearance. Figure 3-8 shows the tip leakage loss coefficient plotted against clearance. The leakage loss varies between designs, with the LP turbine having the lowest leakage loss. The supersonic high work turbine has a low loss slope near zero clearance but has similar loss slope to the transonic and subsonic HP turbines from 0.75 to 1.5% clearance. A nominal industry correlation of 2% loss in turbine efficiency per 1% clearance is shown for comparison. Use of this correlation would result, at 2% clearance, in a 20% underestimate of the tip clearance loss for the subsonic and transonic HPTs, and a 20% overestimate for the LPT at 2% clearance.

To assess the control volume description, the leakage loss due to mixing was cal-

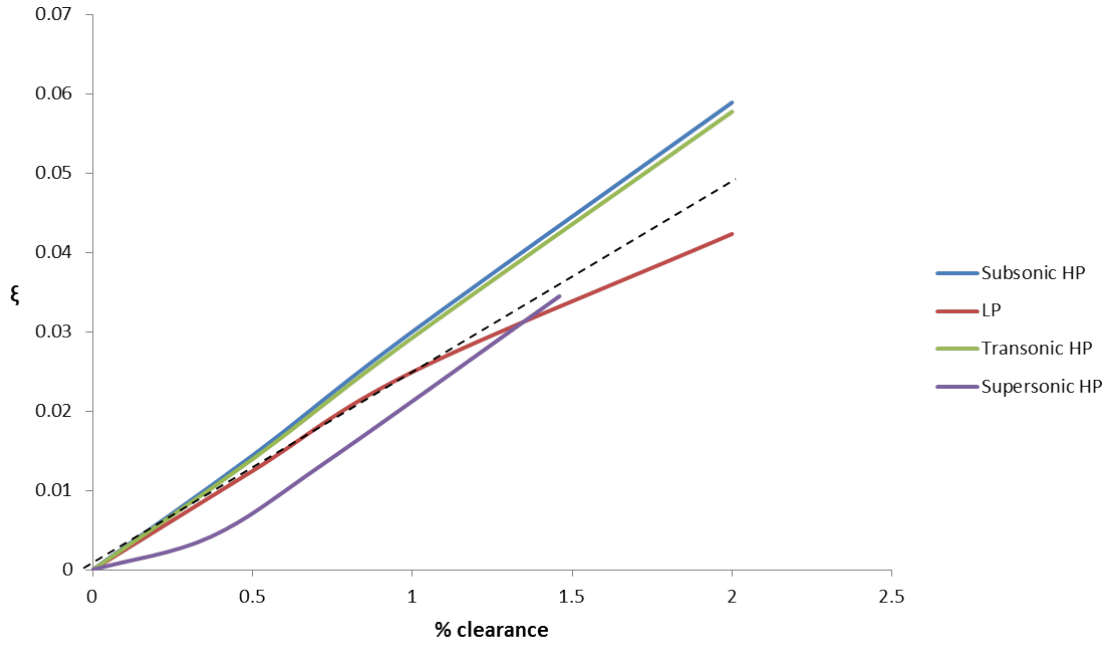

Figure 3-8: Leakage loss coefficient for 0-2% clearance-to-span ratio for four turbine designs

culated. Chapter 2 showed that mixing losses plus losses within the gap account for the leakage loss. The loss within the gap was subtracted from the overall leakage loss to calculate the mixing loss. For leakage flow small compared to mainstream flow, the control volume description shows that the leakage loss is proportional to the leakage massflow. It is thus useful to divide the mixing loss coefficient $\xi = \frac{T_{exit}\Delta s}{\Delta h_t}$ by the leakage massflow ratio $\frac{m_{leak}}{m_m}$ to obtain the mixing loss per unit massflow $\hat{\xi}$, as in equation 3.4.

$$\hat{\xi} = \xi \frac{m_m}{m_{leak}} = \frac{m_m T_{exit} \Delta s}{m_{leak} c_p \left(T_{t,inlet} - T_{t,exit}\right)} \tag{3.4}$$

As with the rectangular ducts, the leakage flow density, temperature, velocity, and angle relative to the freestream were extracted and mixed out to the isentropic suction surface velocity based on 80% span. Table 3.2 shows that for the subsonic HP turbine, the estimated mixing loss is insensitive to the spanwise location used to calculate the suction surface velocity, varying only 5% for spanwise location between 50 and 90% span.

Figure 3-9 shows the mixing loss normalized by leakage flow for each turbine design over a range of clearances. The solid lines show the computed results, while the dotted lines show the control volume estimate. The control volume description gives losses within 25% of the loss from the 3D simulations for three of the four turbines. The calculated loss for the high work turbine at 0.37% clearance is 40% lower than the control volume estimate, but the agreement is within 10% at higher clearances.

Figure 3-10 shows the suction surface isentropic Mach number at 80% span, while figure 3-11 shows the swirl numbers of the tip vortices as a function of axial position at 2% clearance for the four rotors. For the low pressure turbine, the vortex forms further upstream (at 25% axial chord), the vortex is accelerated over the majority of its existence, and the estimated loss is lower than the loss from the 3D computations. The three high pressure turbines have deceleration from 75% axial chord to the trailing edge and the maximum swirl number exceeds $\sqrt{2}$, indicating vortex breakdown. We cannot say whether the control volume analysis should overpredict or underpredict the leakage loss because there are two effects at work: deceleration decreases the mixing losses by decreasing the swirl velocity while vortex breakdown generates additional loss. However, we can say that a design change which causes additional deceleration of the vortex core will increase the losses due to vortex breakdown. This will be demonstrated in Chapter 5.

3.5 Conclusions

The computational studies presented in this chapter showed that vortex mixing losses are affected by changes in pressure. A pressure rise reduces the vortex mixing loss by decreasing the swirl velocity. However, a sufficiently large pressure rise leads to vortex breakdown and increased losses. These two effects are the source of the disagreement between control volume analysis and computed losses. More specific conclusions are listed below.

- A control volume description estimates the mixing loss accurately for a constant area duct.

Table 3.1: Design parameters of turbines used in the assessment of the control volume model for mixing losses

Design	ϕ	ψ	$\frac{P_{t,inlet}}{P_{exit}}$
Subsonic LPT	1.1	2.4	1.6
Subsonic HPT	0.54	2.1	2.2
Transonic HPT	0.58	2.4	2.7
Supersonic HPT	0.41	1.6	4.5

Table 3.2: Difference in loss calculated at X% span and 80% span using control volume model for subsonic HPT

Spanwise Location z/h	Difference in loss / Loss calculated at 80% span
0.5	-.047
0.6	+.009
0.7	-0.004
0.8	0
0.9	+0.01

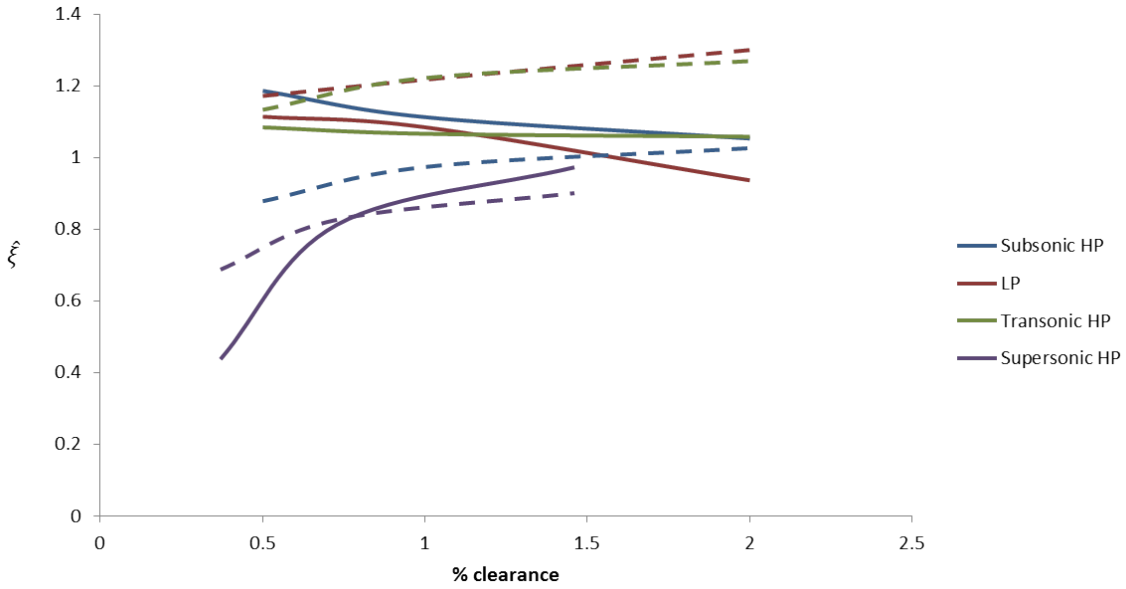

Figure 3-9: Normalized mixing loss per unit leakage flow as a function of clearance-to-span ratio for four turbine designs. Computed losses (solid lines) and control volume estimate (dotted)

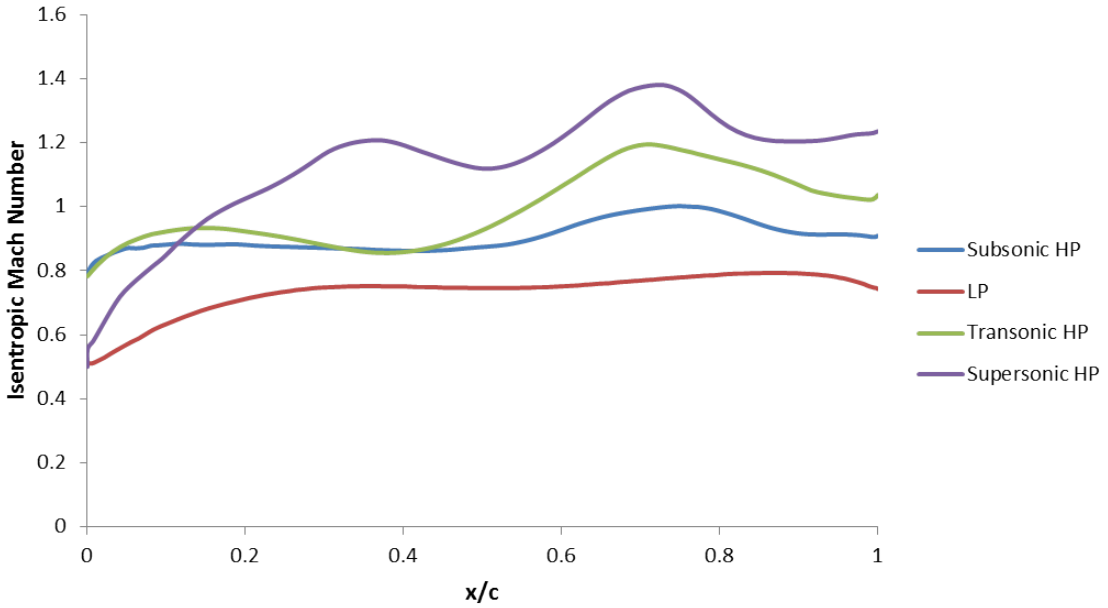

Figure 3-10: Suction surface isentropic Mach number at 80% Span as a function of axial location for four turbine designs

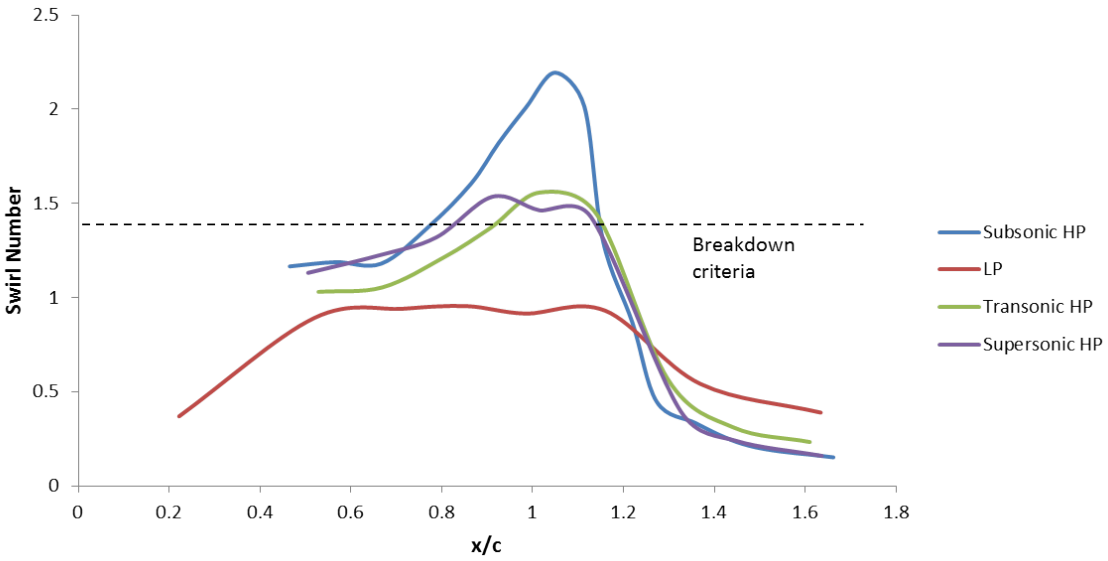

Figure 3-11: Tip vortex swirl number as a function of axial location for four turbine designs

- As a vortex passes through a pressure rise, the swirl velocity and hence the mixing losses decrease, leading to a decrease in the mixing loss. This is the reason the control volume analysis underpredicts the rectangular duct losses for $1 \leq AR \leq 1.5$.

- Vortex breakdown is associated with the increase in mixing losses seen for the rectangular ducts of area ratio $1.3 \leq AR \leq 1.7$.

- A control volume analysis is capable of predicting tip clearance loss to within 40% across a wide range of turbine designs, if the leakage flow is specified. An improvement to the control volume analysis would need to consider the effect of pressure changes on vortex mixing losses.

Chapter 4

Effect of Pressure Changes on Vortex Mixing Losses

4.1 Introduction

Two important concepts discussed in previous chapters are that the majority of turbine tip clearance loss is generated in the mixing of the tip vortex with the mainstream flow as it convects through a pressure rise, and that mixing losses in vortices are altered by changes in pressure level so that constant pressure mixing does not predict the loss. To minimize tip clearance losses, it is useful to examine the effect of a pressure change on mixed-out loss in a vortical flow, because it differs from the effect of a pressure changes on wake mixing losses.

The response of a streamwise velocity defect, or wake, to a pressure change is well understood. An adverse pressure gradient increases the mixing loss for a wake by increasing the axial velocity non-uniformity between wake a freestream; the losses are proportional to the velocity defect squared.

For a vortex, a given freestream pressure rise has a larger effect on the core centerline axial velocity non-uniformity than on a wake [5]. In this context, core stagnation occurs for a lower non-dimensional pressure rise for vortices than for wakes. However, the increase in core area associated with the decrease in core velocity decreases the swirl velocity and hence the mixed-out loss. This chapter illustrates differences

between the response of a wake and a vortex to a pressure change and gives criteria for vortex breakdown, defined here as a stagnation of the flow on the core centerline. Axisymmetric calculations on vortices in ducts with area expansion confirm the effects of vortex line contraction and vortex breakdown on loss.

The ideas discussed also provide a distinction between compressor and turbine tip vortices. The former can be characterized as weakly swirling flows ($S \leq 0.5$) and thus usefully viewed as wakes in pressure gradients. [9], [10]. Turbine vortices, however are strongly swirling ($S \geq 1$) and more prone to vortex breakdown. Because of this difference, a given pressure rise typically increases the mixed out loss for a compressor vortex but can often decrease the loss for a turbine vortex.

4.2 Mixing Losses for a Wake in a Pressure Gradient

The differential form of the one-dimensional momentum equation shows how an adverse pressure gradient increases a wake velocity non-uniformity. The wake velocity is denoted as u while the freestream velocity is denoted U. The pressure p is taken as only a function of x and the momentum equation reduces to conservation of stagnation pressure in the wake and the freestream, Equations 4.1 and 4.2.

$$\frac{du}{u} = -\frac{dp}{\rho u^2} \tag{4.1}$$

$$\frac{dU}{U} = -\frac{dp}{\rho U^2} \tag{4.2}$$

Equations 4.1 and 4.2 show that the fractional decrease in velocity due to the adverse pressure gradient is inversely proportional to the dynamic pressure. The freestream thus decelerates less than the wake does, and the mixed out loss grows as the pressure rises because (as we saw in Chapter 3) mixing losses scale with $(U-u)^2$.

Figures 4-1 shows the velocity non-uniformity and mixed-out loss, normalized by

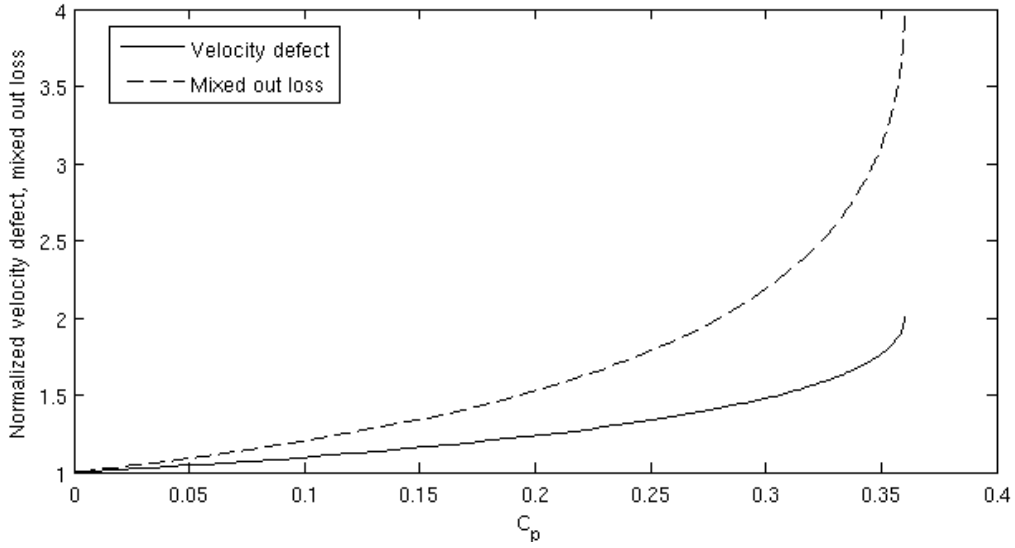

Figure 4-1: Effect of pressure rise on wake: velocity defect (normalized by freestream velocity) and mixed-out loss (normalized by inlet mixed-out loss) as a function of farfield pressure rise $C_p = \frac{\Delta p}{0.5\rho U^2}$.

their initial value, for a wake with velocity ratio $\frac{u(x=0)}{U(x=0)} = 0.6$ as a function of C_p. In equation 4.3, C_p is defined as the pressure rise normalized by inlet freestream dynamic head. Both the streamwise velocity non-uniformity and the pressure rise in Figure 4-1 are representative of turbine tip clearance vortices, but without swirl velocity. As C_p rises to 0.36, the flow in the wake decelerates and stagnates, so the velocity deficit and the mixed out loss increase monotonically.

$$C_p(x) = \frac{P(x) - P(0)}{\frac{1}{2}\rho U(x=0)^2} \tag{4.3}$$

4.3 Control Volume Model for Rankine Vortex Response to Pressure Gradient

We illustrate the behavior of a vortex in a pressure gradient using an incompressible unconfined Rankine vortex description [2]. The Rankine vortex consists of a core undergoing solid body rotation surrounded by a free vortex freestream as in figure

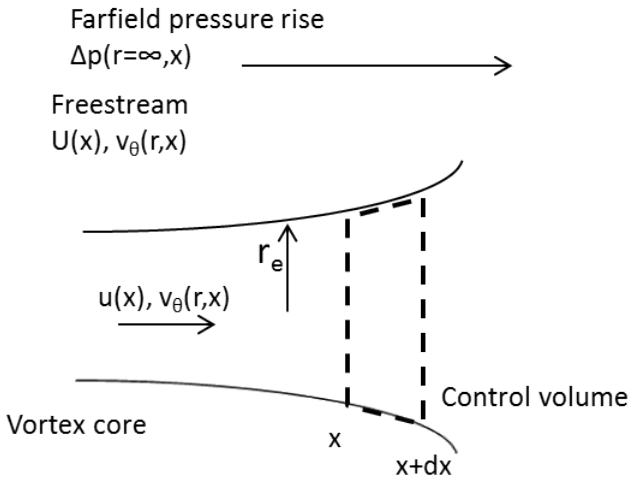

Figure 4-2: Illustration of Rankine vortex model.

4-2.

A control volume for the vortex core is bounded by the core edge streamtube and axial planes. The problem as can be cast in terms of three non-dimensional parameters, the velocity ratio, VR, the swirl number, S, and the farfield pressure coefficient, C_p, defined in equations 4.4, 4.5, and 4.6. Here, u is the vortex axial velocity, U is the freestream axial velocity, v_θ is the swirl velocity, r_e is the radius of the vortex core edge, and the farfield pressure p_∞ is the static pressure at $r = \infty$.

$$VR = \frac{u}{U} \tag{4.4}$$

$$S = \frac{v_\theta \left(r = r_e\right)}{u} \tag{4.5}$$

$$C_p = \frac{p_\infty(x) - p_\infty(0)}{\frac{1}{2}\rho U^2} \tag{4.6}$$

To calculate a mixed-out loss, a mass ratio between the vortex and the freestream must also be specified: $MR = \frac{m_{core}}{m_{freestream}}$. This is necessary because the mixing loss due to dissipation of swirl kinetic energy is infinite if the radius is allowed to extend

out to infinity, as in Equation 4.7.

$$T\Delta s \propto \lim_{R\to+\infty}\int_0^R v^2 r dr \propto \lim_{R\to+\infty}\int_0^R \frac{1}{r}dr = \infty \tag{4.7}$$

At the inlet to the control volume, the vortex initial radius $r_e(x=0)$, circulation Γ, and streamwise velocity ratio $\frac{u}{U}$ are known. The circulation Γ, defined in equation 4.8, is the line integral of the velocity component about a contour of radius r_e. Equations 4.9 and 4.10 describe the axial and swirl velocities in the domain. The farfield pressure at $r=\infty$, $p_\infty(x)$, specified as a function of axial position, determines the evolution of the core flow. The simple radial equilibrium equation, given in equation 4.11 links the farfield pressure to the pressure in the vortex core, resulting in equation 4.12, which gives the radial distribution of pressure as a function of the circulation and the farfield pressure.

$$\Gamma = \oint \vec{V}\cdot\hat{ds} = 2\pi r_e v_\theta\left(r=r_e\right) \tag{4.8}$$

$$v_x\left(x,r\right) = \begin{cases} u(x) & : r \le r_e(x) \\ U(x) & : r > r_e(x) \end{cases} \tag{4.9}$$

$$v_\theta\left(x,r\right) = \begin{cases} \frac{\Gamma r}{2\pi r_e(x)^2} & : r \le r_e(x) \\ \frac{\Gamma}{2\pi r} & : r > r_e(x) \end{cases} \tag{4.10}$$

$$\frac{dp}{dr} = \frac{\rho v_\theta^2}{r} \tag{4.11}$$

$$p\left(x,r\right) = \begin{cases} p_\infty - \rho\left(\frac{\Gamma^2}{8\pi^2 r_e^2}\right)\left[2-\left(\frac{r}{r_e}\right)^2\right] & : r \le r_e \\ p_\infty - \rho\left(\frac{\Gamma^2}{8\pi^2 r_e^2}\right)\left(\frac{r_e}{r}\right)^2 & : r > r_e \end{cases} \tag{4.12}$$

Conservation of mass, momentum, and angular momentum are applied over the control volume shown in Figure 4-2 to give the exit streamwise velocity, swirl velocity and edge radius. Equations 4.13, 4.14, and 4.15 are the differential forms of the mass, momentum, and angular momentum conservation equations. The angular momentum equation is here equivalent to Kelvin's theorem.

$$\rho\left[\pi r_e^2\frac{du}{dx}+2\pi r_e\frac{dr_e}{dx}\right]=0 \tag{4.13}$$

$$\frac{d}{dx}\left[\rho u^2\pi r_e^2+2\pi\int_0^{r_e}Prdr\right]=0 \tag{4.14}$$

$$\frac{d\Gamma}{dx}=0 \tag{4.15}$$

4.4 Mixing Losses for a Vortex in a Pressure Gradient

A vortex in a pressure gradient behaves differently from a wake in a pressure gradient because the pressure in the core is lower than that in the freestream, as in Equation 4.16, and for a given increase in freestream pressure, the pressure change on the core centerline is larger than that with no swirl because r_e increases, and the axial velocity in the vortex core thus decreases more than the axial velocity of a wake with the same initial velocity and farfield pressure rise.

$$p\left(x,0\right)=p_\infty-\rho\left(\frac{\Gamma^2}{4\pi^2r_e^2}\right) \tag{4.16}$$

The other effect of a pressure rise is seen in the swirl velocity, which decreases as the core expands. Figure 4-3 shows the effect of a pressure rise on the axial velocity defect and swirl number for a vortex with initial swirl number 1 and axial velocity ratio 0.6, conditions representative of a turbine tip vortex at the onset of deceleration. As the pressure increases, both velocity defect and swirl number rise, indicating that the decrease in core axial velocity is larger than that of the freestream and swirl velocities. The figure continues until a maximum value of ΔC_p, which is associated with vortex breakdown, as discussed in the next section.

We now examine the change in mixing loss associated with the adverse pressure gradient. The final mixing state is taken to be no swirl and uniform velocity (since the

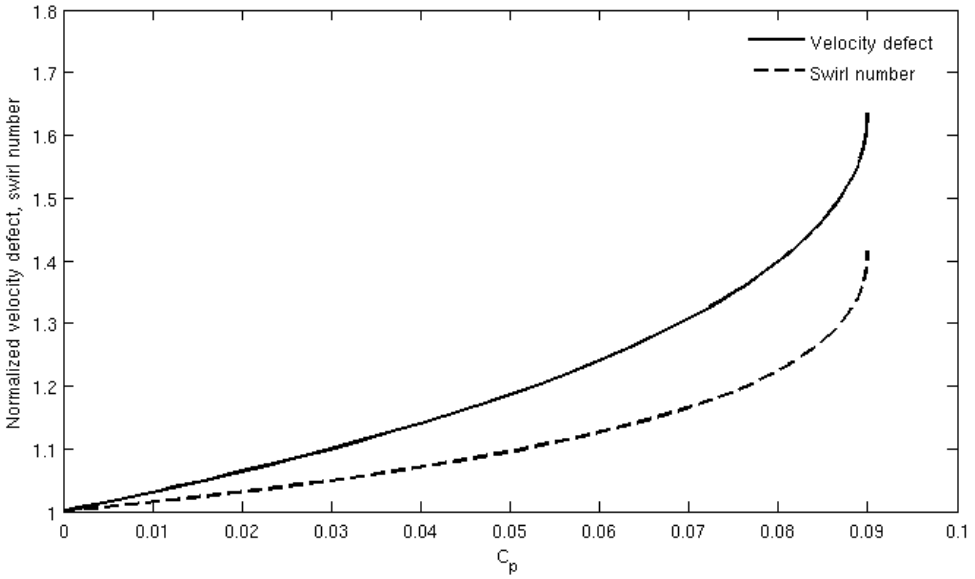

Figure 4-3: Effect of pressure rise on vortex: Normalized velocity defect ($\frac{U-u}{U_{inlet}}$) and swirl number as a function of farfield pressure change $C_p = \frac{\Delta p}{0.5\rho U^2}$

energy associated with swirl velocity in the tip vortex is not recoverable). The swirl kinetic energy is assumed to be dissipated. The mixing loss associated with the axial velocity difference scales as the square of the axial velocity defect $(U-u)$. Figure 4-4 shows the mixing loss, normalized by the initial value, as a function of C_p, for the vortex of figure 4-3 with a mass ratio of 1%. The losses associated with the mixing of the axial velocity nonuniformity and with the dissipation of swirl velocity are given separately to show the dominant effect is in the swirl velocity (because the freestream is swirling as well), and the loss decreases by 20% for C_p=0.09. Deceleration of a vortex decreases the mixed out loss, in contrast to deceleration of a wake, where the mixed-out loss increases. This is the reason that the control volume model (Chapter 3) underpredicted mixing losses for flow injection into diffusers of area ratio 1-1.3 and it also suggests that that deceleration of the tip vortex in the turbine passage can be beneficial to performance.

We are also interested in the dependence of the sensitivity of mixed-out loss to an incremental pressure rise on vortex state (velocity ratio and swirl number). Figure 4-5 shows a contour plot of the derivative of the normalized mixing loss (defined as

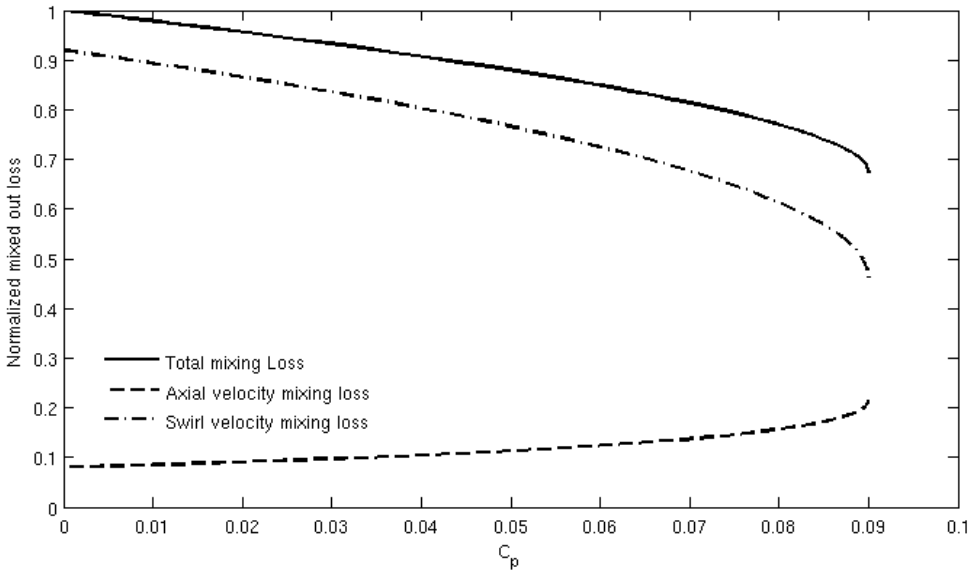

Figure 4-4: Effect of pressure rise on vortex: normalized mixed-out loss (mixed out loss / mixed out loss based on inlet conditions) as a function of farfield pressure change $C_p = \frac{\Delta p}{0.5\rho U^2}$

the mixed-out loss divided by the inlet mixed-out loss) with respect to C_p for vortices of different swirl numbers and axial velocity ratios. The mass ratio used for the computation was 1%, which is close to the ratio between the turbine tip vortex core massflow and the freestream massflow.

One can see the two competing effects of wake behavior and vortex behavior. For a given velocity ratio, the loss derivative decreases as the vortex swirl number increases and the flow becomes more "vortex-like". For a given swirl number, the loss derivative increases as the velocity ratio decreases and the flow becomes more "wake-like". The states of turbine (calculated) and compressor (measured) tip vortices are also plotted in Figure 4-5 [9]. Deceleration of compressor vortex flows results in increases in mixed out losses, while deceleration of turbine vortex flows results in decreases in loss. The magnitude of the change in loss can be an order of magnitude higher for the turbine vortices than for the compressor vortices; swirl velocity in tip vortex flow is more important to leakage loss in turbines than it is in compressors.

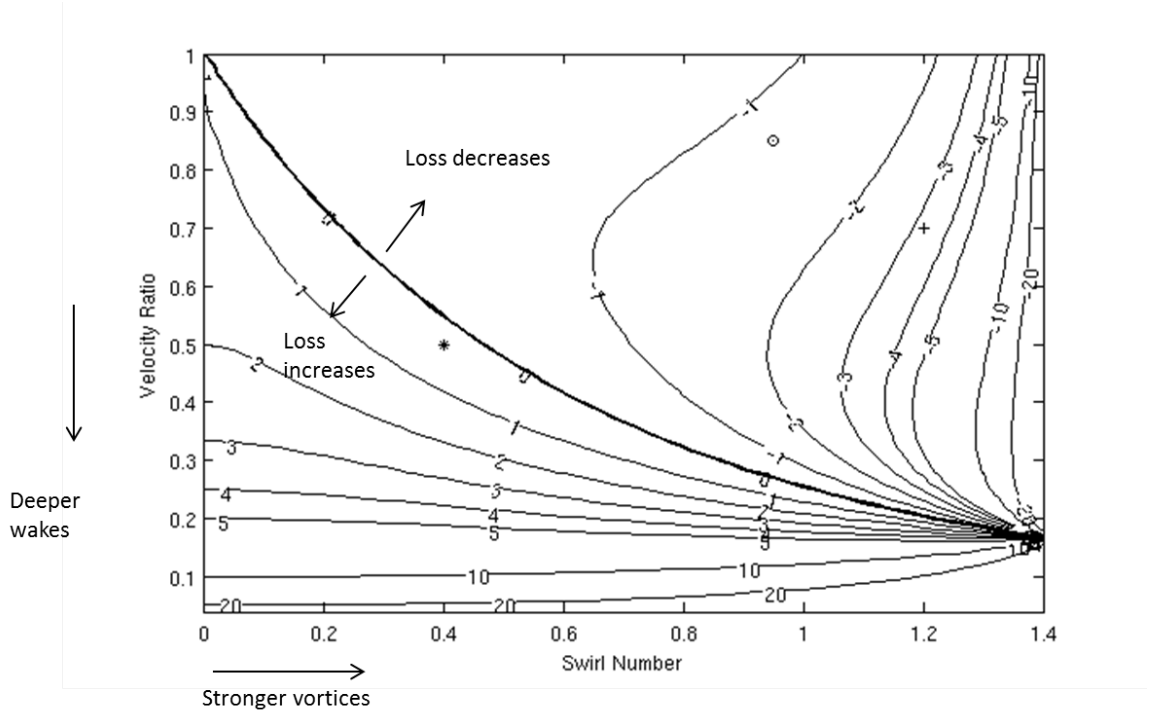

Figure 4-5: Derivative of mixed out loss with respect to $C_p = \frac{\Delta p}{0.5\rho U^2}$ for vortices with specified initial swirl number and velocity ratio. Points plotted represent low pressure turbine ($\circ$, computed), high pressure turbine ($+$, computed), and compressor vortices ($*$, [9]).

4.5 Criteria for Vortex Breakdown

Figure 4-3 shows that there is a maximum pressure rise above which no solutions exist. This represents stagnation in the vortex core and vortex breakdown. Darmofal et al. presented an approximate analysis that indicated that this occurs when the swirl number reaches $\sqrt{2}$ [2]. In Chapter 3 it was shown that vortex swirl numbers in high pressure turbine calculations exceed $\sqrt{2}$. In contrast, measurements of compressor tip vortices at design point showed swirl numbers less than 0.5, indicating that vortex breakdown is much less of a concern in compressors at design point [9].

Figure 4-6 shows the calculated maximum pressure rise for a vortex with a specified initial swirl number, along with results from vortex breakdown experiments [16]. Here the pressure rise is non-dimensionalized by $\frac{1}{2}\rho u^2$ (using the vortex axial velocity). Also shown are swirl numbers and pressure rises associated with the vortex cores observed in the high pressure turbine calculations, based on the state of the vortex at the location at which diffusion begins. Each of the computed vortices experiences a pressure rise large enough to cause vortex breakdown.

The above inviscid analysis admits no solutions for pressure rises larger than the breakdown limit, and so it cannot make a statement about losses beyond this. However, the rectangular duct computations in Chapter 3 show that, in the regime in which vortex breakdown occurs, loss increases rapidly as the duct area ratio, and the vortex swirl number, increases. This implies that vortex breakdown is a loss mechanism whose magnitude depends on the pressure rise experienced by the vortex.

4.6 Computational Study of Vortex in Pressure Rise

To quantify the effect of vortex line contraction and breakdown on the mixed-out loss in turbulent viscous vortices, axisymmetric calculations were carried out to for in circular ducts with area expansions. Figure 4-7 shows the geometry of a duct with area ratio 1.21. The initial core radius r_e is 0.1 of the duct radius. The velocities

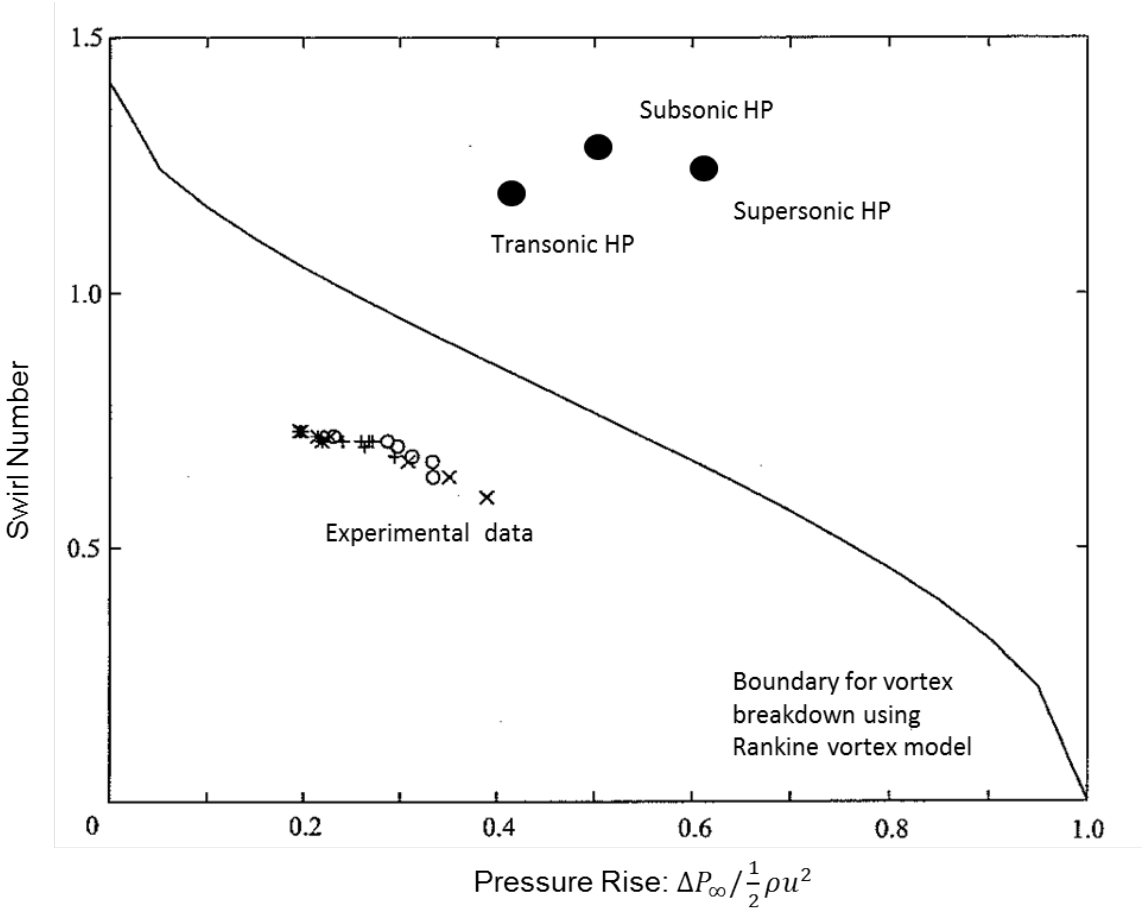

Figure 4-6: Maximum pressure rise resulting in vortex breakdown for specified swirl number, calculated from Rankine vortex model [2]. Also plotted are experimental data for vortex breakdown [16], and computed turbine vortex parameters.

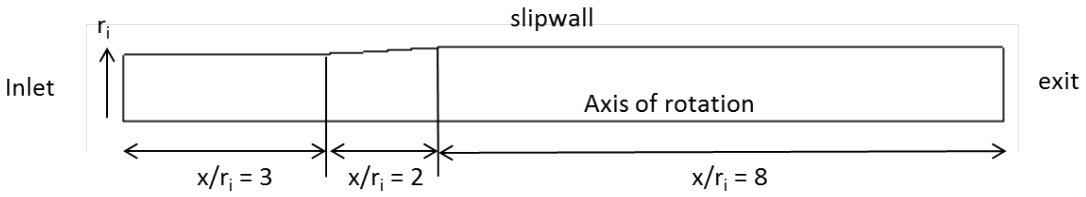

Figure 4-7: Geometry of axisymmetric duct, area ratio 1.21

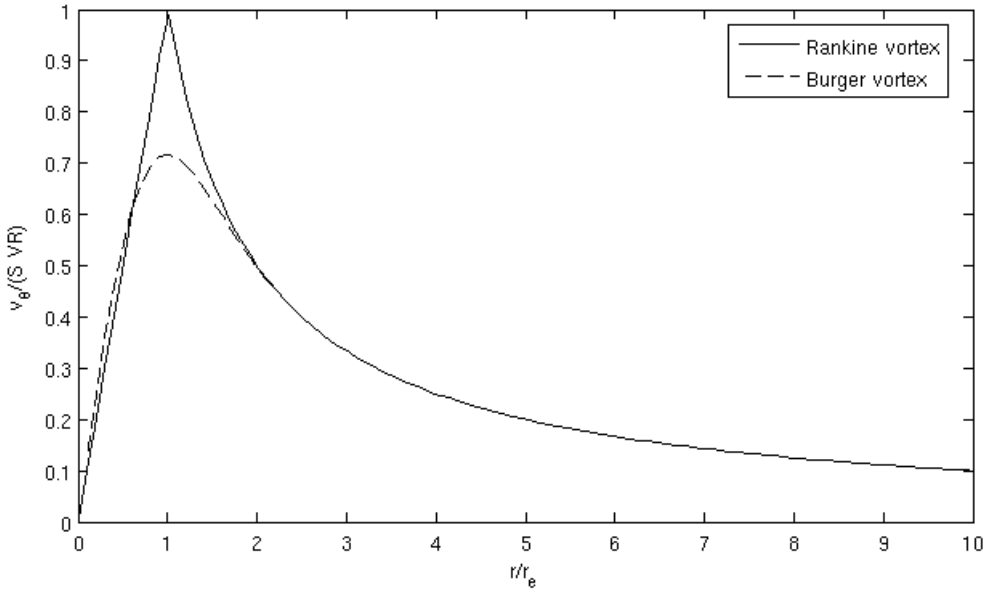

Figure 4-8: Swirl velocity, normalized by freestream velocity as a function of radius for Burger, Rankine vortices

specified at the inlet are given in Equations 4.17 and 4.18 as,

$$\frac{v_x}{U}(r,x) = \begin{cases} VR & : r \leq r_e(x) \\ 1 & : r > r_e(x) \end{cases} \tag{4.17}$$

$$\frac{v_\theta(r,0)}{U} = S\,VR\frac{r_e}{r}(1 - e^{-1.26(r/r_e)^2}) \tag{4.18}$$

The swirl velocity specified in equation 4.18 is that of a Burger vortex, which resembles the Rankine vortex but is defined by a smooth function and has a lower peak swirl velocity [2]. Figure 4-8 shows the swirl velocity distribution as a function of radius for Burger and Rankine vortices with the same total circulation.

The exit boundary sets the derivatives of flow variables in the axial direction equal

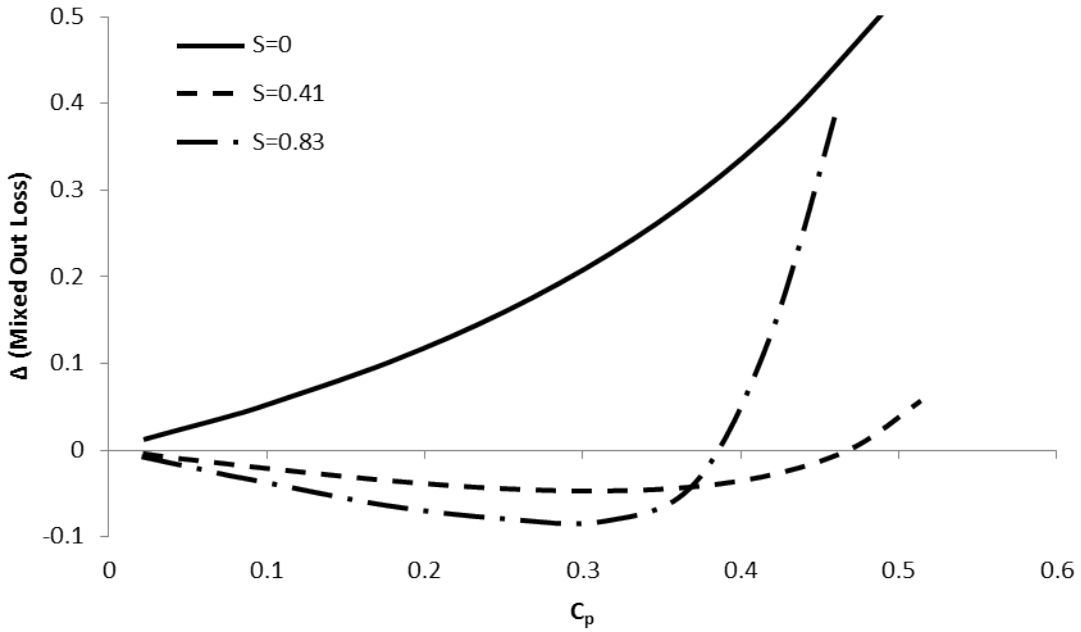

Figure 4-9: Calculated change in mixed out loss, normalized by inlet mixed out loss as a function of duct endwall pressure rise $C_p = \frac{\Delta p}{0.5\rho U^2}$ for vortices in ducts with area expansion. Velocity ratio 0.6, Swirl numbers 0, 0.42, 0.83.

to zero, which is appropriate for a flow which is slowly mixing out. The outer wall is a slipwall to minimize losses unrelated to vortex behavior. Turbulence is modeled using the RNG k-ϵ model [19], and the Reynolds number, based on the vortex core radius and the freestream velocity, is 8×10^4, approximately the Reynolds number of the tip vortex in the subsonic high pressure turbine.

Figure 4-9 shows the difference in mixed out loss between the inlet and exit plane, normalized by the inlet mixed out loss, as a function of the pressure rise coefficient (pressure rise along the duct maximum radius normalized by freestream dynamic pressure) for vortices with velocity ratio 0.6 and swirl numbers 0 (a wake), 0.42, and 0.83. The wake mixed-out loss increases monotonically with pressure rise. The mixed-out losses of the vortices decrease for $0 \leq C_p \leq 0.3$, because of vortex line contraction. Figure 4-10 shows contours of swirl velocity (normalized by freestream inlet velocity) for $C_p = 0.05, 0.19$, and 0.31. As the pressure rise increases, the swirl velocity ratio decreases from 0.32 to 0.27, and the mixed out loss drops accordingly.

Referring back to Figure 4-9, the loss for the $S = 0.83$ vortex begins to increase

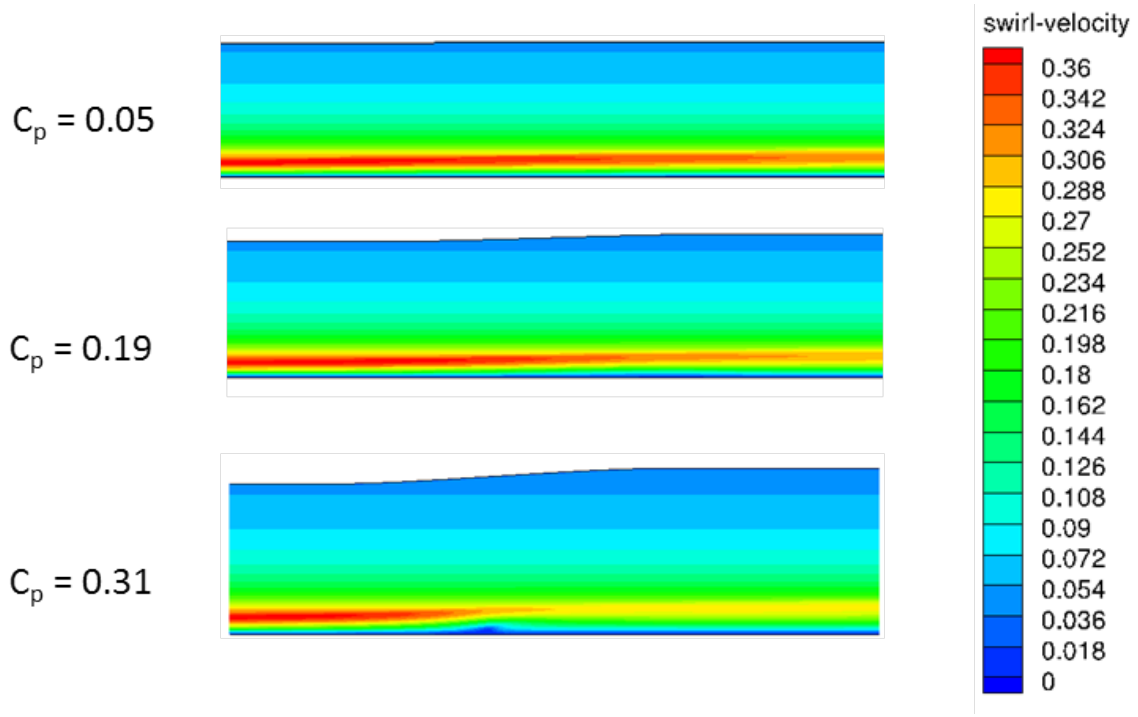

Figure 4-10: Contours of swirl velocity, normalized by inlet freestream velocity for vortex with velocity ratio 0.6, swirl number 0.83 passing through duct with endwall pressure rise $C_p = \frac{\Delta p}{0.5\rho U^2} = 0.05, 0.19, 0.31$.

at $C_p = 0.3$. At $C_p = 0.38$, the exit mixed-out loss becomes greater than the inlet mixed-out loss. This increase in loss is due to vortex breakdown and flow reversal. Figure 4-11 shows contours of axial velocity ratio for the $S = 0.83$ case for pressure rises $C_p = 0.31, 0.37$ and 0.42. For $C_p = 0.31$, the reversed flow region occupies a maximum of 0.07% of the duct area, but as the pressure rise increases, the region of reversed flow grows by more that an order of magnitude to occupy 0.8% of the duct area at $C_p = 0.42$.

The calculations show changes in loss of lower magnitude than predicted by the Rankine vortex model, since viscous effects mix the flow before and during the area expansion. Figure 4-12 shows a comparison of the change in mixed-out loss given by the Rankine vortex model and the axisymmetric CFD. For the control volume, the loss slope with respect to C_p is about five times greater than that for the computations for $C_p \leq 0.1$. Vortex breakdown is predicted to occur earlier than in the axisymmetric calculations, at $C_p = 0.16$. However, the qualitative behavior for the two descriptions are in accord and show that a vortex which passes through a pressure rise less than that sufficient to cause vortex breakdown will experience a decrease in mixed-out loss. As the pressure rise increases past a critical value, the vortex breaks down, and the control volume approach cannot capture the increase in exit mixed-out loss as the vortex experiences increasingly more flow reversal.

4.7 Conclusions

The effect of pressure gradients on flow non-uniformities has been explored. It has been shown that an adverse pressure gradient always increases mixing losses for a wake, but not necessarily for a vortex. However, a vortex core experiences stagnation at a lower freestream pressure change, leading to a large expansion in the vortex core. Turbine tip vortices can have initial swirl numbers near unity, implying the swirl component must be considered when examining the effect of pressure gradients on the flow. This is in contrast to the compressor tip clearance vortex, for which a wake is a reasonable model because of the lower swirl number [9]. It is seen that a small

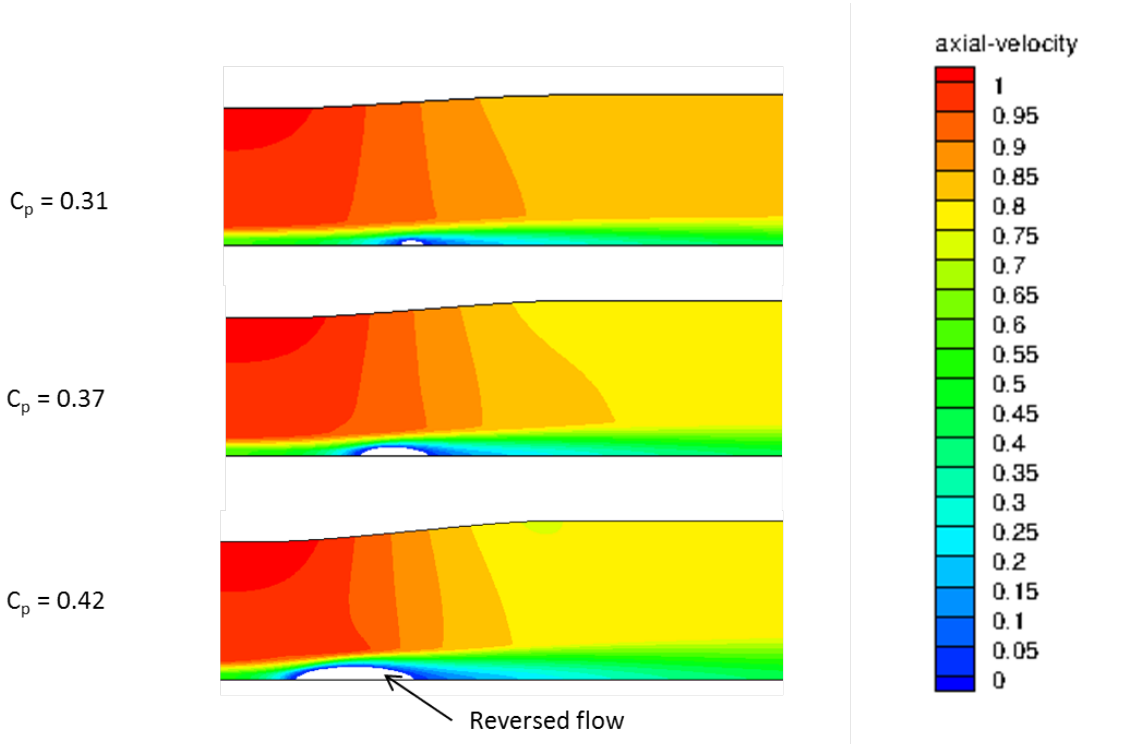

Figure 4-11: Contours of axial velocity, normalized by inlet freestream velocity for vortex with velocity ratio 0.6, swirl number 0.83 passing through duct with endwall pressure rise $C_p = \frac{\Delta p}{0.5\rho U^2} = 0.31, 0.37, 0.42$. Reversed flow regions indicated in white.

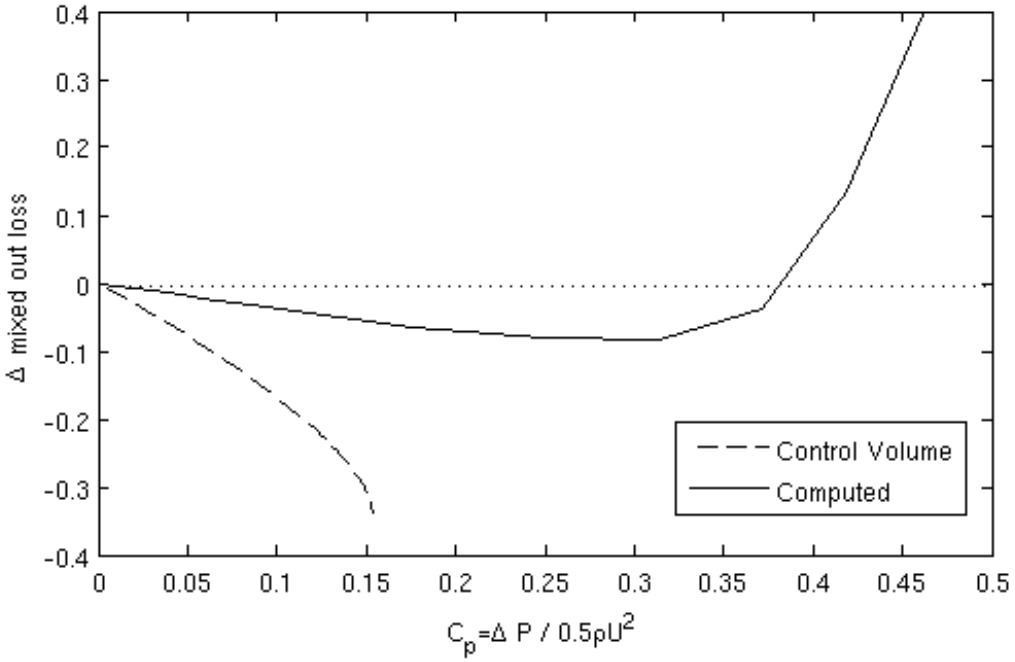

Figure 4-12: Comparison of change in mixed out loss from axisymmetric computations with Rankine vortex model as a function of duct endwall pressure rise $C_p = \frac{\Delta p}{0.5\rho U^2}$.

amount of diffusion has the potential to decrease the mixing loss, but that the current turbine designs subject the vortex to an amount of diffusion sufficient to cause vortex breakdown, a loss mechanism controlled by the freestream pressure rise. Chapter 5 describes the direct application of this observation to a turbine through a numerical study in which vortex breakdown was made more and less severe in an attempt to reduce the tip clearance loss.

Chapter 5

Effect of Turbine Pressure Rise on Clearance Loss

5.1 Introduction

In the previous chapter, it was shown that the tip leakage vortex core in the subsonic high pressure turbine passage encountered a pressure rise sufficient for vortex breakdown, in which the flow in the vortex core is decelerated through flow reversal This leads to the question of whether tip clearance loss can be decreased by designing the turbine with decreased pressure rise near the trailing edge. To answer this question, two blades were designed. One blade was designed with a forward loaded tip section to decrease the suction surface pressure rise. The second had an aft loaded tip section to increase the suction surface pressure rise. For the remainder of the chapter, the forward loaded, and aft loaded designs will be respectively referred to as the F and A blades.

This chapter describes the results of simulations which showed that, relative to the baseline, denoted by B, the A blade had 7% increased tip clearance loss, while the F blade had 9% decreased clearance loss. The entropy generation associated with the tip vortex breakdown region was higher for A blade with more reversed flow in the vortex core.

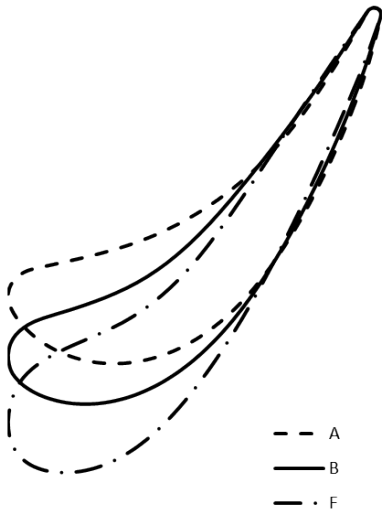

Figure 5-1: Tip geometries: Aft loaded (A), baseline (B), and forward loaded (F).

5.2 Tip Design Strategy

The effect of vortex breakdown on loss was assessed by computing the flowfields around airfoils which increased (the aft loaded or A design) and decreased (the forward loaded or F design) the pressure rise and hence the vortex core deceleration in the aft 25% axial chord of the blade.

Figure 5-1 shows the A, B (baseline), and F tip section geometries. In shifting the loading from aft to forward, the blade is uncambered and suction surface is flattened. The blade was re-stacked to include the new tip design, with the tip blended linearly into the 50% span airfoil shape. Meshes were generated to the same wall spacings as the baseline, and the flow in the blade passages was examined for clearances from 0-2% under the same conditions as the baseline mid-loaded tip (see table 2.1).

Figure 5-2 shows the isentropic suction surface Mach number extracted from the computations at 80% span as a function of axial position for 0.5% clearance. The desired effect has been achieved in that, from $x/c = 0.75$ to 1, the slope of the suctions surface isentropic Mach number is more negative for the A blade than for the F blade.

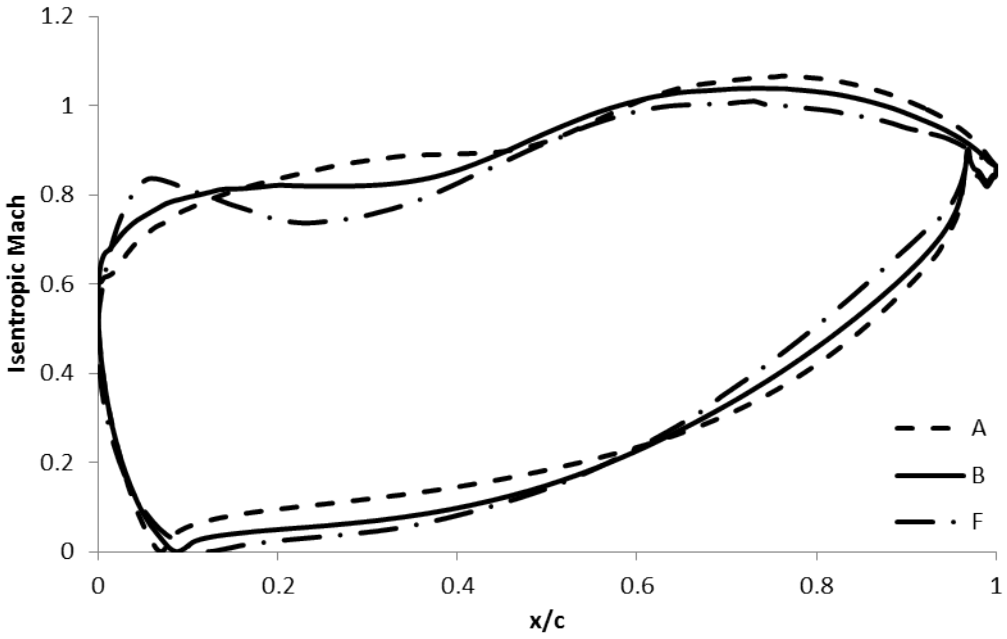

Figure 5-2: Isentropic suction surface Mach number at 80% Span from 3-D calculations at 0.5% clearance.

5.3 Results

5.3.1 Overall Loss

The F blade has 9% less leakage loss than the baseline design. Figure 5-3 shows the leakage loss coefficient (Chapter 2) against clearance for the three different tips. As the loading goes from forward to aft, the tip clearance loss slope increases by 15%.

The difference in *mixing loss per unit leakage flow* between the F and A blades is 30%, which is twice as large as the difference in total leakage loss. Though there is less massflow emerging from the gap for the A blade, the mixing loss is higher. Figure 5-4 shows the computed normalized loss per unit leakage flow for the three different blades at 2% clearance, as well as results from the control volume loss analysis, as described in Chapter 3. The gap loss per unit massflow is the same for each design, indicating that gap loss scales with massflow. The control volume approach captures the effect of pressure distribution, that forward loading decreases the clearance loss due to the decrease in the suction surface peak velocity, however, it underpredicts

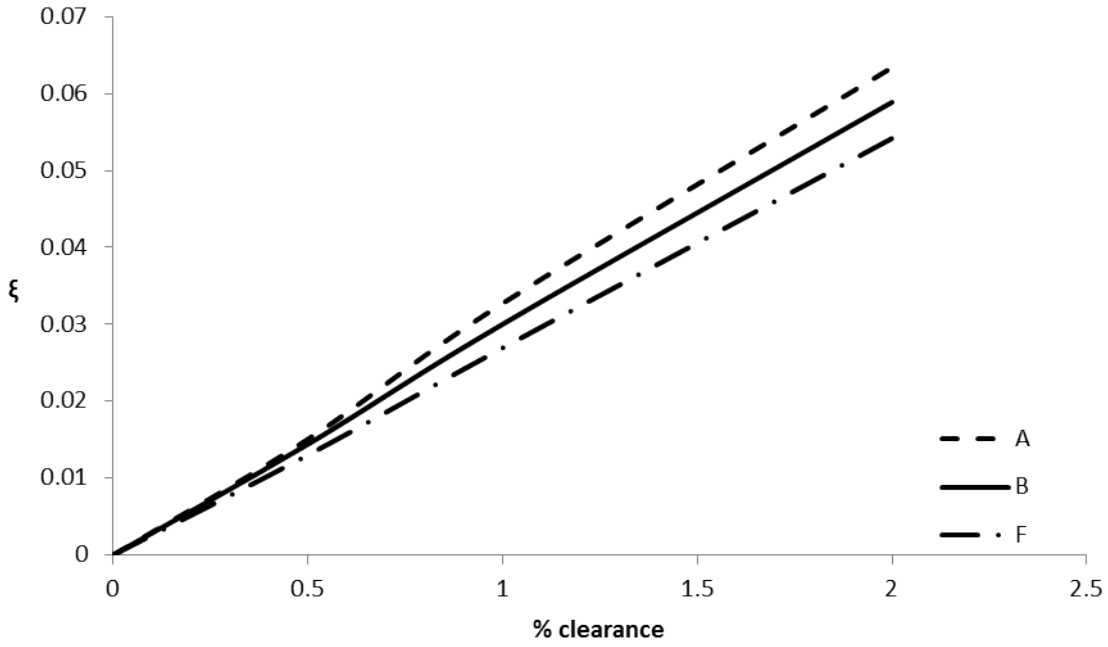

Figure 5-3: Leakage loss coefficient as function of clearance for A, B, F blades.

the magnitude of the effect, indicating that another mechanism is operating. It will be shown that the increase in mixing losses is due to a decrease in vortex streamwise velocity ratio between the F and A cases.

5.3.2 Leakage Mass Flow

The leakage mass flow increases as the blade design changes from aft loaded to forward loaded. Figure 5-5 shows the massflow for the A, B, and F blades as a function of clearance. The difference in leakage flow between the F and A blades cases is 14%. Figure 5-6 shows that the difference in massflow between the F and A blades is primarily associated with the region $x/c = 0.4 - 0.8$.

The massflow through the tip is determined by the gap exit stagnation-static pressure ratio, the viscous losses, and the area, as well as the angle at which the flow exits relative to the mainstream. Figure 5-7 shows the isentropic Mach number at the gap exit for the three blades. The gap pressure ratios are similar from $x/c = 0.4$ to 1 where the majority (85%) of the massflow exits, indicating that the difference in gap exit pressure ratio is not the reason for the increase in leakage massflow. The change

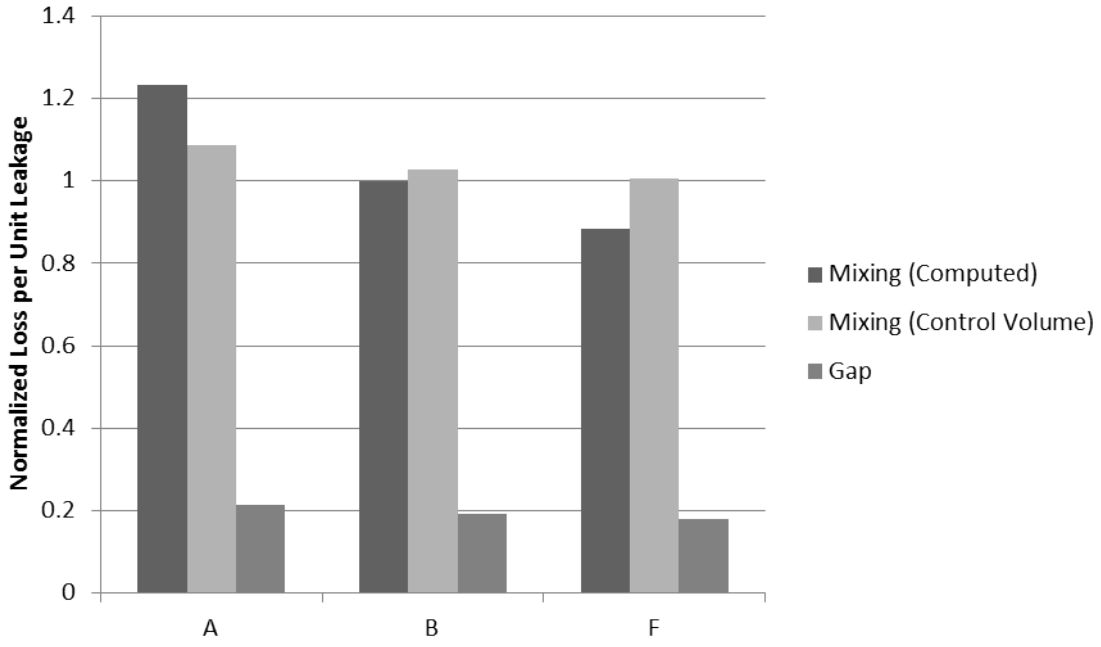

Figure 5-4: Normalized loss per unit leakage massflow for A, B, F blades. Computed mixing loss, control volume estimate for mixing loss, gap losses at 2% clearance

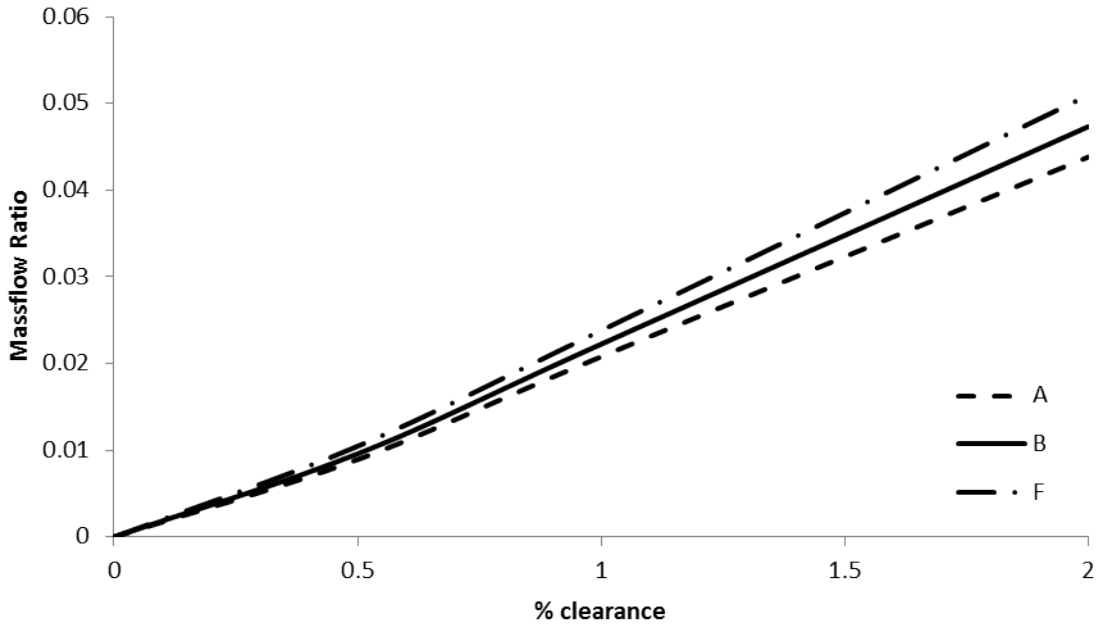

Figure 5-5: Ratio of leakage massflow to passage massflow as a function of clearance for A, B, F blades at 2% clearance.

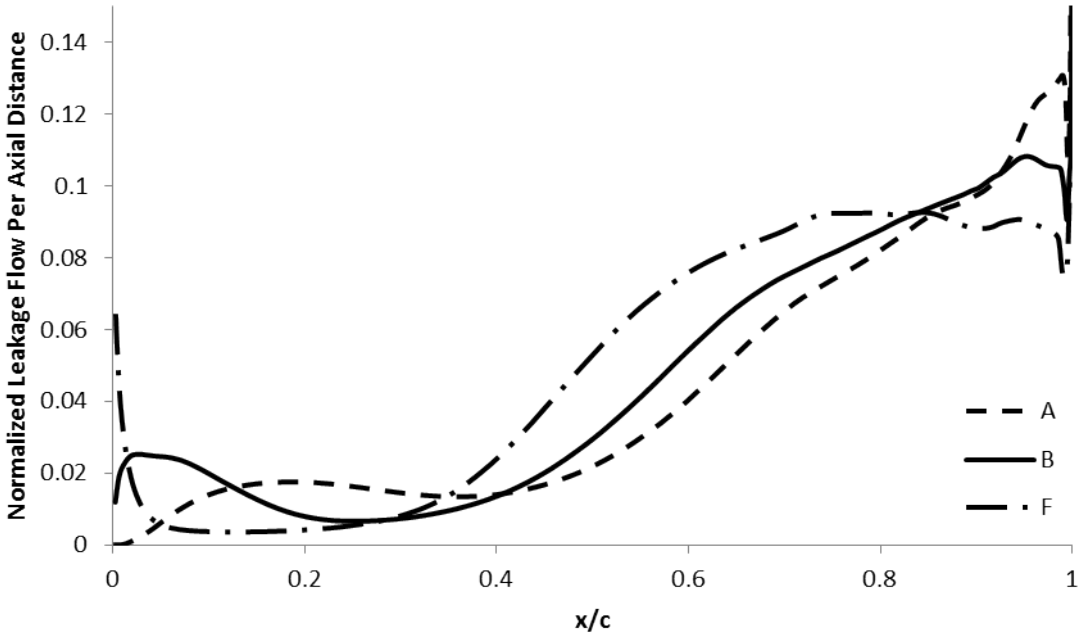

Figure 5-6: Normalized leakage massflow per unit axial chord as a function of axial position for A, B, F blades at 2% clearance.

in viscous losses within the gap account for only 9% of the change in tip clearance loss. Figure 5-8 shows that the discharge coefficients of the three tips differ by no more than 10% from $x/c = 0.4$ to 1.

The factors that do change between the F and A blades are the gap area and the angle between the leakage flow and the mainstream. Figure 5-9 shows the gap perimeter per unit axial chord at each axial location. From $x/c = 0.4$ to 0.8, the F tip gap has more perimeter, and hence area for the flow to exit, than the A tip gap. The angle at which the leakage flow emerges from the gap is given in Figure 5-10. Between 40%-80% axial chord, the leakage flow exits from the F tip gap at a $10 - 15°$ higher angle (closer to perpendicular to the freestream) than that from the A tip gap, meaning that more flow can exit per unit area. In summary, there is a difference in leakage massflow of 14% between the A and F blades because the F blade has a larger perimeter and the leakage flow exits the gap in a direction closer to the gap normal vector.

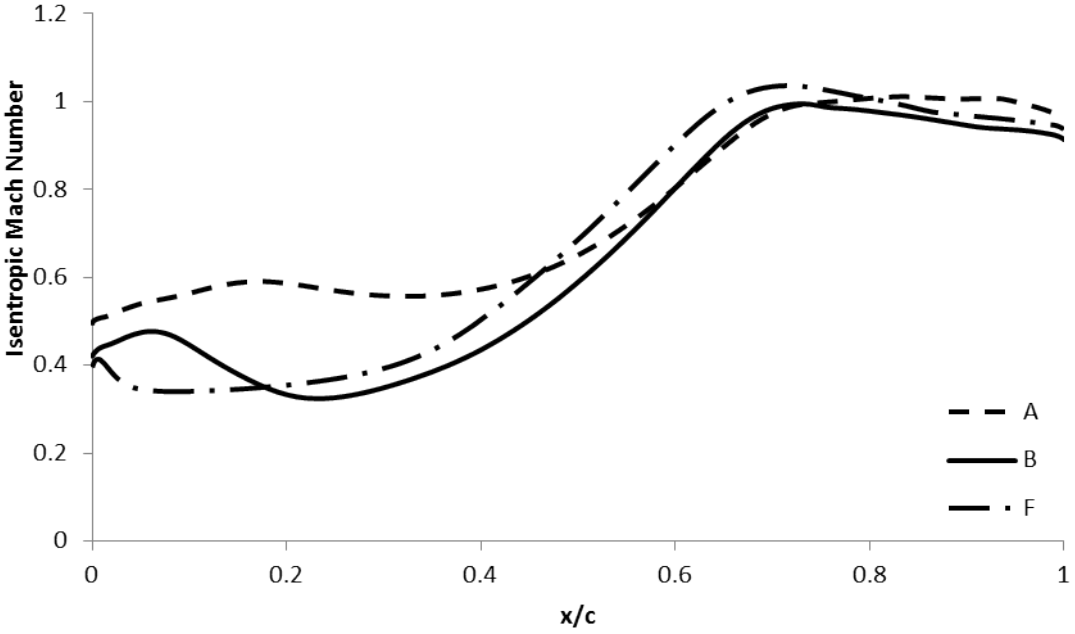

Figure 5-7: Relative isentropic Mach number at suction side gap exit as function of axial position for A, B, F blades at 2% clearance.

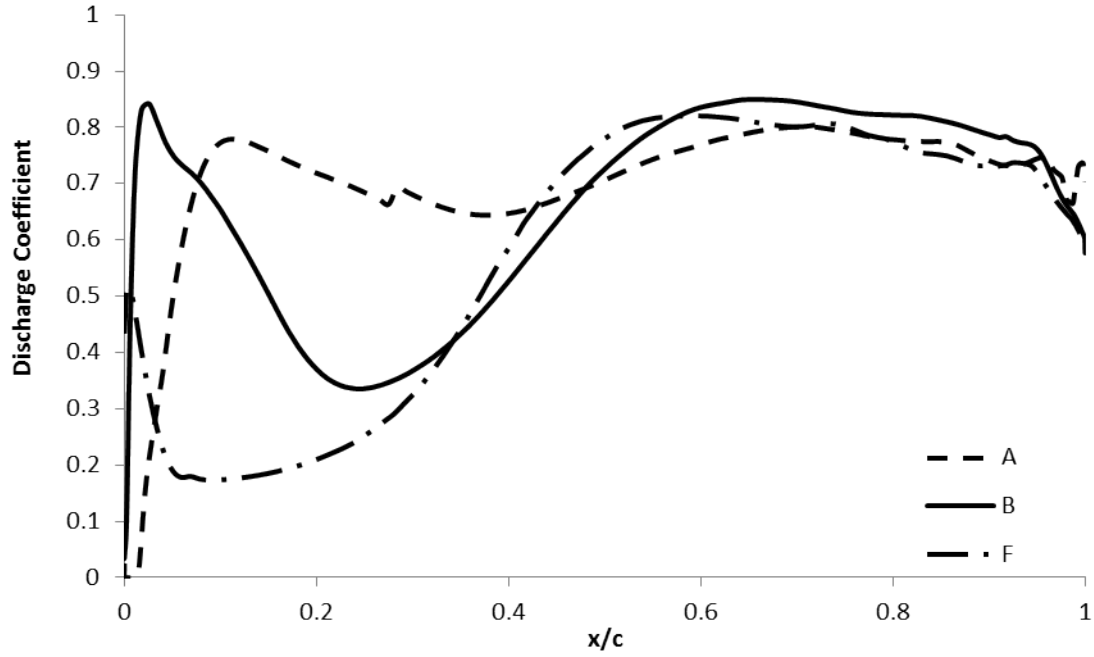

Figure 5-8: Computed tip gap discharge coefficient as a function of axial position for A, B, F blades at 2% clearance.

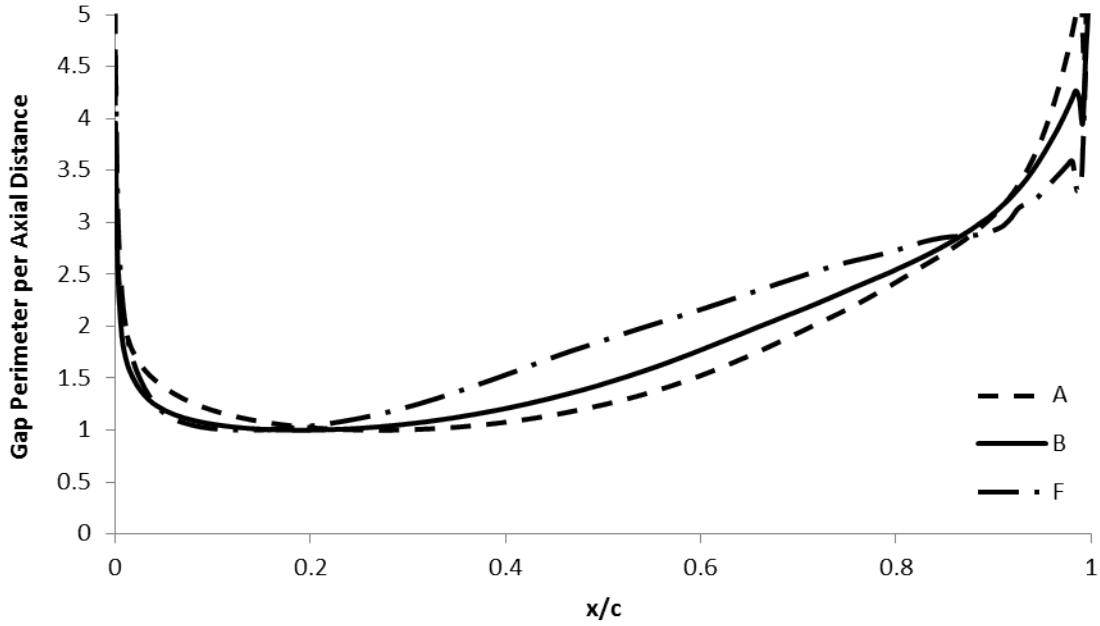

Figure 5-9: Gap perimeter per unit axial chord as a function of axial position for A, B, F blades.

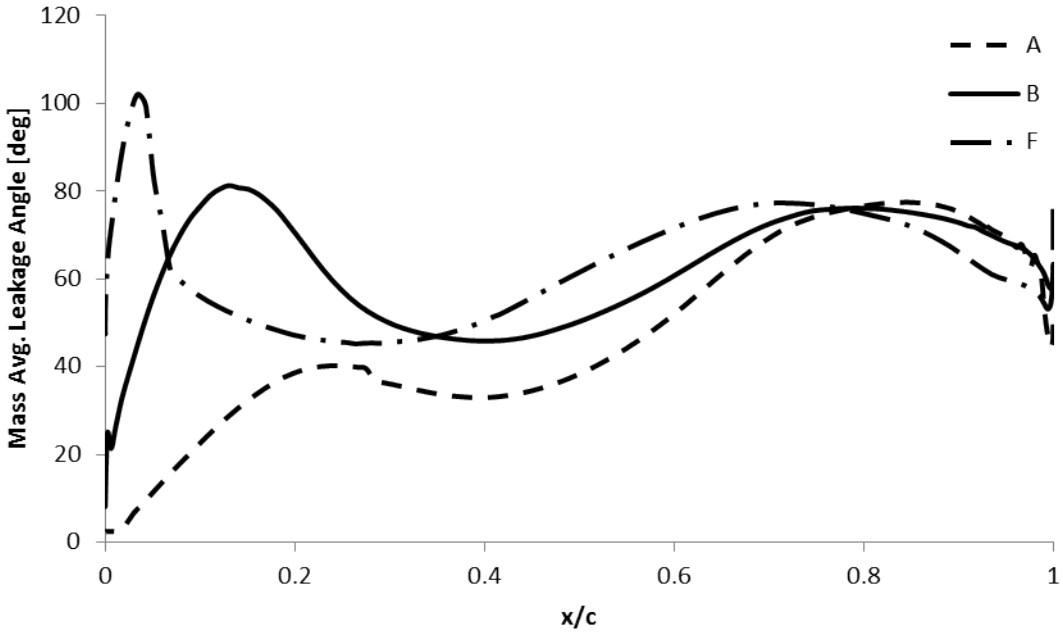

Figure 5-10: Mass average leakage angle in the tip gap as a function of axial position for A, B, F blades at 2% clearance.

5.3.3 Tip Clearance Vortex

In the baseline turbine, vortex breakdown was seen under the influence of the static pressure rise from 75% axial chord to the trailing edge. The aft and forward loaded tips change the pressure rise to which the vortex is exposed, alter the deceleration of the core flow, and alter the losses generated in this breakdown.

Figures 5-11, 5-12, 5-13 and 5-14 show the evolution of the tip clearance vortex properties for the forward and aft 2% clearance cases, extracted using the methodology defined in Chapter 2. Slices were taken normal to the streamwise direction, and the vortex was defined by including cells with positive vorticity (greater than the baseline relative vorticity -2Ω) outside of the tip gap and blade boundary layers. Figures 5-11 and 5-12 show the average and mimimum streamwise velocity ratios in the vortex core for the A, B and F blades. In terms of the average streamwise velocity ratio, the flow in the core of the vortex in the A blade is decelerated more than that in the F blade. The core centerline velocity shows the same trends, but magnified. In the A blade, the core centerline velocity ratio reaches a minimum of -0.13, indicating that the vortex core is reversed, while the F blade does not experience any flow reversal. Figure 5-13 shows this in contours of the streamwise velocity normalized by exit velocity. The reversed flow at the center of the vortex core for the aft loaded turbine is shown in the last two slices, indicated by the white area.

Figure 5-14 shows the swirl numbers for the vortices for the F and A blades. The vortex in the F blade barely reaches the nominal vortex breakdown criterion. It also has a swirl number lower than that in the A blade by a factor of 2 because of the larger pressure rise in the A blade.

5.3.4 Loss Mechanisms

The increase in mixing loss between the F and A blades occurs in the region of vortex breakdown. To illustrate this point, Figure 5-15 shows the difference in loss generation per axial distance(computed from the viscous dissipation, see Chapter 2) between the 0 and 2% clearance cases as a function of axial location for the F and

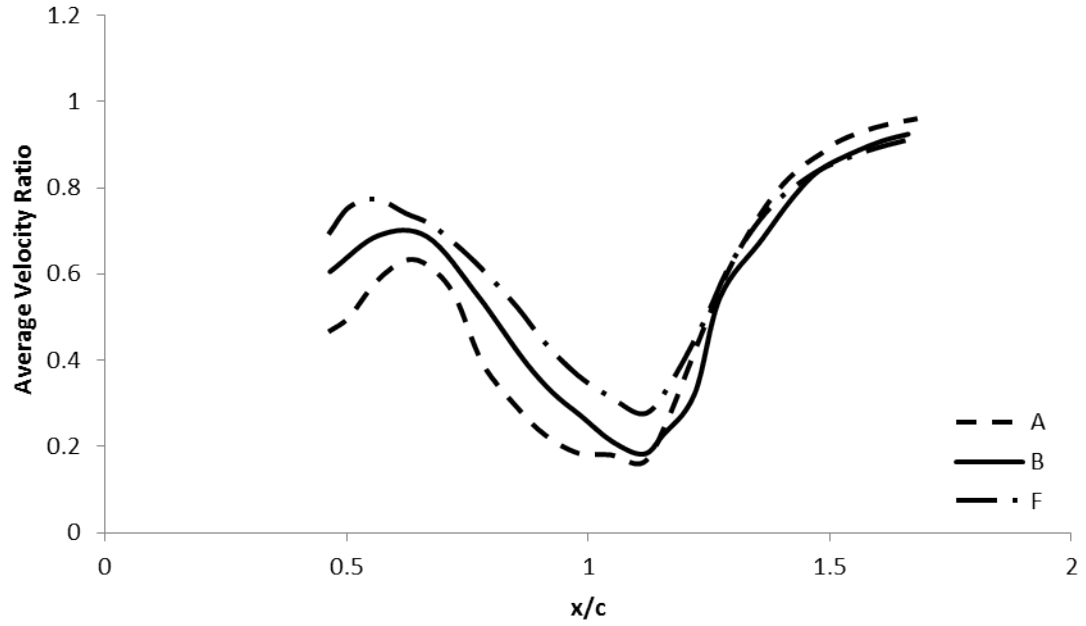

Figure 5-11: Vortex core average velocity ratio as a function of axial position for A, B, F blades at 2% clearance.

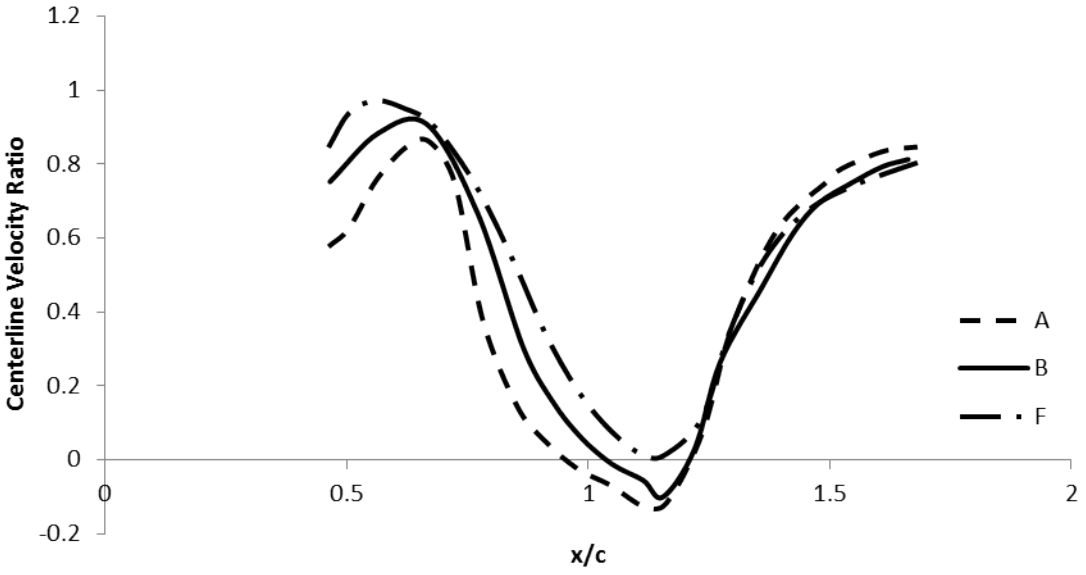

Figure 5-12: Vortex centerline velocity ratio as a function of axial position for A, B, F blades at 2% clearance.

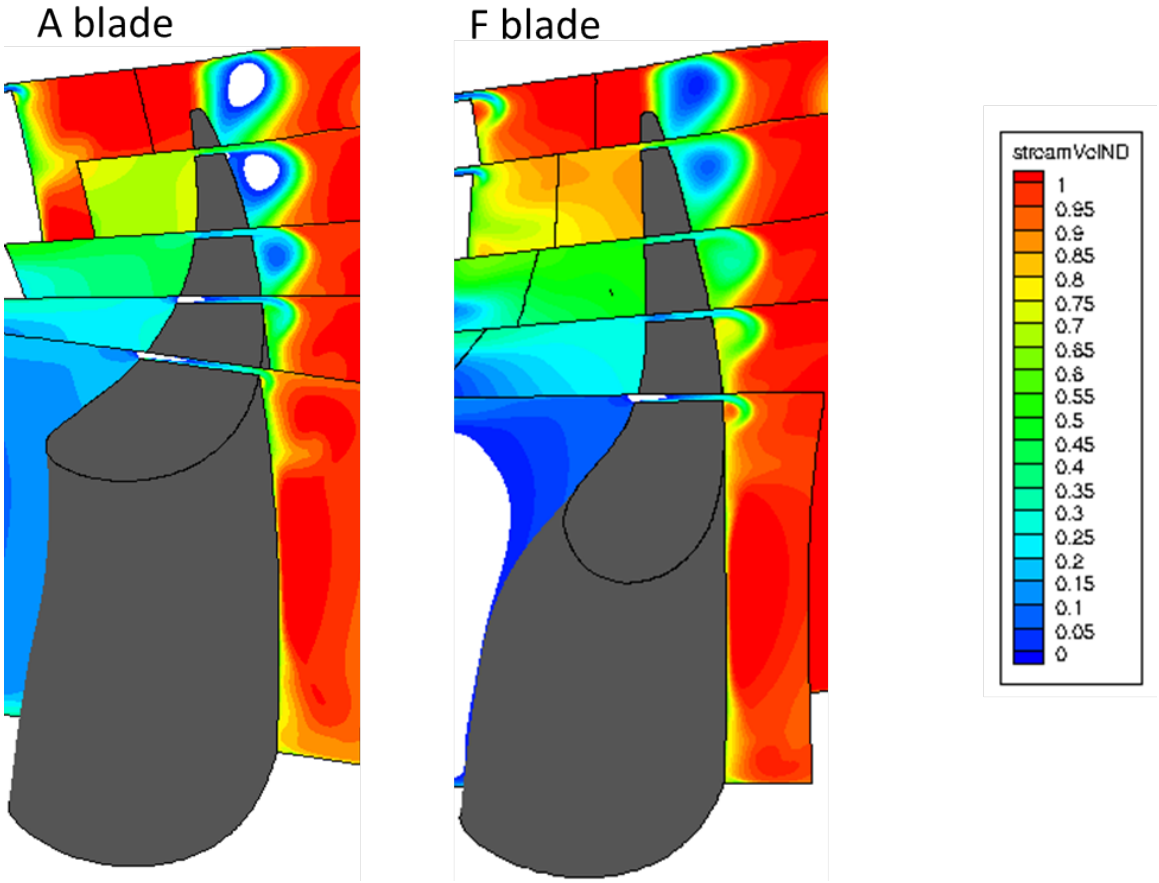

Figure 5-13: Contours of streamwise velocity ratio for A (left), F (right) blades at 2% clearance. Reversed flow regions shown in A blade vortex in white.

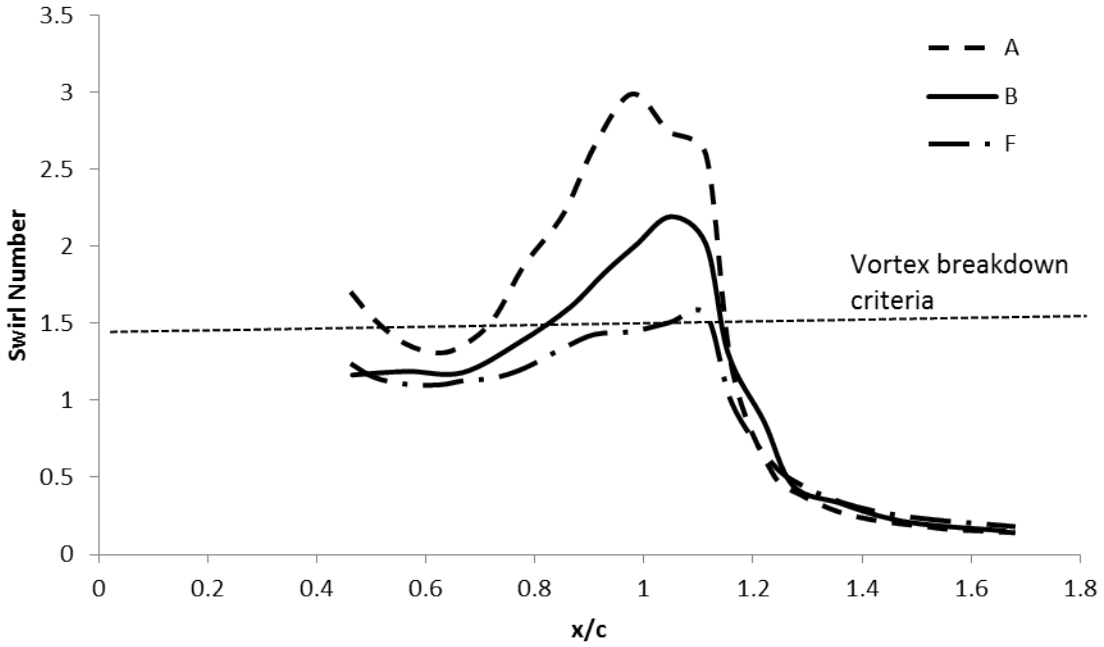

Figure 5-14: Vortex swirl number as a function of axial position for A, B, F blades at 2% clearance.

A blades. The A blade has a 35% higher mixing loss per unit distance in the region $x/c = 1$ to 1.4, where the tip clearance vortex has broken down and is mixing out. From this, we conclude that vortex breakdown is a loss mechanism which contributes to the difference in loss per unit leakage between the A and F blades.

Figure 5-16 compares the viscous dissipation in the F and A blade at the location of maximum entropy generation, $x/c = 1.15$. The volumetric entropy generation has been non-dimensionalized by the massflow through the turbine passage, the exit static temperature, and the specific enthalpy rise through the the turbine. The maximum local dissipation in the plane shown is located in the region of mixing of the tip vortex with the surrounding flow and is a factor of two larger for the A blade than for the F blade, confirming that the increase in viscous dissipation between the A and F blades occurs in the vortex breakdown region.

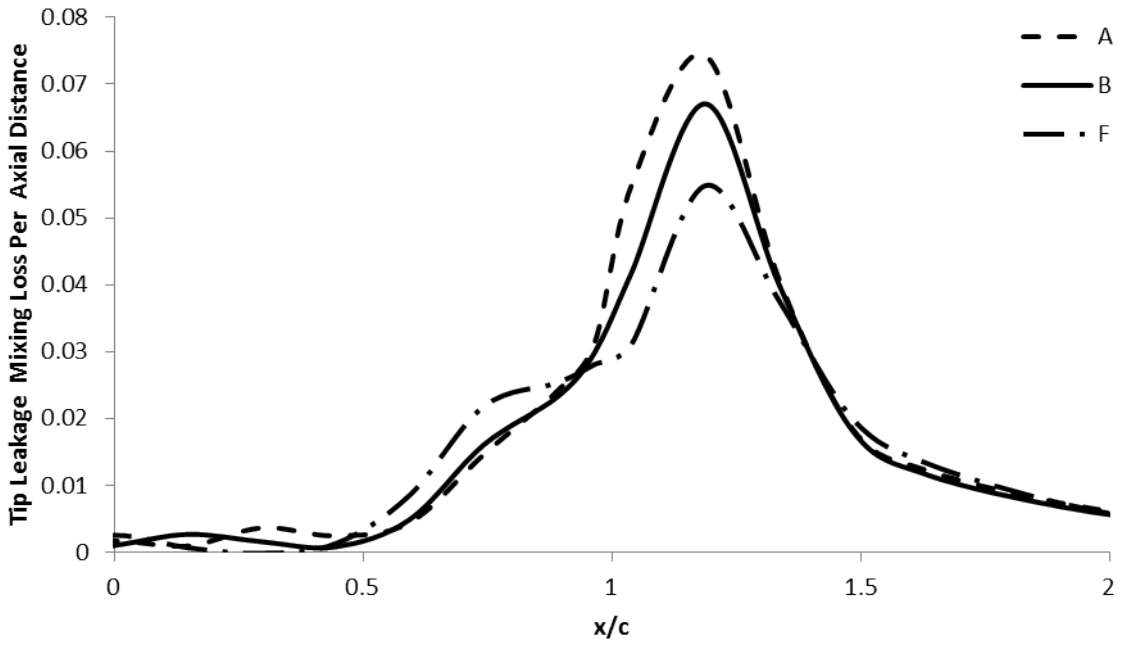

Figure 5-15: Difference in mixing loss per axial chord between 0%, 2% clearance for A, B, F blades.

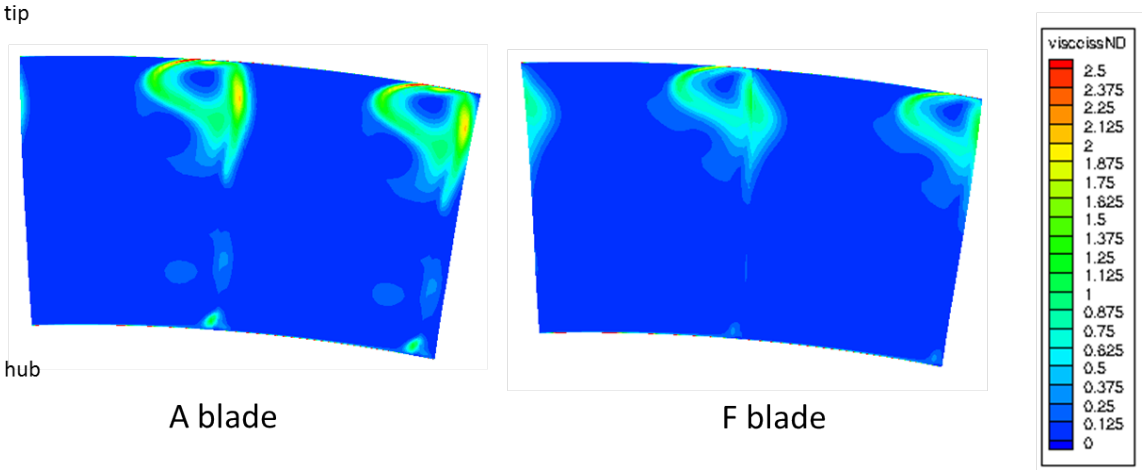

Figure 5-16: Contours of normalized viscous dissipation at $x/c = 1.15$ for F, A blades at 2% clearance. Two adjacent passages shown.

5.4 Conclusions

It has been shown in this chapter that the tip loading distribution can affect tip clearance loss by affecting vortex breakdown, which is a source of tip clearance losses. Two turbine blades were designed to alter the pressure rise experienced by the tip clearance vortex. Computations showed that, relative to the baseline blade, a forward loaded tip (F blade) decreased the tip clearance loss by 9% while an aft loaded tip (A blade) increased the tip clearance loss by 7%. The reason for the difference in clearance loss was found to be the decrease in streamwise velocity ratio in the vortex core, which is directely attribuete to the difference in pressure rise at the aft region of the blade. The A blade, compared to the F blade, had more reversed flow in the vortex core and twice the loss in the region where the vortex broke down and mixed out. These results indicate that leakage vortex breakdown and hence the leakage loss can be moderated by reducing the trailing edge pressure rise through design of the near-tip airfoil shape.

We have seen that a change in the tip section geometry, resulting in a small change in the pressure distribution (see figure 5-2), results in a 9% change in clearance loss (between the B and F blades). The alteration of the pressure distribution was constrained in that the velocity triangles and axial chord were kept constant, and only the tip section airfoil was changed. The pressure distribution can be further altered by changing the airfoil loading along the entire span, the inlet flow angle, or the solidity. Chapter 6 shows the effect of these three variables on tip clearance loss.

Chapter 6

Effect of Overall Blade Loading, Incidence and Solidity

In the previous chapter, we saw that when the the tip airfoil section is changed to reduce the pressure rise encountered by the vortex, the vortex breakdown is mitigated and the clearance loss reduced. Because only the tip section was altered, the pressure distribution was unable to be varied much for the geometries considered. In this chapter, we remove that limitation and evaluate the effect of changes in overall blade pressure distribution on tip clearance loss.

The first section in this chapter addresses the effect of blade loading using linear cascades with the airfoil geometries in figure 5-1. It is shown that the forward loaded cascade has 50% lower loss per unit leakage flow than the aft loaded cascade, mainly because of a decrease in vortex breakdown losses.

Inlet incidence angle affects the pressure distribution for a given blade geometry. The second section shows that as the incidence angle increases, the blade becomes more forward loaded. The tip clearance loss thus decreases because the losses due to vortex breakdown decrease.

Solidity is examined in the third section. It is demonstrated that as the solidity of the baseline rotor increases, the tip clearance loss decreases.

6.1 Effect of Blade Loading

6.1.1 Computational Details

Tip leakage loss was evaluated for linear cascade blades extruded from the A, B, and F tip sections. These will be referred to as the A2, B2, and F2 designs.

Relevant cascade parameters are found in table 6.1. The mesh is spaced to resolve boundary layers near the tip, with $y+ \leq 1$ and 48 cells across the tip gap. The calculation was done in the absolute frame, holding the blade stationary and translating the casing. The inlet total pressure, inlet total temperature, and exit static pressure were specified. No boundary layer was specified at the inlet.

Table 6.1: Linear Cascade Parameters

Midspan Inlet Angle	40.3°
Midspan Exit Angle	67.2°
Exit Mach Number	0.58
Total-Static Pressure Ratio	1.2477
Solidity	1.0
Aspect Ratio	1.26
Exit Re_c	1.82e5

6.1.2 Blade Loading Study Results

As intended, the differences in suction surface pressure distribution between the A2, B2 and F2 are larger than between the A, B, and F cases. Figure 6-1 shows the suction surface isentropic Mach number at 50% span as a function of axial position for the A2, B2, and F2 blades. The Mach number of the F2 blade peaks at $x/c = 0.05$ and falls to the exit Mach number over the remainder of the blade, with 75% of the decrease in velocity taking place upstream of $x/c = 0.5$. The B2 Mach number is 0.65 for $x/c = 0$ to $x/c = 0.6$, and then falls to 0.58 over $x/c = 0.6$ to $x/c = 1$. The A2 Mach number rises from $x/c = 0$ to $x/c = 0.65$, peaks at $M = 0.7$ and then falls to the exit Mach number from $x/c = 0.75$ to 1.

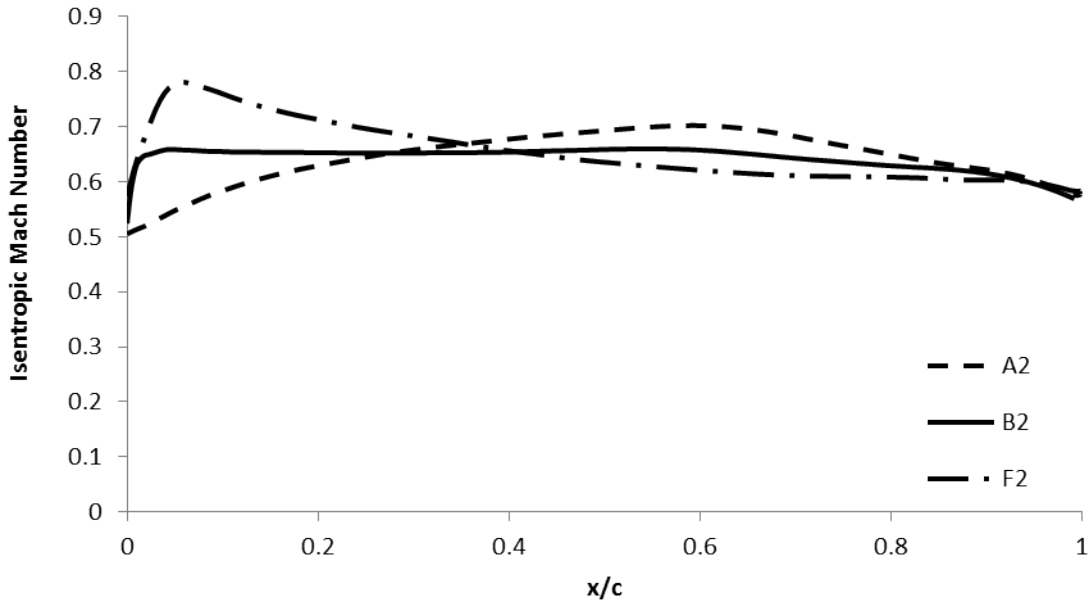

Figure 6-1: Suction surface isentropic Mach number at midspan as a function of axial position for A2, B2, F2 blades at 2% clearance

The difference in pressure distribution results in a 9% decrease in tip clearance loss between the B2 and F2 blades. The difference in loss per unit leakage however is more extreme, because the leakage mass fraction is 18% higher for the F2 blade relative to the B2 blade.

Figure 6-2 shows the calculated mixing loss per unit leakage flow, and the gap loss per unit leakage flow, for the A2, B2, and F2 cascades, along with the control volume estimate for the mixing loss. The gap loss per unit leakage flow is the same to within 5% between designs, indicating that the viscous losses in the gap scale with massflow. The control volume analysis predicts a decrease in loss as the loading changes from aft to forward, but underestimates the magnitude of the decrease by roughly 60%, indicating that not all the losses are captured.

As with the turbine calculations, the increased entropy generation between the A2 and F2 blades can be associated with vortex breakdown. Figure 6-3 shows the swirl numbers for the tip vortices in the A2 and F2 blades as a function of axial position. Each vortex exceeds the nominal breakdown criteria, but the vortex in the

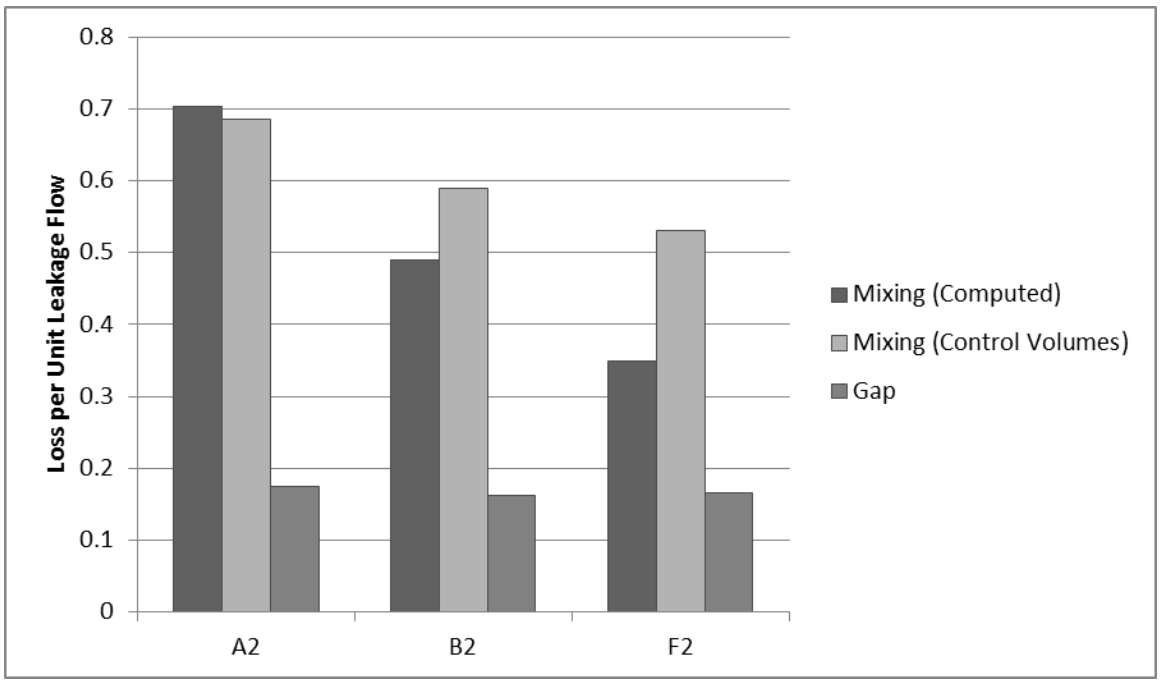

Figure 6-2: Loss per unit leakage flow for A2, B2 and F2 blades at 2% clearance. Computed mixing losses, estimated mixing loss from control volume analysis, and gap losses.

F2 case has lower maximum swirl number and is already broken down at $x/c = 0.5$ due to the adverse pressure gradient from $x/c = 0$ to 0.5. At $x/c = 0.5$, the F2 vortex has accumulated only 43% of its eventual circulation and so the losses due to vortex breakdown are likely lower than had the breakdown occurred at the trailing edge, involving all of the leakage flow.

Figures 6-4 and 6-5 show the core centerline velocity ratio (6-4) and entropy generation per axial distance (6-5) for the A2 and F2 blades as a function of axial position. The vortex breakdown occurs further upstream for the F2 blade than for the A2 blade, and so the loss per axial distance is higher for the F2 blade upstream of the trailing edge. Over the region $x/c = 1$ to 1.4, flow reversal is observed in the A2 blade, the streamwise velocity ratio for the A2 blade is 30% lower than for the F2 streamwise velocity ratio, and the loss per axial distance of the A2 blade is twice that of the F2 blade. These support the conclusion of Chapter 5 that vortex breakdown is a mechanism in tip clearance loss.

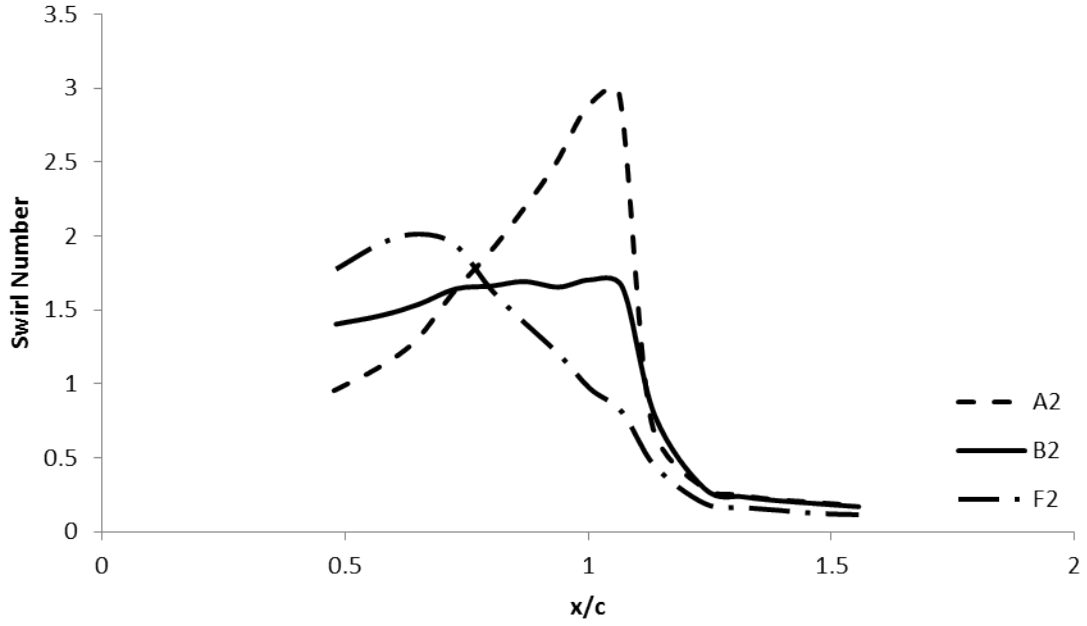

Figure 6-3: Tip vortex swirl number as a function of axial location for A2, B2, F2 blades, 2% clearance.

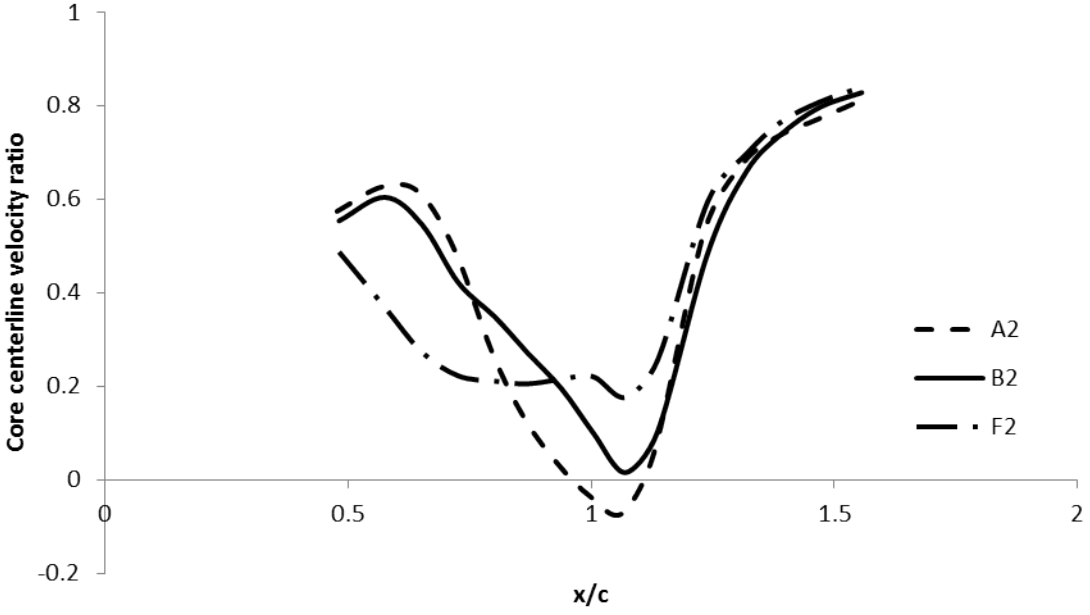

Figure 6-4: Tip vortex streamwise velocity ratio as a function of axial location for A2, B2, F2 blades, 2% clearance.

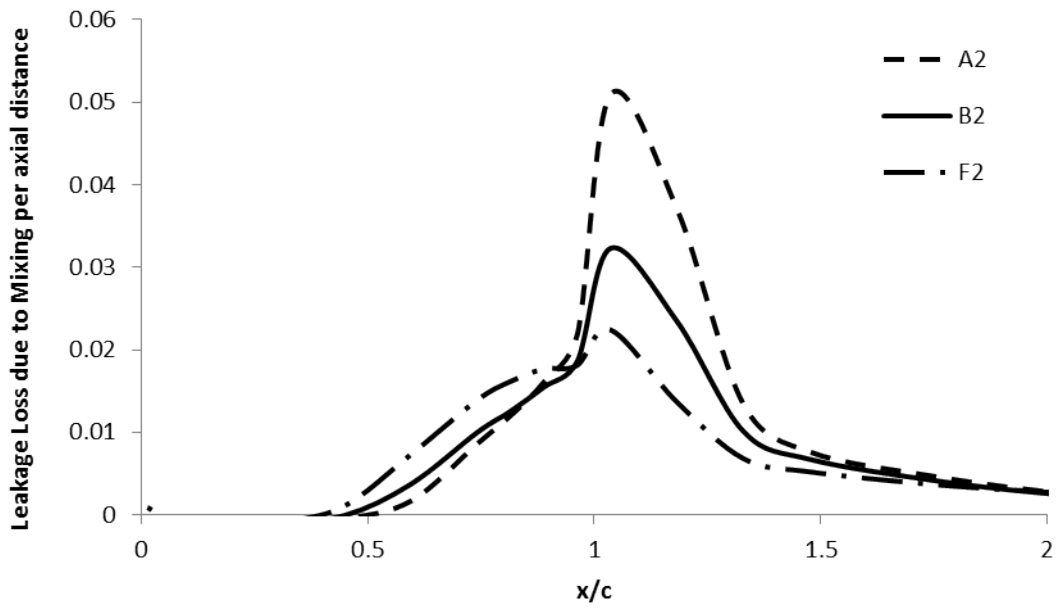

Figure 6-5: Loss per unit axial distance as a function of axial location for A2, B2, F2 blades, 2% clearance.

6.1.3 Discussion and Conclusions

The interpretation of the cascade study results can be summarized as follows. The control volume estimate for the mixing losses in the F2 blade is 30% lower than that in the A2 blade, because the Mach number of the main flow at the suction surface midspan is lower (for the F2 blade relative to the A2 blade) from $x/c = 0.5$ to 1. Put another way, the mixed-out losses estimated from the control volume are modified by vortex line contraction and breakdown to give the actual loss.

For the F2 blade, the pressure rise encountered by the tip vortex is sufficient for vortex breakdown at $x/c = 0.5$. Since the vortex breakdown occurs when only 20% of the leakage flow has exited the gap, the loss due to breakdown is small. The rest of the leakage flow then rolls up into the vortex, which goes through a pressure rise from $x/c = 0.5$ to 1 that is smaller than that in the A2 blade. The pressure rise from $x/c = 0.5$ to 1 decreases the swirl velocities so that the mixing loss per unit leakage flow is lower than that given by the control volume analysis.

For the A2 blade, the pressure rise occurs between $x/c = 0.6$ and 1, and the vortex

breakdown occurs at the trailing edge and involves the entire leakage flow. The vortex breakdown generates enough loss so the loss per unit leakage is slightly higher than that predicted by the control volume model.

The F2 and A2 results illustrate that a pressure rise upstream of midchord is less harmful (in terms of leakage loss) than a pressure rise downstream of midchord since the vortex is not completely formed at midchord. Vortex breakdown in the former situation will produce lower losses than in the latter.

6.2 Effect of Incidence

A change in incidence alters the pressure distribution on the suction surface and thus the tip leakage loss. It will be shown that the leakage loss decreased 16% when the inlet flow angle (relative to the blade) was increased from 30° to 50° for the B2 linear cascade. Figure 6-6 shows the computed suction surface isentropic Mach number at midspan for inlet flow angles 30°, 40° (baseline) and 50°. As the incidence increases, the drop in isentropic Mach number from $x/c = 0.55$ to $x/c = 1$ decreases slightly. Since the leakage mass fraction did not change with incidence [1], the loss per unit leakage flow, shown in figure 6-7, also decreases by 16% between 30° and 50° incidence. The mixing loss predicted by the control volume model is roughly uniform (to within 1%) with incidence, while the actual mixing loss decreases linearly and is lower in value than the control volume estimates.

The change in pressure distribution also affects the vortex evolution. Figure 6-8 shows the tip vortex centerline velocity ratio for the three inlet angles, and Figure 6-9 shows the entropy generation per axial distance. As the incidence angle increases, the minimum centerline velocity rises and the loss generation in the vortex mixing region (between $x/c = 1$ to $x/c = 1.4$) decreases. In other words, the vortex breaks down with lower losses.

Comparing figures 6-1 and 6-6, there are qualitative similarities between the F2

[1]The leakage mass fraction does not change with incidence because most of the massflow exits downstream of 40% axial chord, and the loading in that region is not changed much by incidence (Isentropic Mach number varies by only 0.04.

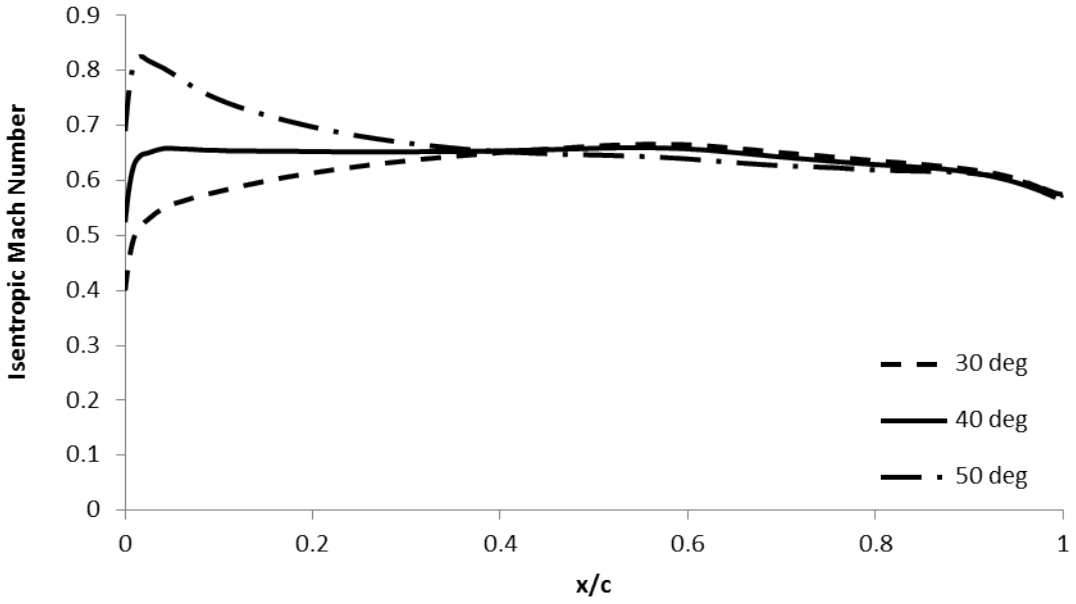

Figure 6-6: Suction surface isentropic Mach number at midspan for incidences 30° to 50°

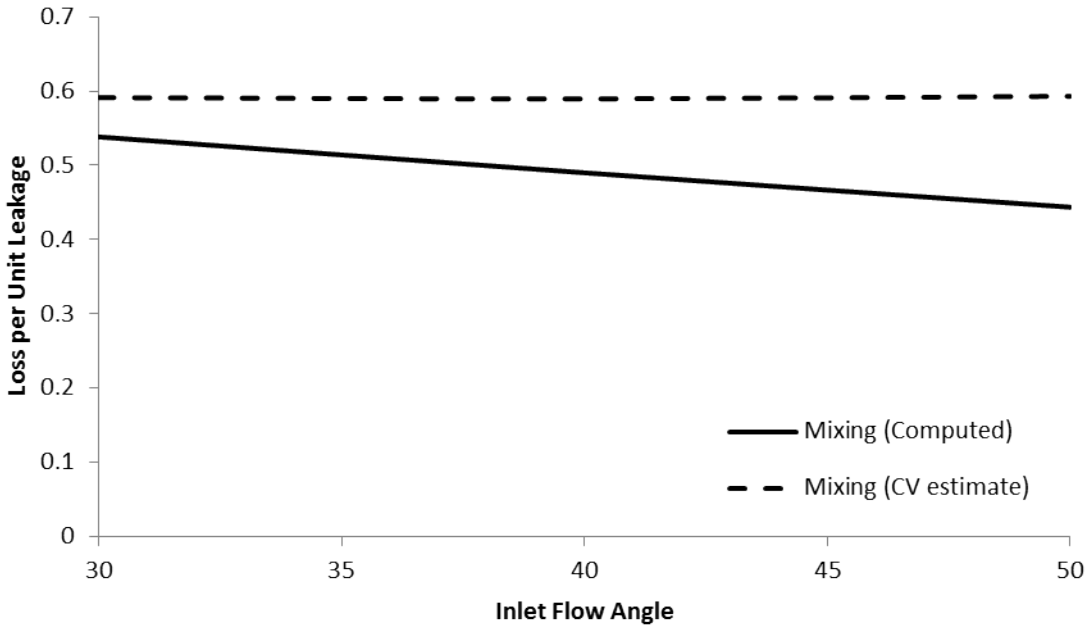

Figure 6-7: Mixing loss per unit leakage flow as a function of inlet flow angle for B2 blade. Computed losses, control volume model estimate

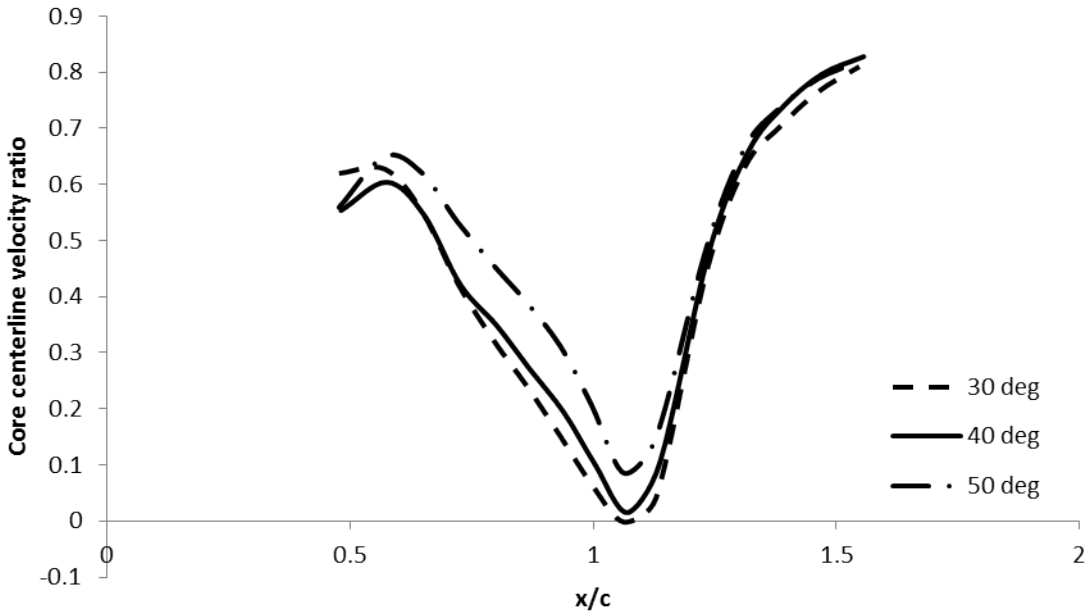

Figure 6-8: Vortex centerline streamwise velocity ratio for B2 blade, inlet flow angles 30°, 40°, 50°.

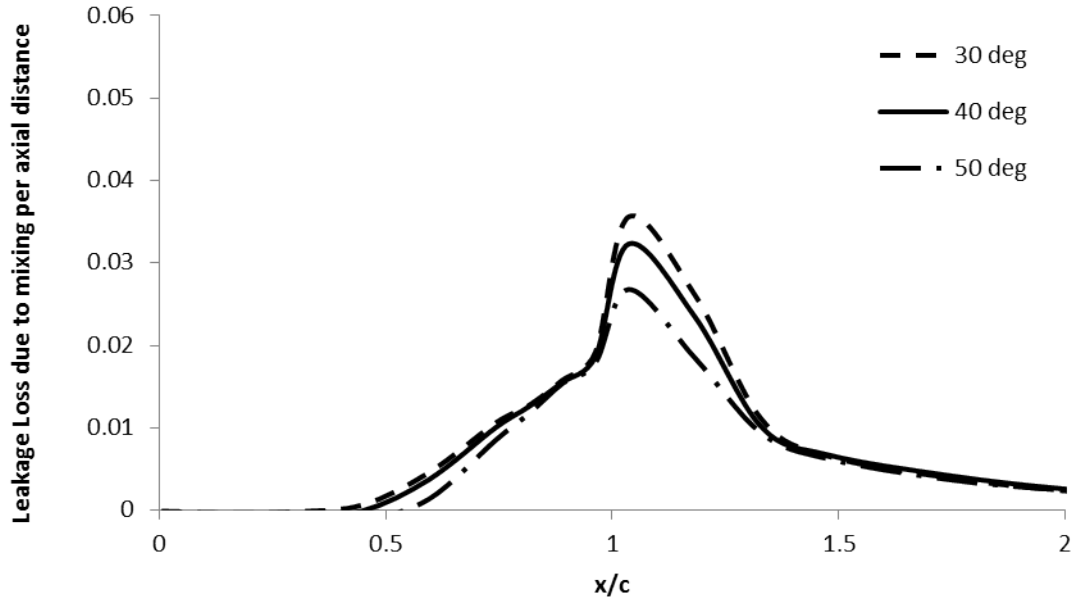

Figure 6-9: Entropy generation per unit axial distance as a function of axial distance for B2 blade, inlet flow angles 30°, 40°, 50°.

blade and the 50° incidence case, and between the A2 blade and the 30° incidence case, although the differences in isentropic Mach number are greater for the tip loading study. Increasing the incidence forward loads the blade, reduces the pressure rise experienced by the vortex, and leads to lower losses from vortex breakdown.

6.3 Effect of Solidity

Solidity is defined in equation 6.1 as the ratio of midspan chord c to pitch p.

$$\sigma = \frac{c}{p} \tag{6.1}$$

An increase in solidity decreases the loading and is therefore expected to affect both the loss per unit leakage flow and the leakage mass fraction. This can be seen using Denton's tip clearance loss analysis [3]. Consider a rectangular pressure distribution. Using the blade circulation and continuity, we obtain expressions for the suction side and pressure side velocities, Equation 6.2 and 6.3, where V_x is the axial velocity, $\psi = \frac{\Delta h_t}{(\omega r)^2}$ is the work coefficient, $\phi = \frac{V_x}{\omega r}$ is the flow coefficient, and α is the local relative flow angle [3].

$$V_{ss} = \frac{V_x}{cos(\alpha)} + \frac{V_x \psi}{2\phi\sigma} \tag{6.2}$$

$$V_{ps} = \frac{V_x}{cos(\alpha)} - \frac{V_x \psi}{2\phi\sigma} \tag{6.3}$$

Following Denton, we assume that the leakage flow dm emerging from the gap over a small axial distance dz is two-dimensional. Equation 6.4 gives an expression for dm, where C_d is the discharge coefficient, g is the gap height, and ρ is the density.

$$dm = C_d g \sqrt{2(p_{ps} - p_{ss})\rho} dz = C_d g c \rho \sqrt{V_{ss}^2 - V_{ps}^2} d(z/c) \tag{6.4}$$

The mainstream massflow is given by $m_m = \rho V_x h p$. Using Equations 6.3 and 6.2 in Equation 6.4 and dividing by the mainstream massflow we obtain an expression

for the leakage massflow in Equation 6.5

$$\frac{dm}{m_m} = C_d(g/h)\sqrt{\frac{2\psi\sigma}{\phi\cos\alpha}}d(z/c) \tag{6.5}$$

The massflow through the gap decreases as $1/\sqrt{\sigma}$ due to the loading change, but the passage massflow decreases at a rate of $1/\sigma$. The result is that the leakage mass fraction is predicted to increase as the square root of solidity.

Equation 6.6 gives the loss per unit leakage flow, where $V_{leak,x}$ and $V_{leak,y}$ respectively refer to the velocity component of the leakage flow aligned and perpendicular to the suction surface velocity.

$$T\Delta s_{gen} = \frac{dm}{m_m}\frac{1}{2}\left[(V_{ss} - V_{leak,x})^2 + V_{leak,y}^2\right] \tag{6.6}$$

$V_{leak,x}$ is equal to the pressure side velocity because the streamwise velocity of the fluid is unaffected as it passes through the gap. $V_{leak,y}$ is computed from the leakage massflow. The resulting expression for loss per unit leakage flow is given in equation 6.7.

$$\frac{m_m T\Delta s_{gen}}{dmV_x^2} = \frac{\psi^2}{2\phi^2\sigma^2} + \frac{C_d^2\psi}{\phi\sigma cos(\alpha)} \tag{6.7}$$

The first term on the right hand side is associated with the equilibration of streamwise velocity between the leakage flow and the mainstream, and decreases at a rate of $1/\sigma^2$. The second term is associated with dissipation of the crossflow kinetic energy, depends on the leakage massflow, and decreases at a rate of $1/\sigma$.

Three-dimensional calculations of the B blade showed the tip clearance loss decreased 15% as the solidity increased from 0.88 to 1.07 [2]. Comparison of the 3-D results with the scaling arguments discussed above for leakage massflow and mixing losses are discussed below.

[2]The solidities of the geometries evaluated were obtained by varying the blade count for the subsonic high pressure turbine of chapter 2 between 53 and 64 (the baseline design has 58 blades).

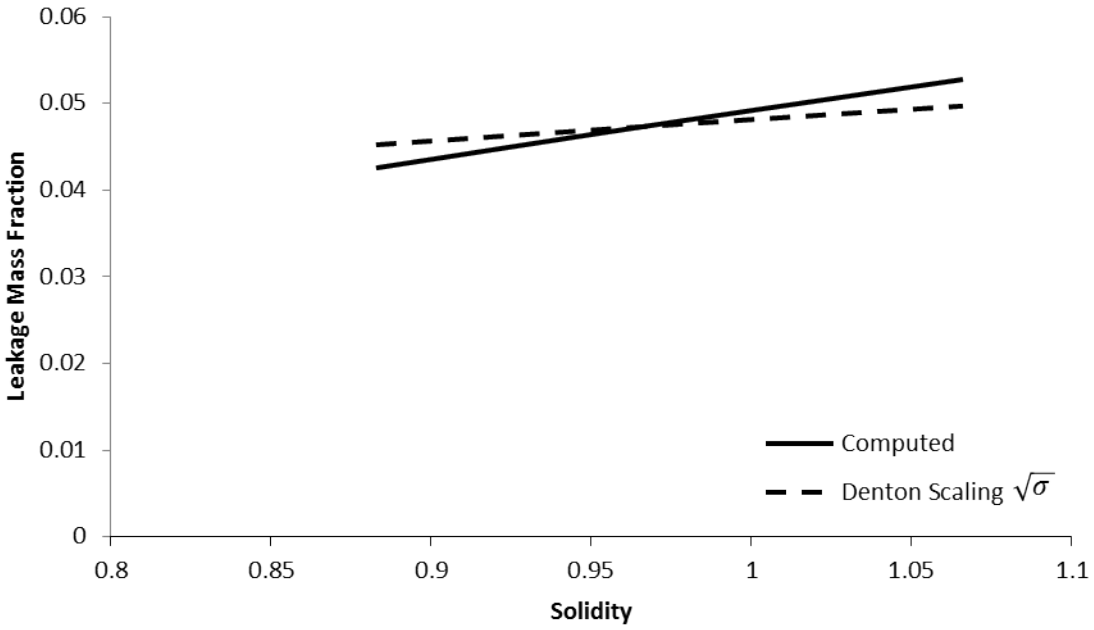

Figure 6-10: Leakage mass fraction as a function of solidity for B blade, 2% clearance.

6.3.1 Leakage Massflow

Figure 6-10 shows the change in leakage massflow ratio ($MR = \frac{m_{leak}}{m_m}$) with solidity. Also shown is the scaling predicted by the Denton's analysis as the solidity changes from $\sigma = 0.97$, given in Equation 6.8.

$$MR(\sigma) = \sqrt{\frac{\sigma}{0.97}} MR(\sigma = 0.97) \tag{6.8}$$

The computed leakage massflow increases linearly with solidity, rather than as $\sqrt{\sigma}$; the computed massflow through the tip gap remains constant as solidity changes, because the total-to-static pressure ratio across the tip gap is unaffected by solidity downstream of $x/c = 0.25$, as shown in figure 6-11. The only effect of solidity on the mass ratio is the change in pitch, so that the mass ratio scales linearly with σ.

6.3.2 Mixing Losses

Three-dimensional computations confirm that the mixing loss per unit leakage flow decreases as solidity increases, but more rapidly than predicted by the control volume

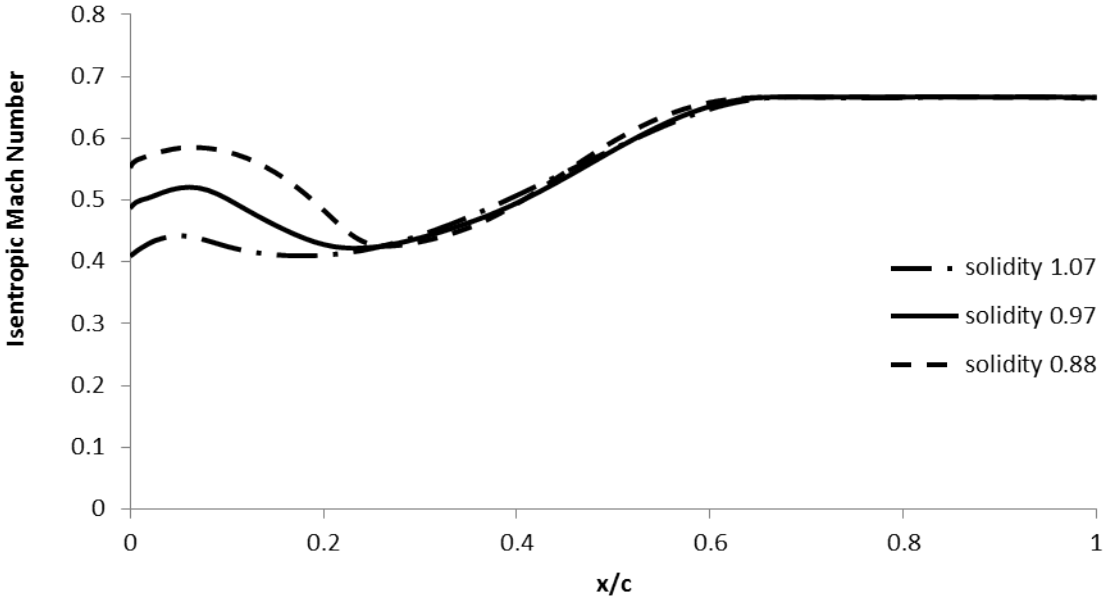

Figure 6-11: Suction surface gap exit isentropic Mach number for B blade, $\sigma = 0.88, 0.97$ and 1.07, 2% clearance.

analysis or scaling arguments presented above. Figure 6-12 shows the mixing loss per unit leakage massflow as a function of solidity, along with the control volume estimates for mixing losses and the scaling. Because the leakage massflow and thus $V_{y,leak}$ are unaffected by the change in solidity, the first term in Equation 6.7 is the only one that varies with solidity, the change in mixing loss should scale as $1/\sigma^2$. Since the two terms in Equation 6.7 are roughly of equal magnitude ($V_{leak,y} \approx V_{ss}$ and $V_{leak,x} \ll V_{ss}$), the mixing loss will scale as given in equation 6.9.

$$\frac{m_m T \Delta s}{m_{leak} \Delta h_t}(\sigma) = 0.5 \frac{m_m T \Delta s}{m_{leak} \Delta h_t}(\sigma = 0.97) + 0.5 (\frac{0.97}{\sigma})^2 \frac{m_m T \Delta s}{m_{leak} \Delta h_t}(\sigma = 0.97) \qquad (6.9)$$

The control volume estimates for the mixing losses decrease at a rate similar to that predicted by the scaling arguments. The computed loss is more sensitive to solidity than the control volume analysis predicts, because of changes in vortex breakdown loss with solidity. Figure 6-13 shows the midspan suction surface isentropic Mach number for the three solidities, while Figure 6-14 shows the vortex core centerline

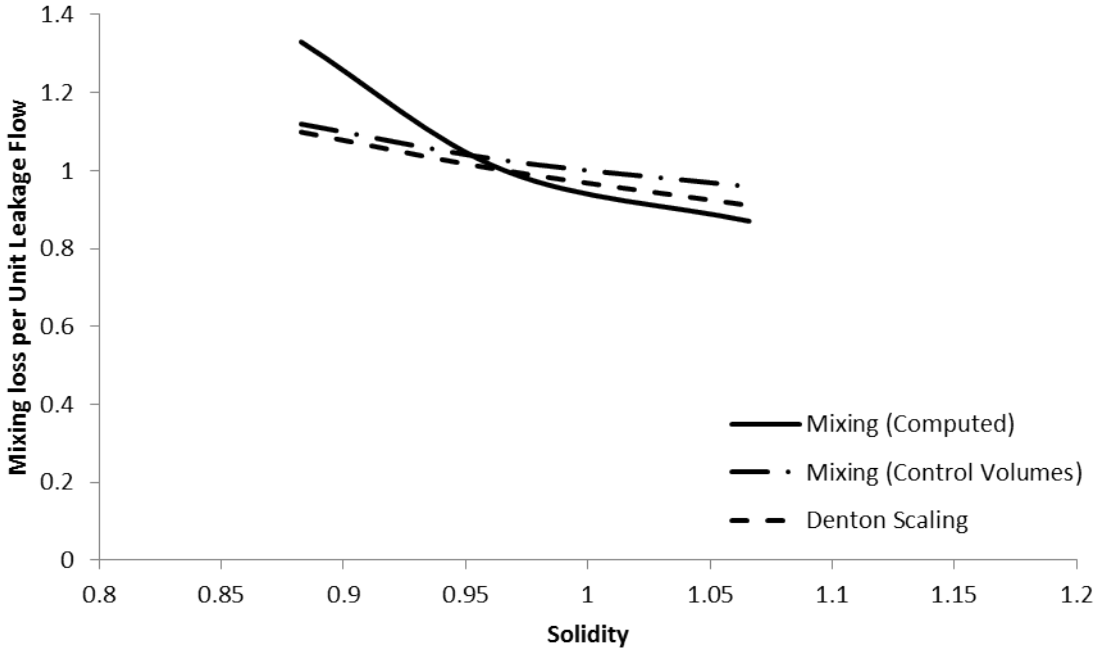

Figure 6-12: Mixing loss per unit massflow as a function of solidity for B blade, 2% clearance. Computed losses and control volume estimate.

velocity ratio as a function of axial position for $\sigma = 0.88, 0.97$ and 1.07. As solidity decreases, the flow decelerates more in the aft region of the blade, and the minimum streamwise velocity ratio at $x/c = 1.15$ decreases. For the three solidities considered, the mixing loss peaks at the location of minimum streamwise velocity in the vortex, as in figure 6-15. This increase in loss is due to both the increase in suction surface Mach number (which is captured by the control volume analysis) and to increased losses from vortex breakdown.

6.4 Conclusions

Blade loading affects tip clearance loss both through increased suction surface mixing velocities, which are captured by the control volume model, and through altering the extent of vortex breakdown, which is not captured by the control volume model.

With the entire blade front-loaded (the F2 blade), the tip clearance loss is decreased 9% relative to the baseline B2 blade, but the loss per unit leakage flow is decreased 30%. The pressure rise from $x/c = 0$ to 0.5 in the F2 blade did not con-

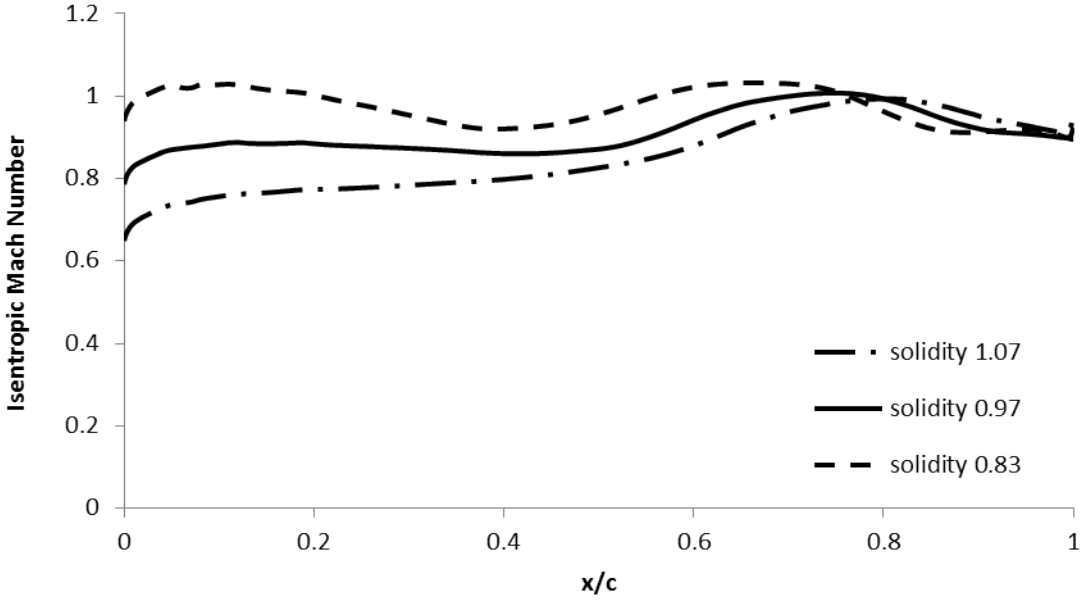

Figure 6-13: Midspan suction surface isentropic Mach number for B blade, $\sigma = 0.88, 0.97$ and 1.07, 2% clearance.

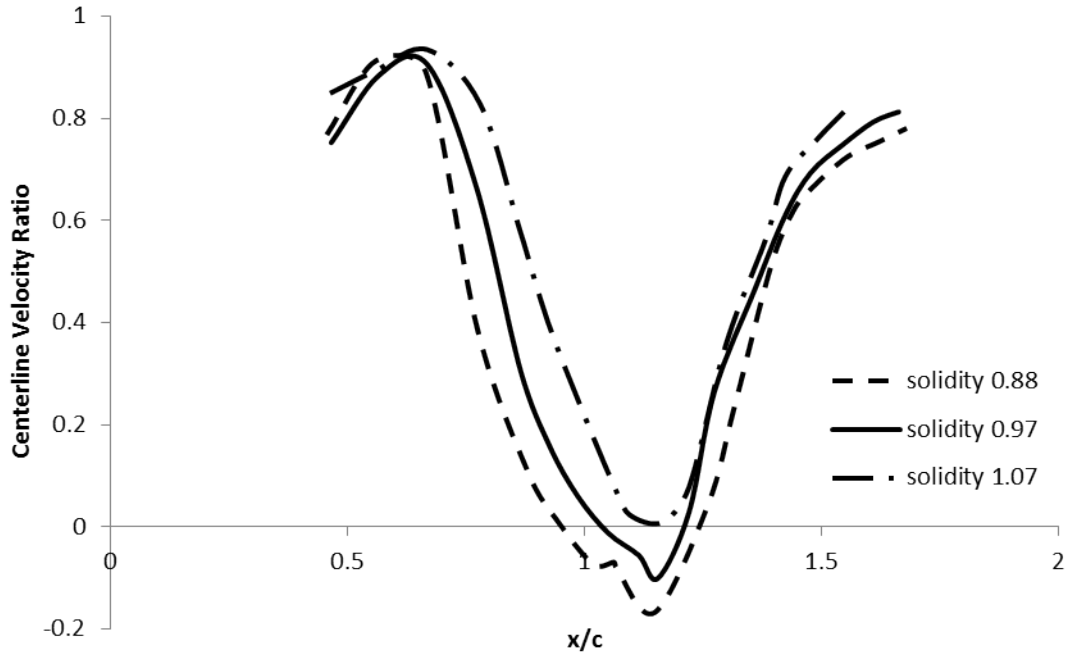

Figure 6-14: Vortex centerline velocity ratio as a function of axial distance for B blade, $\sigma = 0.88, 0.97$ and 1.07, 2% clearance.

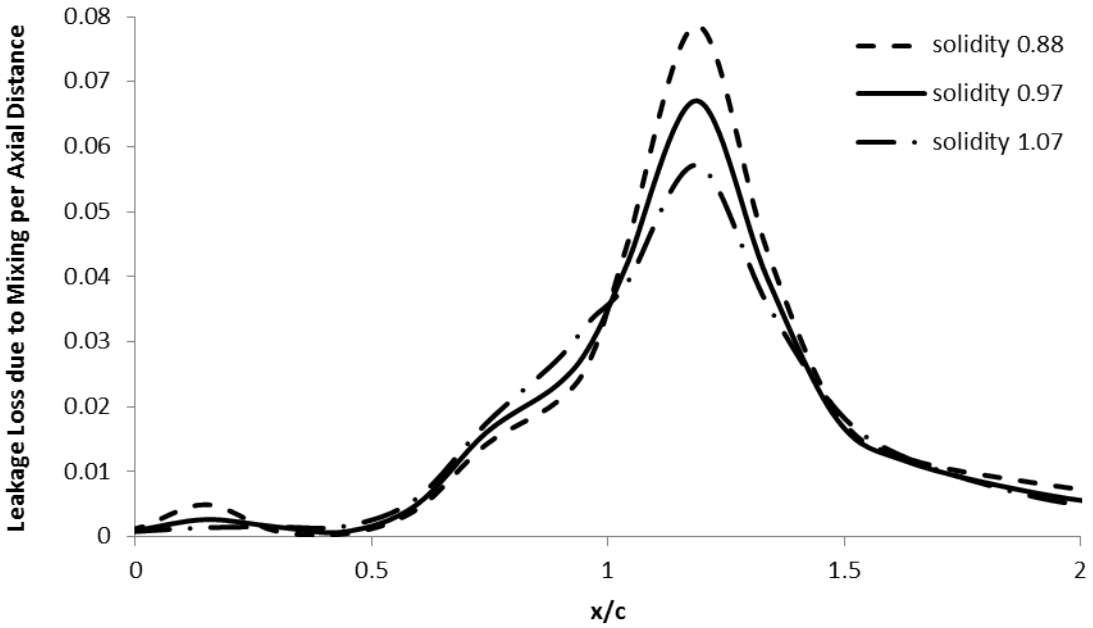

Figure 6-15: Entropy generation per unit axial distance as a function of axial distance for B blade, $\sigma = 0.88, 0.97$ and 1.07, 2% clearance.

tribute to the loss because it caused vortex breakdown while the vortex was still small. If the entire blade is aft loaded, the tip vortex breakdown causes more losses than in the baseline blade, and the tip clearance loss per unit leakage flow is increased 40%.

Positive incidence change shifts the airfoil surface loading forward, while negative incidence change shifts the loading aft. Increasing the inlet flow angle by 10° decreases tip clearance losses by 9% while decreasing the inlet flow angle by 10° increases tip clearance loss by 8%.

Finally, an increase in solidity reduces tip clearance loss by decreasing the freestream Mach number and vortex breakdown losses, even though the leakage mass fraction increases. A 10% increase in solidity was found to decrease the loss per unit leakage flow 13%, while a 10% decrease in solidity increased loss per unit leakage flow by 33%. As solidity increases, the leakage mass fraction grows linearly because the the leakage massflow is unaffected by the solidity change, while the passage massflow decreases. The loss per unit leakage massflow decreases with an increase in solidity because the losses due to vortex breakdown are reduced.

Chapter 7

Conclusions and Recommendations for Future Work

7.1 Summary

The dependence of tip clearance loss on turbine blade pressure distribution was examined through three-dimensional RANS turbine computations, control volume analyses, and computations of flow in rectangular ducts with area changes.

- A control volume approach was assessed against the leakage mixing process in rectangular ducts with area expansion and flow injection as well as in four turbine blade passages. It was found that while control volume analysis is useful for estimating turbine tip clearance losses, there is a large ($\sim 30\%$) uncertainty, because the the change in loss as the vortex passes through a pressure gradient is not addressed.

- Axisymmetric computations of vortices in area expansions showed that strongly swirling tip clearance flows ($u_\theta/u_x \geq 1$) in the vortex core) respond differently to pressure rises than do wakes, because of vortex line contraction and vortex breakdown.

- Based on the observations, it was hypothesized that tip clearance loss due to vortex breakdown could be reduced for blade designs that lower the pressure

rise in the aft section of the suction surface near the tip. Computations for turbines with forward and aft loading, as well as with different incidences and solidities, confirmed this hypothesis.

7.2 Contributions

There are four main contributions made by this work, presented below.

- Turbine tip leakage vortices are found to be qualitatively different from compressor tip leakage vortices at the design point. Turbine vortices have initial swirl numbers greater than 1, while compressor vortices have swirl numbers (u_θ/u_x) less than 0.5. Because of this, a turbine clearance vortex is susceptible to vortex breakdown under a large pressure rise, but it can experience a reduction in mixing loss under a small pressure rise (large and small are defined in Chapter 4). A compressor clearance vortex is more like a wake, whose mixed out loss increases as it passes through a pressure rise.

- The use of control volume analysis to capture the mixing loss between the leakage stream and the mainstream was assessed to be accurate to within 40% for the cases studied. The reason for the discrepancy is that much of the mixing takes place downstream in the tip clearance vortex, which passes through a pressure rise (for the cases considered), rather than at the clearance exit condition.

- Tip clearance vortex breakdown is an important loss mechanism in turbine tip clearance flow. Axisymmetric vortex breakdown calculations showed that as the pressure rise increased above a certain level, the amount of reversed flow in the vortex core and the mixed-out loss both increased.

- Tip clearance loss can be decreased by designing the turbine with a lower pressure rise in the aft 50% axial chord. A forward-loaded blade reduced the tip clearance loss by 16%, relative to an aft-loaded blade, by reducing the pressure

rise and hence the vortex breakdown in the turbine passage. Tip clearance loss also decreases as solidity and incidence increase, consistent with the above ideas.

7.3 Recommendations for Future Work

One major recommendation concerns unsteady flow. The turbine calculations in this thesis treated the blade in isolation. In reality, the upstream vane provides an unsteady inlet flow which can affect the tip clearance flow and the vortex. More importantly, in a real turbine, the tip clearance vortex will not mix out before it encounters the next stationary blade row, and the effect of the unsteady interaction of the vortex with the downstream blade row is not known. One-and-a-half stage unsteady calculations, along with simplified analyses, should be done to assess and to clarify the unsteady effects of tip clearance flow, in particular to determine the behavior of the tip loss in a multi-row unsteady environment.

A second recommendation concerns the design features. The turbines studied in depth were all subsonic. The suggestion is thus to examine the physical features of the mixing process for a supersonic turbine to see if the trends are similar to those of subsonic flow.

Bibliography

[1] T. C. Booth. Importance of tip clearance flows in turbine design. In *Tip Clearance Effects in Axial Turbomachines*, VKI Lecture Series 1985-05. VKI, 1985.

[2] D. L. Darmofal, R. Khan, E. M. Greitzer, and C. S. Tan. Vortex core behaviour in confined and unconfined geometries: a quasi-one-dimensional model. *Journal of Fluid Mechanics*, 449:61–84, 2001.

[3] J. D. Denton. Loss mechanisms in turbomachines. *Journal of Turbomachinery*, 115(4):621–656, 1993.

[4] E. M. Greitzer, C. S. Tan, and M. B. Graf. *Internal Flow*. Camridge University Press, 2004.

[5] M.G. Hall. The structure of concentrated vortex cores. *Progress in Aerospace Sciences*, 7:53 – 110, 1966.

[6] N. W. Harvey. Aerothermal implications of shroudless and shrouded blades. In *Turbine Blade Tip Design and Tip Clearance Treatment*, VKI Lecture Series 2004-02. VKI, 2004.

[7] F. J. G. Heyes and H. P. Hodson. Measurement and prediction of tip clearance flow in linear turbine cascades. *Journal of Turbomachinery*, 115(3):376–382, 1993.

[8] S. C. Kacker and U. Okapuu. A mean line prediction method for axial flow turbine efficiency. *Journal of Engineering for Power*, 104(1):111–119, 1982.

[9] S. A. Khalid. *The Effects of Tip Clearance on Axial Compressor Pressure Rise*. PhD thesis, Massachusetts Institute of Technology, Cambridge, MA, USA, May 1995.

[10] S. A. Khalid, A. S. Khalsa, I. A. Waitz, C. S. Tan, E. M. Greitzer, N. A. Cumpsty, J. J. Adamczyk, and F. E. Marble. Endwall blockage in axial compressors. *Journal of Turbomachinery*, 121(3):499–509, 1999.

[11] S. K. Krishnababu, H. P. Hodson, W. N. Dawes, P. J. Newton, and G. D. Lock. Numerical and experimental investigation of tip leakage flow and heat transfer using idealised rotor-tip models at transonic conditions. *The Aeronautical Journal*, 111(1141):165–186, 2009.

[12] S. K. Krishnababu, P. J. Newton, W. N. Dawes, G. D. Lock, H. P. Hodson, J. Hannis, and C. Whitney. Aerothermal investigations of tip leakage flow in axial flow turbines—Part I: Effect of tip geometry and tip clearance gap. *Journal of Turbomachinery*, 131(1), 2009.

[13] P. K. Kundu and I. M. Cohen. *Fluid Mechanics*. Elsevier Academic Press, 2008.

[14] W. Li, W. Qiao, K. Xu, and H. Luo. Numerical simulation of tip clearance flow passive control in axial turbine. *Journal of Thermal Science*, 17:147–155, 2008.

[15] J. Moore and J. S. Tilton. Tip leakage flow in a linear turbine cascade. *Journal of Turbomachinery*, 110(1):18–26, 1988.

[16] D. Pagan. *Contribution à l'étude expérimentale et théorique de l'éclatement tourbillonnaire en air incompressible*. PhD thesis, Université Pierre et Marie Cure, Paris, Paris, France, May 1989.

[17] A. H. Shapiro. *The Dynamics and Thermodynamics of Compressible Flow, I and II*. The Ronald Press Company, 1953.

[18] P. R. Spalart and S. R. Allmaras. A one-equation turbulence model for aerodynamic flows. *La Recherche Aerospatiale*, 1(1):5–21, 1994.

[19] V. Yakhot, S. A. Orszag, S. Thangam, T. B. Gatski, and C. G. Speziale. Development of turbulence models for shear flows by a double expansion technique. *Physics of Fluids A: Fluid Dynamics*, 4(7):1510–1520, 1992.

[20] D. Yang, X. Yu, and Z. Feng. Investigation of leakage flow and heat transfer in a gas turbine blade tip with emphasis on the effect of rotation. *Journal of Turbomachinery*, 132(4), 2010.

[21] M. Yaras and S. A. Sjolander. Development of the tip-leakage flow downstream of a planar cascade of turbine blades: Vorticity field. *Journal of Turbomachinery*, 112(4):609–617, 1990.

[22] M. I. Yaras and S. A. Sjolander. Prediction of tip-leakage losses in axial turbines. *Journal of Turbomachinery*, 114(1):204–210, 1992.